MODELING THE BEHAVIOR OF A VESSEL UNDER RUNAWAY CONDTIONS

A Thesis

by

RYM KANES

Submitted to the Office of Graduate and Professional Studies of
Texas A&M University
in partial fulfillment of the requirements for the degree of

MASTER OF SCIENCE

Chair of Committee,	Luc N. Vechot
Co-Chair of Committee,	Marcelo Castier
Committee Members,	Reza Sadr
	Valeria Casson Moreno
Head of Department,	M. Nazmul Karim

August 2015

Major Subject: Chemical Engineering

ABSTRACT

Reactive chemicals may proceed into uncontrolled chemical reactions with significant evolutions in temperature and pressure due to vapor/gas production. This happens when there is loss of control of the temperature of the system, and self-heating occurs, thereby leading to a runaway reaction. The overpressurization of the vessel following the runaway may lead to an industrial accident, a thermal explosion, resulting in damages to people, property and the environment. Emergency relief systems (ERS) act as a last line of defense against vessel overpressure. It is therefore critical to the safe operation of chemical processes that they are adequately sized.

Much effort is needed to overcome the limitations presented by the current ERS sizing method used. Also, reliance solely on experimental work can prove to be time consuming and provide difficulties during scale-up to industrial scale. Thus, there is a need to employ a comprehensive dynamic model that describes the vessel behavior throughout the reaction, during depressurization and relief action. This involves the understanding of the phenomenological links between thermodynamics, kinetic and fluid dynamics inside the vessel from the onset of the runaway until the end of the venting through an ERS. These outputs of this model could then to be used to enhance ERS sizing methods and consequence analysis.

This work represents a step forward in this direction. It proposes a model that takes all these factors into account, with the exception of level swell. To achieve this, this work includes: (i) an experimental study of the reactive system using calorimetric techniques; (ii) determination of the kinetic rate expression for the reactive system; (iii) formulation of dynamic lumped model; (iv) dynamic simulations of a closed vessel and partial experimental validation; (v) a sensitivity analysis of the effects of ERS area and ERS set pressure on vessel behavior. This approach was carried out through the evaluation of the decomposition of *di-tert*-butyl peroxide in toluene, a potentially hazardous reactive system.

ACKNOWLEDGEMENTS

I would like to express my utmost gratitude to my committee chair, Dr. Luc N Véchot, for his guidance, sincere advice, infinite optimism and laughter at times where there should have been tear, and unwavering support throughout this research. Special thanks also go to my co-chair, Dr. Marcelo Castier, for his unlimited support and guidance, ever relevant stories about everything and nothing, greatly enthusiastic noise effects during successful simulation runs, and sincere advice. A thank you also goes to Dr. Reza Sadr for his collaboration, perspective and serving as an advising committee member.

I wish to recognize the extent to which conversations and cooperation with Dr. Valeria Casson Moreno have contributed to this project. She has been a source of knowledge and much encouragement. Thank you for the long calls, the explanations, the advice as well as the nudges and pushes.

Much appreciation is expressed to the Mary Kay O'Connor Process Safety Center (MKOPSC) for supporting this research work.

Finally, I first thank my family for their unconditional patience, love and support: My father and mother for their perspective, wisdom and advice; my sister for simply being herself. I also thank friends, colleagues and TAMUQ staff for all their support and help.

NOMENCLATURE

Roman Nomenclature

A	Helmholtz energy	J
A_{ers}	Area of the ERS	m^2
A_{or}	Area of the Orifice	m^2
A_j	Area of a hole that is exposed to phase	m^2
Bi	Biot number	
Cp	Heat capacity of the reacting mixture	J/g.K
D	Diameter of the Reactor	m
E_a	Activation Energy	J/mol
f	Volume function	
G	Vented mass flux	$kg/m^2\ s$
g	Acceleration due to gravity	m/s^2
h	Heat transfer coefficient	$W/(m^2.K)$
h_j	Vertical level of the upper interface of phase j	m
H	Enthalpy	J/kg
H_B	Vertical level of the bottom of the vessel	m
H_T	Vertical level of the top of the vessel	m
ΔH_R	Heat of reaction	J/kg
k	Thermal conductivity	W/(m.K)
k_0	Pre-exponential factor of reaction	1/s

m	Reactant mass	kg
M_m^{out}	Molar mass of stream	g/mol
n	Number of moles	mol
n_c	Number of components	
n_p	Number of phases	
dm/dt	Rate of change of reactant mass	kg/s
ns_{in}	Number of input streams	
ns_{out}	Number of output streams	
$\dot{n}_{im}^{in}$	Molar flow rate of component i in input stream m	
n_{im}^{in}	Cumulative amount of component i that entered the vessel through stream m	
$\dot{n}_{im}^{out}$	Molar flow rate of component i in output stream m	mol/s
n_{im}^{out}	Cumulative amount of component i that left the vessel through stream m	mol/s
m_g	Gas mass	kg
n	Kinetic parameter	
m	Kinetic parameter	
p	Kinetic parameter	
P	Absolute pressure	Pa
P_{atm}	Atmospheric Pressure	Pa
P_{max}	Second pressure peak	Pa
P_{set}	Set pressure for the venting opening	Pa

dP/dt	Rate of pressure rise	Pa/s
$(dP/dt)_{max}$	Maximum pressure rise rate	Pa/s
Q+	Heat gain	W
Q-	Heat lost	W
$\dot{Q}$	Heat transfer rate to the vessel	W/s
R	Gas Constant	J/mol.K
$\dot{R}_i$	Rate of generation of component i	mol/s
$\dot{r}_k$	Rate of reaction k	
S_A	Exchange surface area	m^2
S	Entropy	J/K.mol
t	Time	s
T	Absolute temperature	K
T_{onset}	Onset temperature	K
T_i	Initial Temperature	K
T_{max}	Maximum temperature peak	K
T_s	Vent opening temperature	K
dT/dt	Adiabatic rate of temperature rise due to runaway	K/s
$(dT/dt)_{max}$	Maximum temperature rise rate	K/s
U	Internal energy	J
v_j	Molar volume of phase j	m^3/mol
V	Volume of the Reactor	m^3
Vj	Volume of phase j	m^3

x_{ij}	Mole fraction of component i in phase j	m^3
X	Reaction Conversion	%
dX/dt	Kinetic model used to describe the reaction	1/s

Greek Nomenclature

β	Heating rate	K/min
ρ	Density	kg/m^3
δ	Frank Kamenetskii parameter	
ζ	Extent of reaction	
ϕ	Thermal inertia factor	

TABLE OF CONTENTS

Page

LIST OF FIGURES

LIST OF TABLES

Page

CHAPTER I

INTRODUCTION

Chemical reaction hazards are a principal source of concern in the chemical industry, where various manufacturing processes involve exothermic reactions (polymerizations, hydrogenations, neutralizations, combustions). One of the main hazards associated with exothermic reactions is the loss of the thermal control of the reactor vessel, thereby triggering a runaway reaction that occurs when the rate of heat production rate from the exothermic reaction exceeds the vessel heat removal rate. A runaway reaction is characterized by the exponential increase of the temperature and the pressure of the vessel [1]–[3], that may lead to the vessel explosion along with the release of potentially flammable and toxic substances.

In order to manage the hazards associated with runaway reactions, a risk assessment of the process should be carried out and appropriate safety measures have to be selected, implemented and maintained [4]. These measures include: (i) reduction of the hazards by inherently safer design; (ii) prevention of the risk by process control; and (iii) mitigation of the consequences by protective measures. Emergency relief systems (ERS), such as bursting disks or relief valves, belong to the third category. They are generally used as the last barrier to protect reactor vessels for exothermic reactive systems from a catastrophic explosion. ERS are designed to open at a given set pressure and relieve the vessel pressure during the critical phase of the runaway reaction (when its maximum rate is reached). The prediction of the behavior of a runaway reaction in a reactor vessel, in terms of temperature and pressure evolution, is of utmost importance to perform the correct design of an ERS.

The prediction of the behavior of a reactor vessel under runaway condition during venting is quite complex. Indeed, it requires the extensive knowledge of the reaction kinetics, thermodynamics and fluid dynamics within the vessel, the flow regimes through the venting device [3]. Such phenomena and their interaction are yet to be fully understood. This is especially true for reactive systems categorized by the Design Institute for Emergency Relief Systems (DIERS) as *Gassy* or *Hybrid* systems, i.e. chemical systems for which the pressure generation is mainly or partially due to the production of permanent gases [3], [5]–[7]. Many peroxide compounds tend to decompose by producing permanent gases, and are therefore belong to this particular category [8]. Currently, experimentally validated models to accurately predict the behavior of reactor vessels containing *Gassy* or *Hybrid* systems during venting, are lacking. The work presented in this thesis was done as a first step to fill this gap.

The objective of this research work is to simulate the dynamic behavior of a gassy/hybrid reactive chemical system, within a reactor vessel, under runaway conditions. Many peroxide compounds exhibit behavior indicative of a gassy/hybrid system under runaway, the reactive chemical system chosen in this study is the decomposition of di-terty-butyl peroxide (DTBP) in toluene. The results of this work include the experimental determination of the kinetic of the decomposition reaction and the simulation of the pressure and temperature profiles in the reactor vessel before and during the operation of an ERS (bursting disk).

In this research, a description of the theory behind thermal runaways, the methods of experimentally characterizing them, as well as the use of emergency relief system as mitigation barrier are given in Chapter 1. A review of the methods employed to conduct a kinetic study based on experimental characterization of runaway reactions is presented in Chapter 2. A comprehensive study of fluid flow models for vessel discharges was carried out in Chapter 3. The scope and approach to carry out the research work is developed in Chapter 4. The results for the experimental characterization of the chemical system under runway conditions as well as the kinetic study is presented in Chapter 5. The formulation of the dynamic simulator to include ERS action and chemical reactions is developed in Chapter 5. The results of closed vessel simulation validated against experimental data, a reference ERS venting simulation and a sensitivity analysis is presented in Chapter 7.

The findings of this work capture some capabilities of a dynamic simulator and its role in describing vessel depressurization during ERS action. Although a larger sensitivity analysis is yet to be done in order to fully understand the reliability of such a model for ERS sizing, this work acts a first stepping-stone in that direction.

CHAPTER II

THERMAL RUNAWAY

2.1 Précis

Thermal runaways (runaway reactions or thermal explosions) are characterized by an exponential increase of the temperature and pressure in a reactor or vessel containing a reactive substance [1], [2], resulting from the loss of thermal control of the chemical system. The overpressurization of the vessel following the runaway may lead to its explosion along with the release of potentially flammable and toxic substances.

In this chapter, a brief summary of three major runaway accidents will be provided. Also, the theory behind runaway reactions, and the main experimental techniques used to characterize them will be discussed. Then, prevention barriers and their design techniques will be addressed. The detailed description of these techniques is available in the cited references.

2.2 Major thermal runaway accidents

In 1995, Vilchez et al reported that, out of 5325 incidents involving hazardous materials, thermal explosions are likely to occur mostly during transportation (39%), process (24%), storage (19%), and other operations (19%) [9].The most common initiating causes of runaway reactions include the lack of understanding and the incorrect evaluation of reaction kinetic and thermodynamic conditions of a reactive mixture under runaway condition during the design phase of the process. Very often, the increasing potential for thermal runaways associated to the scale-up of the process is simply not understood and not taken into account. Other initiating causes may be deviations during the process conditions such as failure of the reactor cooling system, failure of the agitation system, wrong addition of chemicals in the vessel, presence of impurities in the reactor, and accumulation of reaction intermediates.

Over the last 30 years, there have been various thermal runaway accidents, but perhaps the three of these accidents that most stand out are:

- Bhopal (India, 1984), where water accidentally entered a storage tank containing 40 tons of methylisocyanate (MIC) causing a runaway reaction. The pressure generated by the runaway, mainly composed of highly toxic MIC vapor and other reaction products, was relieved through the tank pressure relief system causing the death more than 3000 people in one night.
- Seveso (Italy, 1976) where the thermal runaway of the tetra-chlorobenzene hydrolysis to sodium-trichlorophenate reaction formed 30 to 40kg of 2,3,7,8-tetrachlorodibenzo para dioxin (TCDD), a deadly poison, that was released to the surrounding. While no human fatalities resulted from the incident, the health of many people was very seriously affected (several cases of abortions and Chloracne) and many animals in the area died. This event had tremendous impact on the way major hazard plants are regulated in European countries (Seveso Directives).
- T2 Laboratories (Florida, USA, 2007), where the thermal runaway of the reaction that produces methylcyclopentadienyl manganese tricarbonyl led to

the overpressurization of the 9.5 m^3 reactor vessel. The vessel was equipped with a bursting disk that opened to relieve the pressure. However the bursting disk was undersized and the vessel exploded resulted in 4 fatalities onsite and 32 people injured off-site [10].

2.3 Theory of thermal runaways

Runaway reactions are caused due to the failure of the system to remove heat at a rate equivalent to or greater than what is generated by an exothermic reaction. Thus, the study of the energy balance of a process vessel containing a reactive system becomes important with respect to understanding dynamic heat generation and dissipation effects. Semenov [11] and Frank – Kamenetski [12] developed theories to describe quantitatively the conditions at which thermal runaways are initiated in reactor vessels.

2.3.1. Semenov's theory of thermal ignition

Semenov theory assumes that the temperature, T, of a reacting system in a reactor vessel is uniform throughout the entire volume of the vessel. The heat loss rate (Q_- in W) to the surrounding at ambient temperature T_a can simply be represented by Newton's law of cooling:-

$$Q_- = hS\left(T_a - T\right) \tag{1}$$

where h is the heat transfer coefficient (W.K^{-1}.m^{-2}) , S is the heat exchange surface area (m^2). Q_- increases linearly with T, the slope being fixed by hS.

The heat production rate by the reacting system Q_+, assuming a zero order reaction, is given by:

$$Q_+ = m\Delta H_r k_0 \exp\left(\frac{-E_a}{RT}\right) \tag{2}$$

where m is the reactive liquid mass (kg), ΔH_r the heat of reaction (J/kg), k_0 the pre-exponential factor (s^{-1}), E_a the activation energy ($J.mol^{-1}$) and R the universal gas constant ($J.mol^{-1}.K^{-1}$). Q_- increases exponentially with T [11]–[13].

Figure 1 provides a schematic illustration of the temperature dependence of Q_+ and Q_-. There are several cases that can be considered.

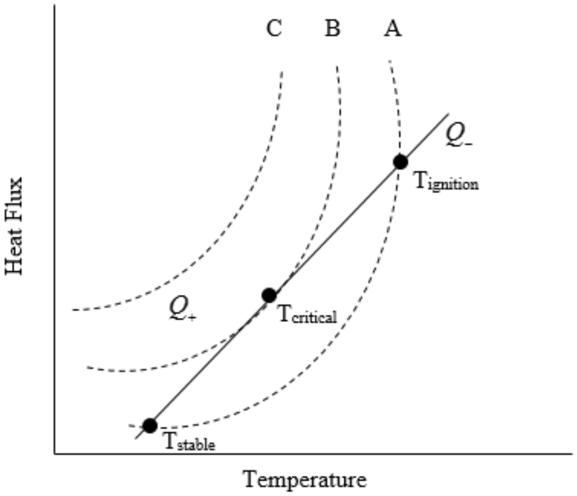

Figure 1. Plot of thermal fluxes against temperature using Semenov's theory. Curves A, B and C are Q_+ , while the straight line is Q_-

Case 1: Q_- line and curve A for $Q+$*:* Two stationary points (T_{stable} and $T_{ignition}$.) can be seen where $Q_+ = Q_-$:

- If the reacting mixture is at a temperature T less than T_{stable} Q_+ will dominate Q-, which will result in an increase of the temperature of the reactive mixture until T_{stable} is reached. For $T_{stable} < T < T_{ignition}$, Q_- will dominate Q_+, which means that the reactive mixture can be cooled down to the T_{stable}. This explains why this temperature is called "stable".
- If the reactive mixture has a temperature higher than $T_{ignition}$, Q_+ will dominate Q_- leading to an increase of the temperature that further accelerate the reaction. The conditions for a thermal runaway are then fulfilled.

Case 2: Q_- line and Curve B for Q_+*:* For this case, Q_- is tangential to Q_+ and intersects Q_+ only at $T_{critical}$ which is a metastable point. Any infinitesimal increase of T from this point will initiate the runaway.

Case 3: Q_- line and Curve C for Q_+*:* Q_- is always less than and never intersects Q_+. There is no stationary point, the reactive systems will undergo a runaway.

Semenov 's theory is used to explain gaseous or liquid systems subject to self-heating in a strongly turbulent regime. It can also be used for small solids particles suspended in a fluid in a turbulent regime, as is the case in sections of plug flow or stirred reactors [11]–[13].

2.3.2. Frank-Kamenestskii's theory of thermal ignition

While Semenov's model is useful, it is limited to systems where there is no temperature gradient within the vessel. The Frank-Kamenetskii theory overcomes this limitation [12], [14]. This theory is relevant to cases where the reactants have low thermal conductivity and are surrounded by highly conductive walls or there is considerable resistance to heat transfer in the reacting system [13]. Figure 2 shows the temperature profile of such a system.

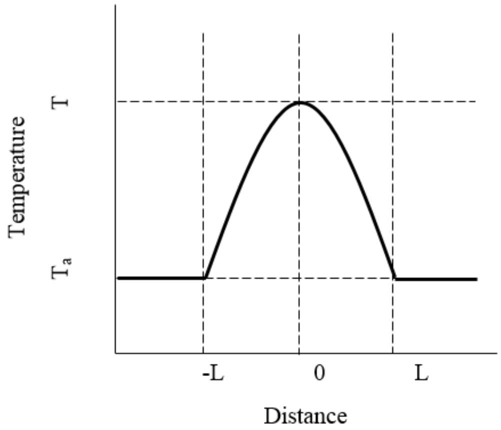

Figure 2. Temperature profile of a system according to Frank-Kamenetskii's theory

Heat production can be expressed in the same manner as Semenov's Q_+.

The reaction is taken to be sufficiently exothermic and thus there is negligible reactant consumption at the ignition point. Also, the activation energy is assumed to be sufficiently high so that the activation energy parameter is sufficiently small [12]–[14]. The activation energy parameter, ε, is given by

$$\varepsilon = \frac{RT_a}{E_a} < 1 \tag{3}$$

With respect to heat transfer, the theory assumes that within the system the mode of heat transfer is conduction only, while at the boundaries both radiation and convection take place. The Biot number is used to show the temperature gradient at the system boundaries, and is given by:

$$Bi = \frac{hL}{k} \tag{4}$$

where *h,* is the effective heat transfer which includes both radiation and convection, *L* is the characteristic length of the body and *k* is the heat conductivity of the solid material. A low Biot number results in the surface temperature not being close to T_a, while a high Biot number results in the surface temperature close to T_a.

The Frank-Kamenetskii parameter, δ, is defined by

$$\delta = \frac{\rho QA}{k} \frac{E_a L^2}{RT_a^{\,2}} \exp\left(\frac{-E_a}{RT_a}\right) \tag{5}$$

This parameter can give indication of how reactive the reactants are, what the dimension of the system involved is, and the effect of ambient temperature on the system [15]. Critical values of the Frank-Kamenetskii paramter, δ_c, for different geometries are compiled by Beever [16], with the interpretation that if $\delta > \delta_c$, then self-ignition will occur [15].

The critical values can be theoretically calculated as the limit of solving the stationary heat conduction equation when no steady state value can be obtained. The classical method of determining δ_c is given by rearranging Eq. (5) [16]

$$\ln\left(\frac{\delta T_a^{\,2}}{L^2}\right) = \ln\left(\frac{E_a}{R}\frac{\rho Q A}{k}\right) - \frac{E_a}{RT_a} \tag{6}$$

A plot of the left hand side (LHS) of Eq. (6) versus $1/T_a$ for varying characteristic lengths would yield a straight line, with a slope of $-E_a/R$. Kinetic parameters can be determined experimentally as discussed in Chapter 2.

This theory describes well systems in non-turbulent motion such as liquids, gaseous, solid and suspensions of solids in reactors that are not agitated and subject to self-heating. However, it does not take into consideration phenomena like hydrolysis, evaporation, condensation. It also does not take into account a larger activation energy parameter, a finite heat transfer correlation, oxygen diffusion or reactant consumption.

2.4 Experimental characterization of thermal runaways

In order to obtain knowledge of exothermic runaway hazards associated with a system under study, experimental thermal hazard assessment tests are performed [17].

2.4.1. Thermal screening

Thermal screening is the first stage when conducting a thermal assessment. Its objective is to identify the potential exothermic behavior potential of a sample over a given temperature range.

Laboratory scale equipment, such as Differential Scanning Calorimeters (DSC), are used for thermal screening. A DSC experiment consists in measuring the heat flow into or out of a small sample amount of a substance (mg to g scale) usually enclosed in a small pressure resistant metal or glass cell as it is exposed to a controlled thermal profile. This is done by measuring the difference between the amount of heat required to increase the temperature of a test pan containing the sample and an empty reference test pan. The tests can be performed in temperature **scan mode** (over a range of temperature a given heating rate) or **isothermal mode** (constant temperature). The temperatures can usually range from -200 to 500 °C.

Data obtained from a thermal screening test are usually thermograms of a heat flow (in W or W.kg^{-1}) *into* or *out of* the sample versus temperature or time. In a thermogram, the direction of the peak indicates whether the process is endothermic or exothermic; conventionally upward pointing peaks are taken to be exothermic. Figure 3 shows an idealized thermal screening curve of an exothermic system.

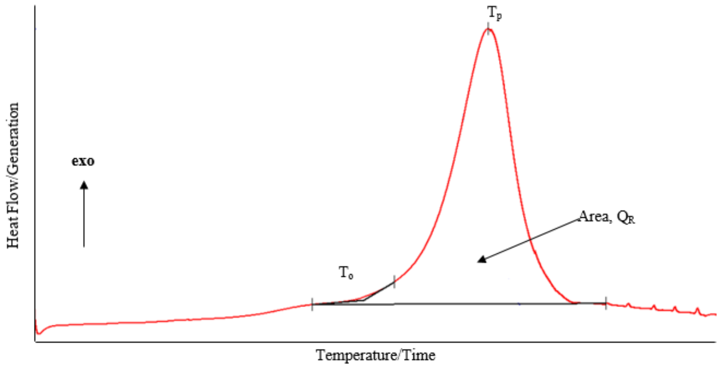

Figure 3. Thermal screening data with an exothermic reaction

The heat flow versus time/temperature curve provides precious information on the following:

- The **total heat of reaction** (ΔH_R in J.kg^{-1}): The integration of the heat flow thermogram over time gives the total heat released, which is equivalent to the heat of reaction of the system. This is a direct indication of the exothermic potential of the chemical reaction. If the heat of decomposition is greater than 500 J/g then the sample maybe explosive.

- The **reaction conversion** at a given time/temperature: The partial integration of the heat flow versus time curve from the start of the test (t=0) to a given time (t) provides the energy of reaction released over that period, ΔH(t). The reaction conversion (X) is then given by:

$$X(t) = \frac{\Delta H(t)}{\Delta H_R} \tag{7}$$

- This reaction conversion profile gives information about the reaction mechanism. The conversion profile is shown in Figure 4 below. A similar profile can be generated for conversion-temperature data as well.
- The **rate of reaction** at a given time and temperature: The derivative of X(t) is a direct measurement of the reaction rate:

$$\text{reaction rate}(t) = \frac{dX(t)}{dt} \tag{8}$$

- The **onset temperature, $\mathbf{T_{onset}}$**, which correspond to the temperature at which an exotherm is detected by the instrument. When using the same instrument the comparison of T_{onset} between several substances can provide the relative thermal stability;
- The **peak temperature ($\mathbf{T_p}$)** and **peak shape**: T_p is an indication temperature at which the maximum heat flow is measured. The peak shape provides an

indication on the type of reaction mechanism as well as the temperature range where the heat is released. The higher and sharper the peak is, the more hazardous the system is.

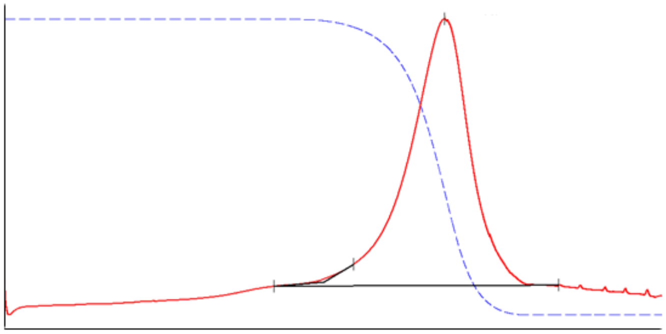

Figure 4. Conversion profile (blue dashed line) for heat flow thermogram (red line)

2.4.2. Adiabatic calorimetry

Following the screening tests, laboratory scale "*adiabatic*" tests should be conducted to study the behavior of reaction under runaway conditions since they are most representative of heat dissipation effects at a large scale.

Adiabatic calorimeters are laboratory bench scale equipment that allow the safe investigations of a runaway reaction. In these equipment, adiabatic conditions (elimination of the heat losses) are achieved by placing the sample (10 – 100 g) in a test cell (metal or glass) surrounded by electrical heater that follow the temperature of the sample during the runaway, as seen in

. The temperature difference between the sample and the surrounding being close to zero, the test can be conducted in adiabatic conditions.

Figure 6 shows typical data obtained with adiabatic calorimeters. The following characteristics of the runaway reactions can be extracted: the onset temperature for the decomposition (T_{on}) in adiabatic condition, the temperature and pressure evolution, the maximum temperature and pressure rise rate, the time to reach maximum rate of reaction and the type of reactive system according to DIERS classification (see part 2.5.1).

In an adiabatic test, the heat released by the reaction goes towards increasing the temperature of the sample and the sample holder. Thus, the thermal inertia of the test cell will play a role in the resulting temperature profile of test. The thicker the wall of the test cell, the higher the thermal mass of the text cell, the more energy is used to heat up the wall (so less for the reactive mixture itself). The relative significance of the thermal inertia of the test cell is quantified by the ϕ factor (phi factor) as follows:

$$\phi = \frac{\left(mCp\right)_{liquid} + \left(mCp\right)_{cell}}{\left(mCp\right)_{liquid}} \tag{9}$$

Large scale vessels tend to have a negligible thermal mass compared to the thermal mass of the liquid they contain, thus their ϕ is close to unity.

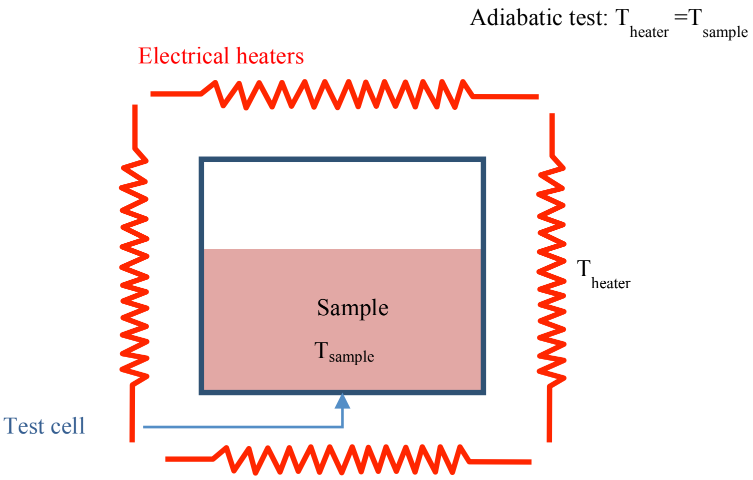

Figure 5. Schematic of an adiabatic calorimeter

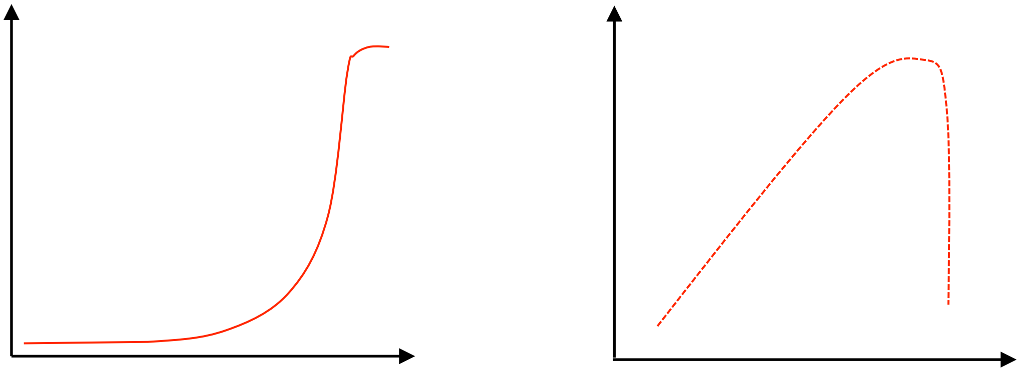

Figure 6. Schematic of adiabatic calorimeter results

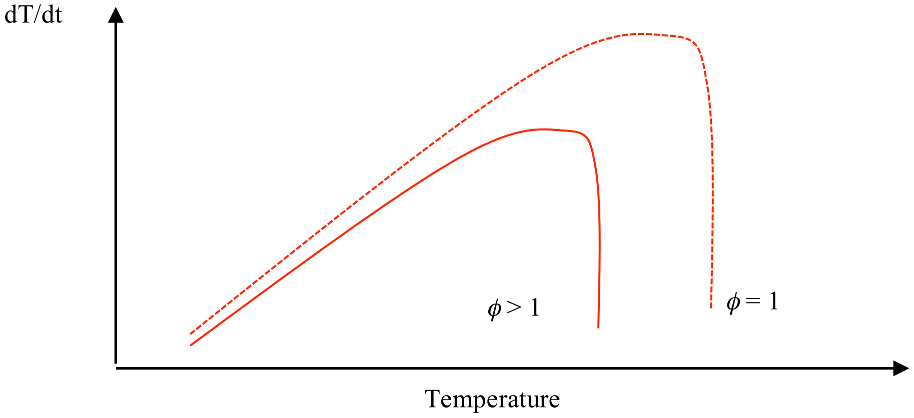

Figure 7. Influence of ϕ on the temperature profile

As shown in Figure 7, experimental data obtained with equipment with $\phi >> 1$ may lead to an underestimation of the temperature and temperature rise rate that will occur at large scale (ϕ close to 1). However, ϕ close to unity is very difficult to achieve at small scale. It is recommended to use equipment with phi-factor within a range of 1.05-1.1 to best approach the industrial conditions. If the ϕ rating of particular instrument is outside this range, the data obtained needs to be corrected before using it for vent sizing [18].

The data obtained from adiabatic calorimetry are used to size emergency relief systems that protect the reactor against explosion should a runaway reaction occur.

2.5 Runaway reactions and vent sizing

In the early 1980's the Design Institute for Emergency Relief Systems (DIERS) under the umbrella of the American Institute of Chemical Engineers (AIChE), made and exceptional effort to develop methods for the design of ERS to handle runaway reaction. The research focused on the prediction of two-phase flow venting resulting from the runaway as well as the use of adiabatic calorimetry data to predict the required relief capacity. These methods are still used to date but in some cases have some serious limitation as explained in chapters 3 and 4.

2.5.1. DIERS classification of reactive systems

The DIERS has proposed to classify reactive systems under three main categories: *vapor*, *hybrid* and *gassy* systems. These systems can have a *tempered* or an *untempered* behavior as described below. To classify the reacting system, the use of adiabatic calorimetry techniques is required.

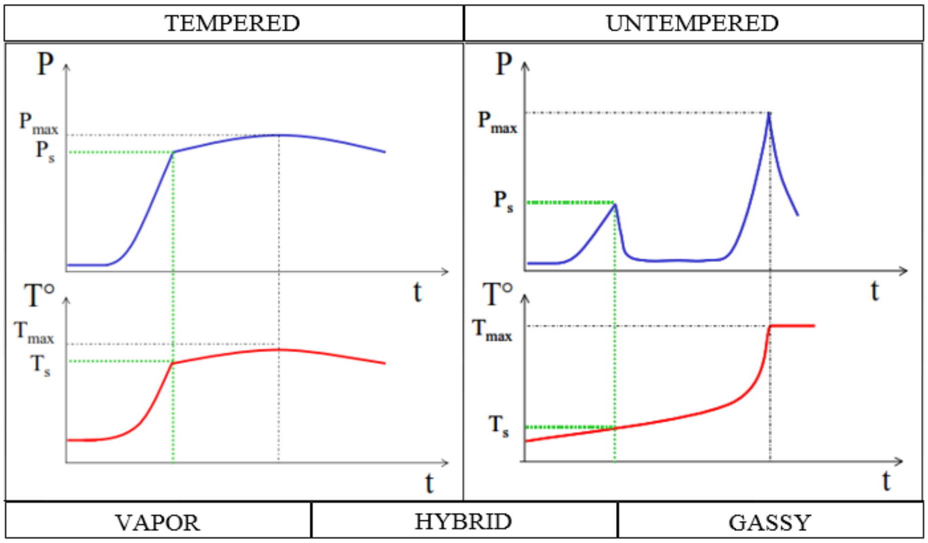

Figure 8. Tempered versus untempered systems during relief operation

Figure 8 shows the typical behavior of the reactive systems according the DIERS classification during the operation of the ERS (with P_S being the ERS opening pressure).

2.5.1.1. Vapor systems

When the pressure generated by the runaway reaction is entirely due to the vaporization of its components, the system is classified as a "*vapor*". These systems are "*tempered*" as during the operation of properly designed ERS, the latent heat of vaporization is absorbed at a sufficient rate to maintain a relatively constant temperature, at constant pressure. Thus, the ERS can temper/control the rate of the reaction by keeping the temperature nearly constant. This temperature may vary slightly at constant pressure due to changes in liquid composition due to a reaction, or preferential boiling of the more volatile components. [3]

2.5.1.2. Gassy systems

When the pressure generated by a runaway reaction is due to the production of non-condensable gas only (e.g. CO_2, CH_4, O_2) and no or very few vapor, the system is classified as a "*gassy*". Such a system has an *untempered* behavior, as the operation of an ERS cannot control the temperature and thus the reaction rate. The ERS simply acts to relief the vessel pressure (by removing material from the reactor). For a gassy system the operation of an ERS may lead to the depressurization of the vessel but will not stop the reacting mixture temperature from increasing exponentially. When the runaway reaches its maximum reaction rate with the associated maximum gas production rate, a *second pressure peak* may arise [3].

2.5.1.3. Hybrid systems

If the pressure generated by a runaway reaction is due to both the production of a permanent gas and vapor, the system is then classified as a "*hybrid*". In this case, the system can experience tempered or untempered behavior, depending on the relative rates of vapor and gas production at the relief pressure. As a rule of thumb, when the vapor pressure constitutes only about 10% of the total pressure, the hybrid systems can usually be treated as gassy systems. [3]

2.5.2. ERS design principles

An adequately sized vent must allow the venting of the vessel material (single or two phase) at a volumetric rate equal or superior to the volumetric gas/vapor generation rate resulting from the runaway reaction. DIERS developed "user friendly" vent sizing calculation methods for the above mentioned reactive systems that require providing an answer to the following questions:

- What will be the maximum gas/vapor generation rate in the vessel considering the worst case scenario during the runaway?

DIERS developed the methodologies to measure the maximum gas/vapor generation rate at laboratory scale using adiabatic calorimetry as described in section 4.2 in chapter 2.

- What is the nature of the fluid entering the vent?

This requires level swell calculation as described in section 2.2 in chapter 4.

- What is the one or two-phase discharge rate through the ERS?

This requires one phase or two phase flow calculation as described in part section 3 of chapter 4.

Figure 9 is a schematic showing the types of reactive systems, their source of pressure generation, and the ERS design criteria under the worst case scenario [3]. The reader can refer to the DIERS Project Manual [19] and UK HSE Workbook for Chemical Reactor Relief System Sizing [3] for a comprehensive description of the vent sizing methods.

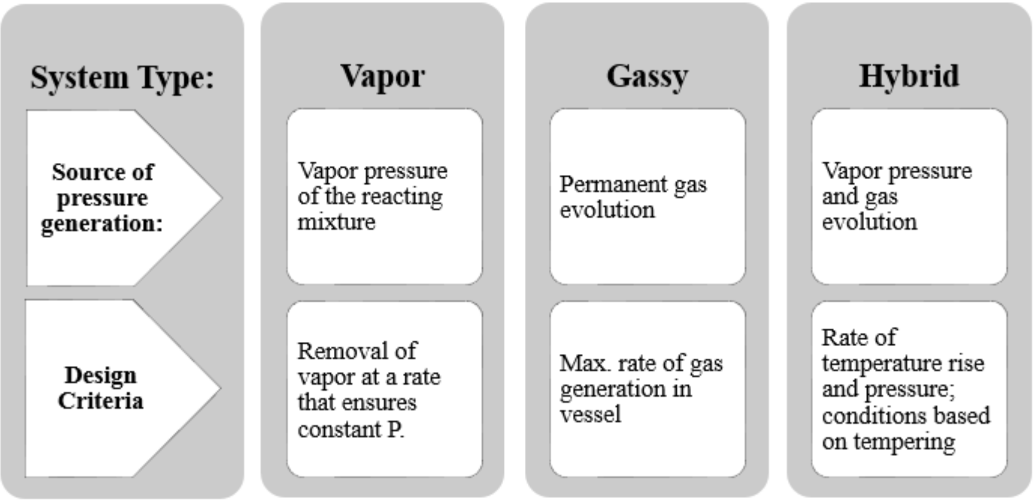

Figure 9. Source of pressure generation, and worst case scenario design for classes of reactive systems under runaway conditions.

2.5.3. ERS design for gassy and hybrid untempered systems

The correct design of an ERS for vapor systems has been extensively studied by DIERS [19]. The developed methodologies have the advantage of being user friendly and provide relatively good results. This is not the case of the vent sizing methods developed for gassy and untempered hybrid systems. The DIERS vent sizing method for gassy system is based on a mass balance at the second pressure peak (see Figure 8) i.e, when the reaction is at a maximum:

$$A = \frac{1}{G} Q_{G\max} \frac{m_R}{V} \tag{10}$$

where m_R is the initial mass or reactant, V the vessel volume, $Q_{G\max}$ the peak gas generation rate and G the mass flow capacity. $Q_{G\max}$ is measured using adiabatic calorimetry. G has to be calculated using an applicable method for non-flashing two-phase flow (see chapter 3). To be conservative, the following assumptions are often made:

- all the reaction mixture remains in the reactor until the maximum gas generation rate; and
- homogeneous two-phase flow occurs at the maximum gas generation rate.

Several authors have raised the issue that the methods for gassy systems are significantly oversizing, meaning that the resulting vent sizes are unrealistic (some times as large as the vessel diameter) impractical and expensive [20]–[22].

In 2009, the UK Health and Safety Laboratory and the French INERIS organized a series of Round Robin tests on vent sizing for gassy systems [23]. The results showed that there is still no consensus on the best approach to measure Q_{Gmax} from calorimetric data. Moreover there is still no reliable method to predict the nature of the vented mass flow (gas or two-phase) at the second pressure peak.

As for hybrid systems, the existing vent sizing methods take into account the contribution of the vapor and gas production to the overall maximum gas/vapor production rate:

$$A = \frac{1}{G}\left(Q_{G\max} + Q_{V\max}\right)\frac{m_R}{V} \tag{11}$$

where $Q_{V\max}$ is the peak vapor generation rate.

This approach is also known to be rather simplistic and lead to oversizing.

An understanding of the behavior of gassy and hybrid systems in runaway conditions during venting is of utmost importance to improve the ERS sizing methods. However, very few studies are available on these systems and several authors have urged for the need of experimental and theoretical research on the topic [20], [24]–[28]. Véchot *et al.* performed reactor venting experiments with untempered hybrid systems (cumene hydro peroxide solution) under runaway conditions at laboratory scale [20], [27]. This work provided for the first time comprehensive experimental data on the temperature, pressure and vented reactant mass evolution versus time. However, the interpretation of the experimental data still requires a better understanding of the phenomena involved in the venting process, which are rather complex and require a more in-depth investigation.

The simulation of the venting of an untempered (gassy or hybrid) systems requires the understanding of the nonlinear links between the reaction kinetic during the runaway, the mass and the heat transfer between the different phases in the vessel, the distribution of components in the different phases, the flow regimes in the vessel and through the venting device. The proper modeling of these combined phenomena can provide the thermodynamic conditions of the vessel contents (temperature, pressure, phase composition) and vented mass evolution as a function of time for a given ERS size. Besides the ability of better sizing ERS, the modeling of the venting of an untempered (gassy or hybrid) systems during the operation of an ERS can be used for a more accurate prediction of the consequences of a runaway reaction [8].

The work proposed in this thesis is a significant step in this direction.

CHAPTER III

KINETIC MODELING

3.1 Précis

The simulation of the venting of a reactor vessel containing a reactive mixture first requires the understanding of the reaction kinetics under runaway conditions. Reaction kinetics studies aim to measure and model the rate of reaction of a global chemical conversion of a system (e.g. in the case of a peroxide system, the rate of decomposition). Different kinetic model expressions have been developed to describe the reaction rate depending on the mechanism of the chemical reaction of concern.

Thermal analysis, which refers to the study of heat transfer associated to transformations in a test sample (e.g. reaction or phase change), is one of the methods employed to extract relevant kinetic model parameters from experimental calorimetric data obtained in isothermal and non-isothermal conditions.

In this chapter, the choice of a kinetic expression for a particular reactive system will be discussed, based on available methods in literature. The experimental data and thermal assessment techniques used to extract necessary kinetic parameters used in this work will be explained.

3.2 Kinetic model expressions

A reaction rate is often expressed in terms of the variation of the reaction conversion with time (dX/dt). The rate is a function of the temperature (T), the pressure

(*P*) and the conversion (*X*) [29]. In most cases, the pressure dependence is neglected. The reaction rate expression is:

$$\frac{dX}{dt} = K\left(T\right)f\left(X\right) \tag{12}$$

The temperature dependence, *K(T)*, is given by the Arrhenius equation as follows:

$$K(T) = k_0 \exp\left(\frac{-E_a}{RT}\right) \tag{13}$$

where k_0 (s^{-1}) is the pre-exponential factor that describes molecule vibrations and collisions, E_a ($J.mol^{-1}$) is the activation energy that corresponds to minimum energy barrier to cause the reaction, and R ($J.mol^{-1}.K^{-1}$) is the ideal gas constant.

Combining Eqs. (12) and (13) gives the general expression for the reaction rate:

$$\frac{dX}{dt} = k_0 \exp\left(\frac{-E_a}{RT}\right)f\left(X\right) \tag{14}$$

where the expression of *f(X)* is dependent on the reaction mechanism [30].

Thus, the reaction rate is expressed in terms of the '*kinetic triplet*':

$$\frac{dX}{dt} = F\left(k_0, E_a, f\left(X\right)\right) \tag{15}$$

The kinetics models developed to describe different mechanism models are numerous but are generally classified under three categories: accelerating, decelerating, and sigmoidal (or autocatalytic). Each of these them have defining kinetic profiles, mainly known as conversion-time curves, which can be seen in Figure 10.

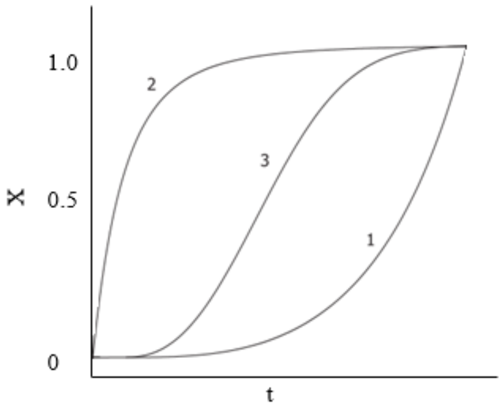

Figure 10. Conversion-time profiles for (1) accelerating (2) decelerating and (3) sigmoidal reaction models [29]

Accelerating models are those wherein the rate increases with increasing conversion, with the maximum rate being reached at a conversion of 1. These types of reactions are described by a power-law model, where *n* is a constant.

$$f(X) = nX^{\frac{n-1}{n}} \tag{16}$$

On the other hand, decelerating models are those wherein the maximum rate is achieved at low conversion and decreases as conversion increases. Diffusion processes usually follow decelerating kinetics. These types of reactions are described by an nth order model, where *n* is the reaction order:

$$f(X) = \left(1 - X\right)^n \tag{17}$$

Sigmoidal models combine both the accelerating and decelerating models in their initial and final stages, respectively. The maximum rate is achieved at an intermediate conversion. These types of reactions are described by the Avrami-Erofeev model, where n is a constant [31]–[33].

$$f(X) = n(1-X)\left[-\ln(1-X)\right]^{\frac{n-1}{n}} \tag{18}$$

More reliable models have been developed that represent all three conversion-time profiles. Šesták and Berggren [34] suggest an empirical model, which considers all three cases depending on the values of parameters *m, n* and *p*:

$$f(X) = X^{m}(1-X)^{n}\left[-\ln(1-X)\right]^{p} \tag{19}$$

Their work provides the study of various cases where sets of of *n*, *m* and *p* are used to describe reaction involving diffusion, nucleation, phase boundary reactions etc.

When *p* is set to zero in Eq. (19), the model is known as the extended Prout-Tompkins equation [33], [35], [36]. It is also known as the truncated Šesták-Berggren model.

3.3 Use of thermal analysis experimental data for the determination of kinetic parameters

The calorimetric experiments described in section 4 of chapter 2 (isothermal and non-isothermal and adiabatic) can be used to identify a suitable kinetic model for the reactive chemical of interest and extract the relevant corresponding kinetics parameters using differential kinetic methods.

3.3.1. Isothermal and non-Isothermal analysis

For isothermal conditions (T = constant), *k(T)* is constant in Eq. (12) and thus the conversion rate is fully dependent on the reaction model, *f(X)*. The most common non-isothermal program is a linear temperature dependence on time proposed by Vallet [37], where β is the heating rate:

$$\beta = \frac{dT}{dt} = \text{constant} \tag{20}$$

This assumes that change from an isothermal to a non-isothermal regime has no bearing on the reaction kinetics. While this is intuitively correct for simple single step processes, it may have serious implications for multi-step reaction kinetics [38].

For a constant heating rate non-isothermal temperature program, the following form of Eq. (14) is used:

$$\beta \frac{dX}{dT} = k_0 \exp\left(\frac{-E_a}{RT}\right) f\left(X\right) \tag{21}$$

For non-isothermal conditions however, the additional effect of *K(T)* yields sigmoidal curves, and it becomes more difficult to be able to classify the reaction type.

3.3.2. Adiabatic tests

For an adiabatic system, since the reaction rate follows the Arrhenius rate equation, it can be expressed in terms of conversion, *X*, as in Eq. (14). The heat generated in an adiabatic system during the reaction is used to raise the temperature of system. Expressed mathematically,

$$\Delta H_R \frac{dX}{dt} = -C_p \frac{dT}{dt} \tag{22}$$

Taking ΔH_R to be the heat of reaction per unit mass, and combining Eqs. (14) and (22) and rearranging constitutes the adiabatic heat balance, given by

$$\frac{dT}{dt} = -\frac{\Delta H_R}{C_p} k_0 \exp\left(\frac{-E_a}{RT}\right) f\left(X\right) \quad (23)$$

The self-heating rate, or the temperature rise rate of each curve, plotted against -1000/T(K) was used to determine the activation energy, E_a. This plot is similar to that shown in Figure 7. The slope of the section of linear part of the curve (before the curvature) where the conversion is zero or low, is equivalent to average value of –Ea/R.

3.4 Model-free isoconversional methods

In the late 1950s, when thermal analysis instruments became commercially available, a large amount of research was done regarding non-isothermal kinetics. There has been an increasing amount of work done since then on methods used to extract the kinetic parameters and the reaction model from non-isothermal data [39]–[49]. Such rapid development came about mainly because the time it takes to run a non-isothermal experiment is much more reasonable that it would take to run a series of isothermal experiments. Also, a non-isothermal run contains enough information on the temperature dependence of the reaction rate, and thus provides sufficient knowledge for kinetic evaluation [43]–[48].

A number of studies have been conducted to confirm whether non-isothermal data allowed for reproducibility of results obtained from isothermal data, only to find out that the results were not consistent [50]–[52]. Vyazovkin and Wight [38] proposed that the formal reason for the inconsistency results from force-fitting experimental data to different reaction models. Experimentally, they believed that the inconsistency is due to the different temperature regions used for both regimes. Thus, it in general, one cannot expected that kinetic parameters derived from isothermal and non-isothermal experiments to be identical.

The alternative is a model-free approach to kinetic analysis [38], [53], [54]. Model-free kinetic analysis methods are based on the isoconversional principle, where at a fixed conversion, the reaction rate is only a function of temperature [29]. This is shown by taking the logarithmic derivative of Eq (12)

$$\left[\frac{\partial \ln\left(\frac{dX}{dt}\right)}{\partial T^{-1}}\right]_X = \left[\frac{\partial \ln\left(k\left(T\right)\right)}{\partial T^{-1}}\right]_X + \left[\frac{\partial \ln\left(f\left(X\right)\right)}{\partial T^{-1}}\right]_X \tag{24}$$

Since the conversion is fixed, *f(X)* is a constant and thus its derivative is zero, making the second term zero. Simplifying Eq. (24) based on this, gives

$$\left[\frac{\partial \ln\left(\frac{dX}{dt}\right)}{\partial T^{-1}}\right]_X = -\frac{E_a}{R} \tag{25}$$

3.4.1. Determining the Activation Energy

Model free isoconversional methods are generally divided into two categories: differential and integral, depending on the experimental data required [29]. For the purpose of this study, only differential experimental data will be used in terms of thermal analysis. The most common differential isoconversional method was suggested by Friedman [55], which uses the logarithmic form of Eq (21) given by:

$$\ln\frac{\beta dX}{dT} = \ln\left[k_0 f(X)\right] - \frac{E_a}{RT} \tag{26}$$

This method requires a series of thermal analysis experiments to be conducted at different heating rates, as shown in Figure 11. For each heating rate, at any given *X*, the value of E_a is found from the slope of a plot of $\ln\left(\beta dX/dT\right)$ versus 1/T, which is known as a ***Friedman plot***. The ICTAC [29] recommends that E_a values be determined at conversions of 0.05-0.95 in order to be able to accurately determine the dependence of E_a on X.

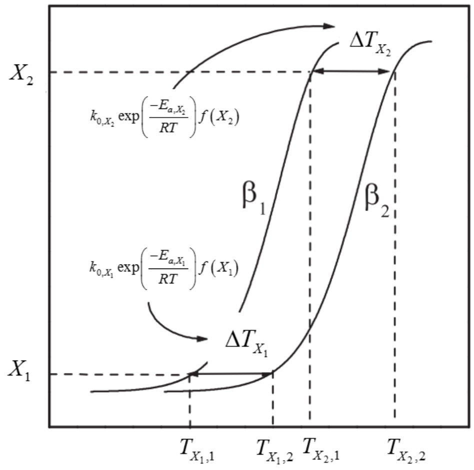

Figure 11. Iso-conversional method using scanning runs with different heating rates.

It should be noted that differential isoconversional methods are subject to some inaccuracy resulting from improper baseline determination, and having a heat of reaction that varies noticeably with the heating rate [56], [57]. The obtained value for E_a can be compared with that estimated using adiabatic calorimetry data.

3.4.2. Determining the Reaction Model and Pre-exponential Factor

In order to determine the reaction model, Flynn [58] proposed to assume a reaction order model of $f(X) = (1\text{-}X)^{n}$, where in at low conversions ($X \approx 0$), the intercept for a Friedman plot at low conversion yields $\ln(k_0)$. Once this is known, a plot of $f(X)$ versus X then in turn yields n. Malek et al. also [59]–[61] proposed a method that allows for the determination of the analytical form of the reaction model once the activation energy has been obtained. Two special functions are defined: $y(X)$ and $z(X)$ which as used to transform experimental thermal analysis data. The function $y(X)$ is given by:

$$y(X) = \frac{dX}{dt}\exp(x) \tag{27}$$

where X is $-E_a/RT$ and $z(X)$ is given by

$$z(X) = g(X)f(X) = \pi(x)\frac{dX}{dt}\frac{T}{\beta} \tag{28}$$

where $\pi(X)$ is an approximation of the temperature integral given by the Senum and Yang [62]

$$\pi(x) = \frac{x^3 + 18x^2 + 88x + 96}{x^4 + 20x^3 + 120x^2 + 240x + 120} \tag{29}$$

Using obtained experimental values, y(X) against X curves can be plotted, and then normalized since the pre-exponential factor is still unknown. Then, they are compared to theoretical y(X) vs X plots called master plots, as shown in Figure 12. The best model is the one that matches one of the curves of the master plots, with their labels relating to specific rate expressions listed in the ICTAC report [29]. For a series of tests at different heating rates, a plot of dX/dt vs T for each heating rate yields a series of experimental *y(X)* plots; the resulting curves should not reflect dependence on β [29]. The shape of *y(X)* curve is very sensitive the value of E_a obtained, and thus an accurate value for it is necessary [61]. As can be seen, some y(*X*) curves do have maximum value, denoted by X_M.

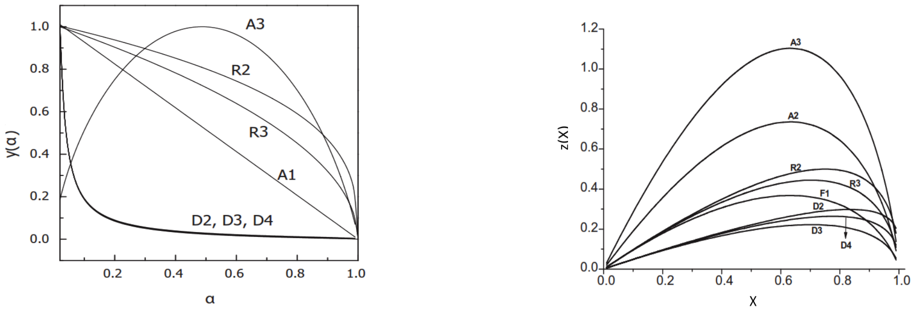

Figure 12. Theoretical master plots of (left) *y(X)* as a function of *X* and (right) *z(X)* as function of *X* for reaction models.

Similarly, *z(X)* plots combine both integral and differential forms of the reaction models. The plots are obtained by plotting the product of *f(X)g(X)* against *X*, and all theoretical curves have a maximum value at certain conversion, denoted as $X_{p,}$ as can be seen from Figure 12. The value of X_p is independent of E_a. These values have been calculated [63] for some reaction models. They provide another indication as to which model represents the better fit. From this, the pre-exponential factor can be calculated using [63]

$$k = \frac{-\beta E_A}{R T_{\max}^2 f'\left(X_{\max}\right)} \exp\left(\frac{E_A}{R T_{\max}}\right) \tag{30}$$

where maximum values are related to the maximum of a kinetic curve for a given heating rate [29], [63].

Another method is that of invariant kinetic parameters [64] which uses the compensation effect. This is a linear correlation of the Arrhenius parameters evaluated for the same reaction with different models. Despite the variation in parameters with different reaction models, *f(X)*, they all follow that

$$\ln k_0 = eE_a + b \tag{31}$$

where *e* and *b* are dependent on *β*. The invariant kinetic parameters, denoted by ln $k_{0,inv}$ and $E_{a,inv}$ are evaluated from different sets of *e* and *b* for various heating rates using

$$b = \ln k_{0,inv} + eE_{\mathrm{a},inv} \tag{32}$$

This method however is more computationally challenging than any of the other isoconversional methods, and has proven to be difficult in terms of error estimation; thus, it is rarely used.

3.4.3. Limitations of Isoconversional Methods

Despite their advantages, there are a few problems associated with using isoconversional methods. The most apparent problem is that there is no direct way presented to evaluate the pre-exponential factor nor the reaction model [40], [41], [55]. The more serious problem however, is the variation of the kinetic triplet parameters with the extent of reaction. This creates difficulties concerning the interpretation of data. Agrawal [65] concluded that for multistep reactions, the Friedman method yields values of E_a that are have no physical meaning. Flynn and Wall [41] also observed that E_a was subject to variation with X for multi-step kinetics. Vyazovkin and Lesnikovich [66] proved that the dependence of E_a on X gives insight into the complexity of a chemical process, as well as its mechanistic path. The shapes of this dependence have been developed from simulated data for competing [66], independent [67], reversible [68], consecutive [69], and diffusion reactions [70]. The problem of varying E_a values can be solved without averaging, by assuming that the partial kinetic triplet for a given X remains the same under variable temperature [38].

CHAPTER IV

FLUID FLOW MODELS

4.1 Précis

Pressure vessels are equipped with emergency relief systems (ERS) as a measure of protection from overpressure. The correct design of an ERS requires in depth understanding of vessel depressurization phenomena, the flow regimes in the vessel and in the venting device, along with an accurate description of the kinetic of the reaction under runaway conditions as described in the previous chapter.

At the ERS set pressure, venting occurs through the available ERS area. During the initial stages of ERS action, the fluid within the vessel experiences a sharp decay in pressure, and this pressure gradient accelerates the fluid through the ERS [71].

Initially, the fluid through the ERS may flow at a velocity equal to the sound speed of the fluid at the conditions of the exit point. The fluid flow is then said to be in choking conditions, wherein the fluid’s velocity is independent of the downstream pressure. If the fluid is liquid, upon reaching the saturation boundary, it may flash and become a two-phase mixture. During the depressurization, the difference between the internal pressure and pressure at the ERS exit decreases and the flow becomes subsonic. Also, the fluid flow progressively changes from turbulent to laminar until there is no flow and no pressure difference between the vessel and the release environment [71]. Thus, it is important to predict when the flow reaches choking conditions (sonic) and non-choking conditions (subsonic).

The factors that affect the behavior of the fluid in the event of a release from a vessel are: the initial pressure within the vessel; the temperature of the fluid; the number of phases and their compositions; the size, location and orientation of the ERS; and the level swell, which influences the type of flow, and mass flow rate significantly [72]. Modeling the depressurization of a vessel requires an accurate description several interacting phenomena such as thermodynamic equilibrium, heat transfer, reaction kinetics, fluid flow dynamics for a closed and open system, as well as transport properties, for both the contents of the vessel and inside the ERS.

The literature on fluid releases from pressure vessels and their simulation is vast. This chapter reviews part of it, focusing on vessel depressurization, the factors that affect it, its consequences, and existing computer programs to simulate it.

4.2 Flow regime in the vessel

In order to appropriately design an ERS system that allows for vessel depressurization, it is important to determine whether the reacting mixture will allow for a single phase fluid to be relieved, (usually all vapor relief in the case of an ERS located at the top of the vessel) or a two-phase fluid mixture. In some cases, single phase venting can be followed by two-phase flow venting at the peak reaction rate [3]. The required ERS area for two phase flow venting is much larger in comparison to single phase venting. DIERS conducted at study [19], wherein they showed that most incidents associated with vessel overpressure evolved during a thermal explosion, are either due to incorrect sizing of the ERS area and/or an inadequate choice of ERS device depending on the type of flow to be discharged (one or two phases). It should be noted that these two factors are mutually inclusive [19]. Based on this study, they recommend that for the purpose ERS sizing using the method of hand calculations, two-phase relief should be assumed for tempered systems, while initial single phase relief followed by two phase relief is a conservative assumption for untempered systems [3], [19].

4.2.1. Level swell

Level swell is the mechanism through which two-phase flow may occur during a runaway reaction. The gas and/or vapor produced during a runaway reaction will form bubbles through the bulk liquid, which due to buoyancy, will rise through it, in effort to disengage from its surface [3]. If the speed of the rising gas bubbles is high enough, it can cause some liquid to move upwards too, such that the bulk liquid level increases and swells. If this level rises to the ERS inlet during venting, two phase flow results. Two-phase flow may also take place because of flashing or gas dissolution due to changes in the thermodynamic equilibrium of the system during venting.

When complete disengagement of the gas bubbles occurs, the phases separate completely leading to single-phase flow release (vapor and/or gas). However, when no disengagement occurs, the two phases are uniformly mixed and the quality of the fluid entering the ERS inlet is the same as that of the bulk fluid. If partial disengagement occurs, then there is a partial separation at the gas/liquid interface such that the two phases have different velocities and properties. Thus, the quality of the liquid at the ERS inlet is higher than that of the vessel fluid, and two-phase flow occurs. A drift flux model can be used to consider the relative motion between phases [7], [73]. In these models, a mixture of momentum equation describes the motion of the whole mixture and kinematic constitutive equations are used to specify the relative motion between phases.

Thus, accurate prediction of such level swell within a vessel is very important during ERS action, as it determines whether the vented fluid is single-phase flow or two-phase flow. Various parameters influence the type of flow at the ERS exit, and these include: the initial fill rate, the level of the vessel, the reactive system, the vessel pressure, the vapor/gas production rate, the vessel flow regime and the vapor/liquid disengagement within the vessel [7], [73].

There are different approaches to modeling level swell. Reference [19] describes a method that incorporates a vapor material balance at the ERS inlet referred to as the 'coupling equation'. This method is computationally intensive, with an iterative procedure to determine the quality of the vapor at the inlet of the ERS. To do this, Fishes suggests coupling the level flow model in the vessel and the fluid flow model in the ERS, and solving for the inlet quality. Etchells and Wilday [3], on the other hand, concentrated more on "hand calculation methods" which do not use the coupling equation. It should be noted that hand calculation methods rely heavily on experimental data, and use many simplifying assumptions, regarding the flow regime, and the vessel inventory at the maximum pressure developed.

4.2.2. Vessel flow regimes

In order to define the flow type at the ERS inlet appropriately, the flow regime of the system within the vessel also needs to be classified. Generally, most reactive systems are inherently foamy, whereby they always vent a two-phase mixture that is homogeneous, as seen in Figure 13 (a) [3]. This means that the quality (ratio of vapor to liquid) of the fluid entering the ERS is the same as the average quality of the bulk fluid. These systems continually vent a two-phase mixture through the ERS, until the vessel contents empty. Trace concentrations of certain substances can bring about inherently foamy behavior, and thus assumptions regarding non-foamy behavior should be made with caution [3], [19], [74].

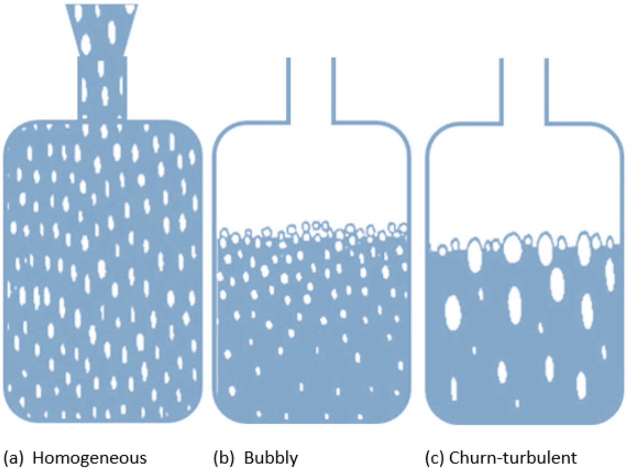

Figure 13. Vessel flow regimes. Adapted from Etchells and Wilday [3]

That being said, some reactive systems do display non-foamy behavior. In these cases, a single-phase flow at the ERS can result from a small vapor/gas production rate and a low initial vessel fill level. At a high enough vapor production rate, and initial fill level, two-phase flow at the ERS may be achieved. Coupled, a high vapor/gas production rate will cause the already high liquid vapor interface (due to a high initial fill level) to move upwards due the level swell phenomena. If this level reaches the ERS inlet, two-phase flow results until enough swelled liquid has been vented, and single-phase flow remains. During the two-phase venting, for the non-foamy vessel flow regime, the quality of the fluid entering the ERS is much higher than for the homogeneous case [3].

The extent of level swell and the quality of the fluid entering the ERS for a certain vapor/gas production rate depends on the two-phase flow regime with in the vessel. The remaining classifications of two-phase vessel flow are either bubbly or churn-turbulent. Bubbly flow, as the name indicated, describes the movement of discrete small bubbles rising through the liquid at low velocities, as seen in Figure 13 (b) [3]. Churn-turbulent flow, however, describes the upwards movement of bubbles, and their coalescence to form large bubbles which rise even faster upwards as seen in Figure 13 (c) [3]. It should be noted that for the same vapor/gas, the amount of level swell in the bubbly flow is higher than in the churn –turbulent regime, meaning that two-phase flow is more likely to occur in a vessel that has a bubbly flow regime [3]. DIERS suggested that for low viscosity systems (< 0.1 Pa·s), churn-turbulent is the more likely regime, while for moderately high viscosity systems (> 0.1 Pa·s) bubbly is the more likely regime [19]. Also, for high viscosity systems (> 0.5 Pa·s), the assumption of a homogenous flow regime is valid [75]–[77].

4.3 Two-phase flow models for venting through ERS

The prediction of the flow rate at the ERS in the case of a fluid discharge from a pressure vessel is a dynamic problem. As the fluid is released, the vessel undergoes depressurization and the fluid inside it expands, with a change in its properties as well as possible phase change. The study of these pressurized releases has generated significant research interest in the past, leading to the development of several fluid flow models that predict discharge rates.

Models for single-phase flow (gas or liquid) are very well established. Two-phase flow models are however much more complex and involve the description of the mass, momentum and energy exchanges between the vapor/gas and liquid phases. They allow for the calculation of two-phase mass flow rater per unit area, as well as the critical pressure for choking. There is currently a lack of understanding of the thermal and fluid-dynamics phenomena occurring between the two phases (relation between pressure drop and vapor quality, non-equilibrium effects with delayed vaporization, different velocities of the two phases, critical flow conditions). This is partly related to the lack of experimental data on two-phase flow. Therefore, two-phase flow models based on simplifying assumptions have been developed over the years.

A large number of two-phase flow models exist in literature. For two-phase flow across orifices [78], they fall into two different: homogeneous and non-homogeneous models. Homogeneous models consider the mixture as single fluid and that the thermodynamic and physical properties can be obtained by averaging phase properties.

They also assume the same speed for all phases. Non-homogeneous models relax these assumptions.

To decide on the most appropriate one, parameters such as flashing/non-flashing flow, flow regime, phase slip, equilibrium and non-equilibrium flow, and turbulent/laminar flow are taken into consideration [3]. Flashing or non-flashing flow may occur depending on the reactive system type. Also, since the vapor/gas phase tends to travel much faster than the liquid phase, some of the models take this into consideration. The assumption of no phase slip is related to homogenous flow [3]. When looking at equilibrium and non-equilibrium flow, the main difference between them is whether the residence time is long enough to allow the fluid to flash to equilibrium saturation condition as the pressure falls along the flow path [79]. For flow through a sharp edged orifices or short pipes, the stored liquid may exit the vessel quickly enough such that thermodynamic equilibrium is not maintained. The residence time is too short for the liquid to experience a phase change, and this happens well after the fluid has exited the vessel. The criterion used to measure the non-equilibrium nature of fluid flow is length of the orifice, which should be less than 0.1m.

An overview of some of the available two-phase flow models will be provided in this section.

4.3.1. Homogeneous Equilibrium Model

The Homogeneous Equilibrium Model (HEM) [19], assumes homogeneity, no phase slip and thermodynamic equilibrium between discharged phases through the orifice, meaning that their equal average speeds can be used. Also, fluid expansion is considered to be isentropic, and that the two-phase mixture has adiabatic flow [3], [71]. The HEM was extensively developed by Leung (1989) [80], [81] and proposes a unified approach for compressible flow of two-phase mixtures through nozzles and pipes, which accounts for the effects due to friction, gravitational change, inlet sub-cooling and presence of non-condensable gases. It is applicable for flashing and non-flashing two-phase flow. DIERS [3], [19] recommends the use of the HEM for relief sizing purposes, as it gave the best fit to their experimental results, and the most conservative (lowest) mass flow rate when compared to other model. However, it should be noted that because the HEM method will tend to underestimate the relief flow capacity, it leads to oversizing of ERS. More so, the HEM is less accurate in estimating critical pressure for choking and, in some cases, a slip flow model would be more conservative.

4.3.2. Homogeneous Frozen Model

The Homogeneous Frozen Model (HFM) [19] describes the flow of a non-volatile liquid phase and insoluble gas phase [71]. It is recommended by DIERS for relief sizing of gassy systems [3], [19]. This model assumes a non-equilibrium nature of the fluid flow, and no mass transfer between the two phases during the efflux, hence the ‘frozen’. Further assumptions include equal phase velocities, isentropic expansion of vapor, and incompressible liquid phase, and negligible wall shear forces. It does not taken into account flashing, and thus the flow maybe greatly overestimated. Thus, this model is not the best choice for tempered system, as per DIERS recommendations [3].

4.3.3. Tangren et al.'s Method

Tangren et al. [82] proposed a method to implement the HFM. Their calculations yield similar, if not slightly lower results than HEM. However, it is only applicable to non-flashing two-phase flow (gassy systems). The model assumes no phase slip, uniform phase mixing, and thermodynamic equilibrium between the phases. The flow is taken to be frictionless, and the vapor phase is treated as an ideal gas. Also, it assumes little gas dissolution in the liquid phase, which brings about an overestimation of the relief rate. The main difference between Tangren et al.'s method and HEM is that the two-phase mixture is isothermal in this case, as opposed to adiabatic, as in the case of HEM. This simplifies calculations, and provides a more conservative value of the relief rate [3], [82]

4.3.4. The Slip Equilibrium Model

The Slip Equilibrium Model is used for both flashing and non-flashing two-phase flow, with the assumption of uniform mixing of the phases. It also considers slip between the phases, and is based on thermodynamic equilibrium. There exist various models that describe phase slip, and they can lead to more conservative (lower) fluid flow determinations.

4.3.5. The Omega Method

In 1995, Leung developed the Omega method, based on the homogeneous flow model, to account for the compressibility of the two-phase mixture using the ω-parameter [5]. It is a method of evaluating HEM or HFM, as it introduces various simplifying assumptions, but its advance lies in the fact that no computer code is required for numerical evaluations [2]. This method is recommended by the American Petroleum Institute (API) [19], [83] for vent sizing purposes as it provides conservative results, as well as DIERS [3], [19]. Thus, it is widely used and has been extensively tested [84]. The model can estimate flow rates and exit pressure for a fluid with an initial state of all saturated liquid, all saturated vapor, or a mixture of two, so long as saturation conditions apply [85]. However, it should be noted that the Omega method is only valid in the cases of spray or wet vapor flow, where few drops of liquid are entrained in the vapor [78]. Diener et al. demonstrated that it was also unsuitable for inlet flow conditions involving boiling liquids with only low vapor contents [86].

4.3.6. Homogeneous Non-Equilibrium Model

Another model that considers a transient state between equilibrium and non-equilibrium is the Henry-Fauske Model, and is known as the Homogeneous Non-Equilibrium Model (HNE) [19], [87]. This model forms the bases for a family of models that describe varying extents of non-equilibrium behavior. It describes the behavior of fluid that subcooled at the inlet pressure, but reach saturation conditions within the exit nozzle [19], [78], [79], [88]. HNE is recommended for short nozzles and orifices where the residence time of the mixture is too short for significant evaporation, and the non-equilibrium nature of the flow is taken into account. It assumes that each phase expands isentropically, and that the liquid is incompressible. It also assumes that there is no heat or mass transfer within the nozzle, due to the short residence time, and that heat transfer rate between the phases is not negligible. To evaluate the actual heat transfer process, it is assumed that the vapor flow at the throat is described by a polytropic process [19], [78], [79], [88].

4.3.7. Simplified Equilibrium Rate Model (ERM)

Fauske and Grolmes [89] derived a simple extension of the HEM that was termed as Fauske's equilibrium rate model (ERM). This model yield similar results to the HEM, but with is faster computationally, and more convenient [2]. It assumes that liquid entering the ERS is a saturated liquid, and no flashing occurs in the ERS until the critical pressure point for choking is reached. It also assumes that the system is a vapor pressure system and that there is no slip between phases (homogenous flow), and that the choked flow through a nozzle is turbulent, frictionless and has enough residence time to flash and reach equilibrium [2].

4.3.8. Homogeneous Non-Equilibrium extention by Diener and Schmidt

Diener and Schmidt [86] proposed an extension to the Omega method by adding an equation that considers boiling delay. This method, called the Homogeneous Non-Equilibrium method by Diener and Schmidt (HNE-DS), and takes into account the boiling delay, hydrodynamic non-equilibrium, and calculates reliably the flow rate in both flashing and non-flashing flow [86].

4.3.9. Other two-phase flow models

Raimondi [8] identified that the Omega method, as proposed by the API cannot be used for multicomponent systems at high pressure where condensation and evaporation may appear, as well as near the thermodynamic critical point. The recent extension of this method by Deiner-Schmidt still does not resolve its limitation at temperature and pressure regions close to the thermodynamic critical point. He proposed to model fluid flow through a nozzle based on a rigorous calculation of critical flow conditions of a mixture by means of equations of state for multicomponent and multiphase mixtures. In his study [8], Raimondi proposes an algorithm for the maximum allowable flow rate discharged through an orifice, based on the evaluation of sonic velocity, using the same equation of state used for evaluation of thermodynamic properties, for given upstream conditions.

Moody (1965) proposed an alternative model, which assumes annular flow, uniform but not equal linear velocities of each phase, as well as equilibrium between liquid and vapor phases. This model predicts the maximum flow rate of a single component, two-phase mixture. The flow rate is maximum when its derivatives with respect to the exit velocity ratio (slip ratio) and the exit pressure are equal to zero [71].

Norris and Puls [90] proposed a mechanistic model for simulating single and multiphase flows, which assumes homogeneous thermodynamic equilibrium. In this model, the fluid phase behavior and the fluid properties are calculated using an equation of state model that carries out either isothermal or isentropic flashes over a range of pressures. This model was tested in 1993 for hydrocarbon blowdown from vessels and pipelines [91]. However, the proposed model was unable to predict the vessel fluid temperature variations, and did not account for the momentum and energy balances, nor gravity segregation [90], [91].

Cumber [72] developed an accurate outflow model that predicts mass flow rates of releases from high pressure vessels in a fast and robust manner. The model assumes a single control volume, no heat transfer (adiabatic vessel walls) as its effect on the mass flow rate is negligible during the initial stages of discharge when the flow rate is the highest. The Peng-Robinson equation of state was used, and thermodynamic equilibrium between two phases is assumed. It should be noted that during rapid depressurization, non-equilibrium effects might have a minor influence on the mass flow rate. Upon testing, the model prediction of the pressure and flow rate were reasonably accurate for a vessel containing a single gas phase. However, some of the assumptions were later found to be invalid, such as that of adiabatic vessel walls. This assumption was based on the fact that, in early stages of depressurization, the heat transfer is less significant. However, over time, the heat transfer to the vessel changes the vessel temperature, which has a second order effect on the mass flow rate. Thus Cumber's model tends to under predict the vessel temperature and slightly over predict the mass flow rate [72].

4.4 Limitations of the discussed models

The DIERS workbook provides a decision tree for selecting the appropriate two phase flow model for the different classifications of reactive systems. An overview of these model was given by Selmer-Olsen [92]. He identified the following difficulties: (i) there is no accepted design method for two-phase flow; (iii) the API method may be inadequate as it leads to large ERS orifice sizes; (iv) the methods available are not sufficiently validated by experimental work, especially at large/industrial scale, (v) there exists a strong relation between the thermohydraulic behavior of the fluid system and the flow through the pressure relief device for which the commonly used modular approach may be inappropriate [87], [92].

In order to overcome these difficulties, rigorous modeling of depressurization of vessels that incorporates and describes phenomena such as thermodynamics, kinetics, and fluid dynamic is necessarily to understand the behavior at large scale.

4.5 Vessel depressurization computer programs

Models for leaks from pressure vessels form the backbone of computer programs developed overtime for the industry. An account has been given by Selmer Olsen (1992) [92]. A benchmark exercise on vessel depressurization methods is described by Skouloudis [93]. Some of these programs are described in Appendix C, and use two-phase flow methods described in section 4.3. The limitations of these models are inherent in the computer programs as well.

More recently, the use of the thermodynamic speed of sound to predict choking conditions has been explored. This is because the sound velocity of fluids in thermodynamic equilibrium exhibits important discontinuities at phase boundaries, as noticed long ago by Landau and Lifschitz in the case of pure fluids [94]. Since then much numerical work has been done to evaluate the sound speed in multiphase systems, in order to study to study leaks inside tanks and pipeline [94]–[101]. Two models that incorporate this concept are discussed below.

4.5.1. BLOWSIM

From 1999 to 2007, Mahgerefteh and co-workers developed mathematical models for simulation of accidental leaks from pipelines. They developed a procedure based on the method of characteristics [100]. Mahgerefteh and Wong developed BLOWSIM, a program that incorporated cubic equation of states, and accounted for heat transfer effects, inter-phase fluxes and effects of sonic flow [97]. Then, Mahgerefteh and co-workers then proposed a numerical simulation method for predicting the blowdown of high-pressure cylindrical vessels subject to a fire, by including transient thermal and pressure stress effects [99]. This model accounts for non-equilibrium effects between phases, heat transfer between fluid phases and their corresponding sections of the vessel wall, interphase fluxes due to evaporation and condensation, and the effects of sonic flow at the orifice.

4.5.2. Rigorous simulation of leaks from high-pressure storage vessels

Castier et al. developed a FORTRAN program that simulates the dynamics of storage tanks and flash drum using a formulation adequate for phase modeling. Rigorous physical property calculations, with the Peng-Robinson (RK) equation of state (EOS), were implemented to account for non-ideal fluid behavior [102]. In their work, a drum of constant volume, V, with s_f input streams and s_w output streams was considered. The model consists of a set of differential and algebraic equations. The differential equations include the mass and energy balances, while the algebraic equations allow for the calculation of the fluid conditions inside the vessels and at any leak points where a fluid may be released.

The mass and energy balance equations are respectively given by

$$\frac{dN_i}{dt} = \sum_{j=1}^{s_f} \dot{f}_{ij} - \sum_{j=1}^{s_w} \dot{w}_{ik} \qquad i = 1 \ldots n_c \tag{33}$$

$$\frac{dU}{dt} = \sum_{j=1}^{s_f} \dot{H}_j^f - \sum_{j=1}^{s_w} \dot{H}_k^w + \dot{Q} \tag{34}$$

where t is the time, U is the internal energy, N_i is the total number of moles of component i within the drum. The number of components is denoted by n_c, and thus i can have a value of 1 up until n_c. The molar flow rate of component i in input stream j, and the enthalpy of stream j are $\dot{f}_{ij}$ and $\dot{H}_{ij}$ respectively. Similarly, the molar flow rate of component i in output stream k, and the enthalpy of stream j are $\dot{w}_{ik}$ $\overset{g}{w_{ik}}$ and $\dot{H}_k^w$. Finally, $\dot{Q}$ is the heat load provided to the vessel. This generates (n_c + 1) equations, whose numerical integration yield the evolution of U and n for any given time step.

Thermodynamic equilibrium is assumed at all times within the tank, and thus the intensive properties of any output streams are the same as those of the phase they are withdrawn from. Given a specific set of *UVn* values, equilibrium is achieved by minimizing, A, Helmholtz energy. This was suggested by Michelsen [103], where in the *UVn* flash uses direct iterations in temperature, phase volumes and moles of each component in each phase, with A being the core function. This is formulated as such

$$Q_F = \frac{A - U^*}{RT} \tag{35}$$

where A is the Helmholtz energy, U^* is the specified internal energy at a given time step, and R is the universal gas constant, and T is the temperature.

Castier’s work [102] uses derivatives of Q_F with respect to the number of moles of each component in one of the phase and to the temperature and one of phase volumes (i.e. phase K). A system with n_p phases would have the following set of algebraic equation resulting from the derivatives of Q_F

$$\left(\frac{\delta Q_F}{\delta T}\right)_{\underline{V},\underline{\underline{n}}} = \frac{U^* - \sum_{k=1}^{n_p} U_k}{RT^2} = 0 \tag{36}$$

$$\left(\frac{\delta Q_F}{\delta V_k}\right)_{T,V_{m\neq k,K},\underline{\underline{n}}} = \frac{P_K - P_k}{RT} = 0 \qquad k = 1 \ldots n_p, \text{ and } k \neq K \tag{37}$$

$$\left(\frac{\delta Q_F}{\delta N_{ij}}\right)_{T,V,n_{km,\ k\neq i,\ m\neq j,J}} = \frac{\mu_{ij} - \mu_{iJ}}{RT} = 0 \qquad i = 1 \ldots n_c, j = 1 \ldots n_p \text{ and } j \neq J \tag{38}$$

where U_k and P_k denote the internal energy and pressure in phase k, μ_{ij} is the chemical potential of component i in phase j, and J is the phase with the largest amount of i . The equations are formulated under the assumption that phase K, the largest phase volume, is a dependent variable. In the same manner, the largest amount of moles of every component in a phase was taken to be the dependent variable.

The Jacobian matrix of this set of equation is the Hessian matrix of Q_F which is symmetrical, and thus the full Newton-Raphson step at each iteration can be obtained by solving the given system

$$\begin{bmatrix} r_{TT} & r_{TV}^T & r_{TN}^T \\ r_{VT} & r_{VV} & r_{NV} \\ r_{NT} & r_{NV} & r_{NN} \end{bmatrix} \begin{bmatrix} \Delta T \\ \Delta V \\ \Delta N \end{bmatrix} = \begin{bmatrix} r_T \\ -r_V \\ r_N \end{bmatrix} \tag{39}$$

where $\underline{\Delta V}$ and $\underline{\Delta N}$ represent the vectors containing independent volumes and component mole numbers [102].

While DAE solvers exist, the approach of solving the algebraic equations of the model at each time step of the differential equation integrator was used. The reason for this is that the algebraic part of the model requires multiple, complex, and conditional calculations that would be cumbersome to implement within a DAE solver. Examples of these are several types of flash calculations that deal automatically with the appearance or disappearance of phases within the vessel and at the exit point, and sound speed calculations to determine whether the output flows are choked. The integration of the differential system was done using the Bulirsch-Stoer algorithm as implemented by Press et al. with a single loop [104] and a lumped approach [105].

The ODE system integration provides the values of internal energy and components amounts inside the vessel, whose volume is fixed. The knowledge of these variables allows the evaluation of all other state properties of the fluid inside the vessel by maximizing its entropy, in what is known as a *UVn* flash problem. The solution of the *UVn* flash problem, which is a saddle point of the Q_F function, determines the state of the fluid and its thermodynamic properties within the vessel for any given time, t [102]. However, Solving a *UVn* flash problem requires various properties: internal energy, pressure, chemical potential (or the logarithm of the fugacity) of each component, and their derivatives with respect to temperature, volume and mole numbers. In order to calculate physical properties, the PR EOS was used, with one-fluid van der Waal mixing rules, so that all fluid phases present inside the vessel can be modeled. Also, binary interaction parameters were set to zero. Derivative properties were calculated using the Thermath computer algebra package [106].

In order to calculate the physical properties of the input streams, a *TPn* flash problem was solved. [107] Then, to calculate the initial vessel conditions, a *TVn* flash procedure was used [108]. Phase appearance and disappearance was determined using the global stability test [109]. A phase, j, was removed when the following condition was met:

$$\frac{V_j}{V} \text{ or } \sum_{i=1}^{n_c} N_{ij} \Big/ \sum_{i=1}^{n_c} N_i < 10^{-6}$$

Should the global stability test allow for the appearance of a new phase, it was initialized to have 10^{-3}% of the total number of moles within the vessel. Castier et al. demonstrated the capabilities of their formulation through various examples. [102]

In 2009, Castier proposed a new algorithm to solve *UVn* flash problems, for non-reactive systems, using direct entropy maximization in a single loop in order to solve two and three phase equilibrium problems [110]. Typically these problems are solved using nested loops, as Michelsen's [103] framework suggests, using ln T, ln$P$, and the number of moles of each component in each phase as the iteration variables. Starting form this framework, and using iteration variables of T, phase volumes, and the number of moles of each component in each phase, a single iterative loop can be used. Figure 14 shows the proposed single loop algorithm.

For stability, a single-phase configuration is tested with the given values of temperature of pressure. If this is feasible, then the system is stable. If the system tests unstable, a new phase is added, and the entropy of the two-phase system is maximized. The initial number of moles assumed for the phase added during the phase stability test corresponds to a fraction of 1×10^{-10} of the total number of moles, with the mole fractions, molar volume, and molar internal energy obtained from the phase stability test. If merging phases results in a state of higher entropy, the algorithm removes a phase by eliminating phases whose number of moles corresponds to a fraction less than 1×10^{-6} of the total number of moles. Its internal energy, volume, and number of moles of each species are added to those of the other phase. If the algorithm fails to converge numerically, the nested loops approach is activated [110].

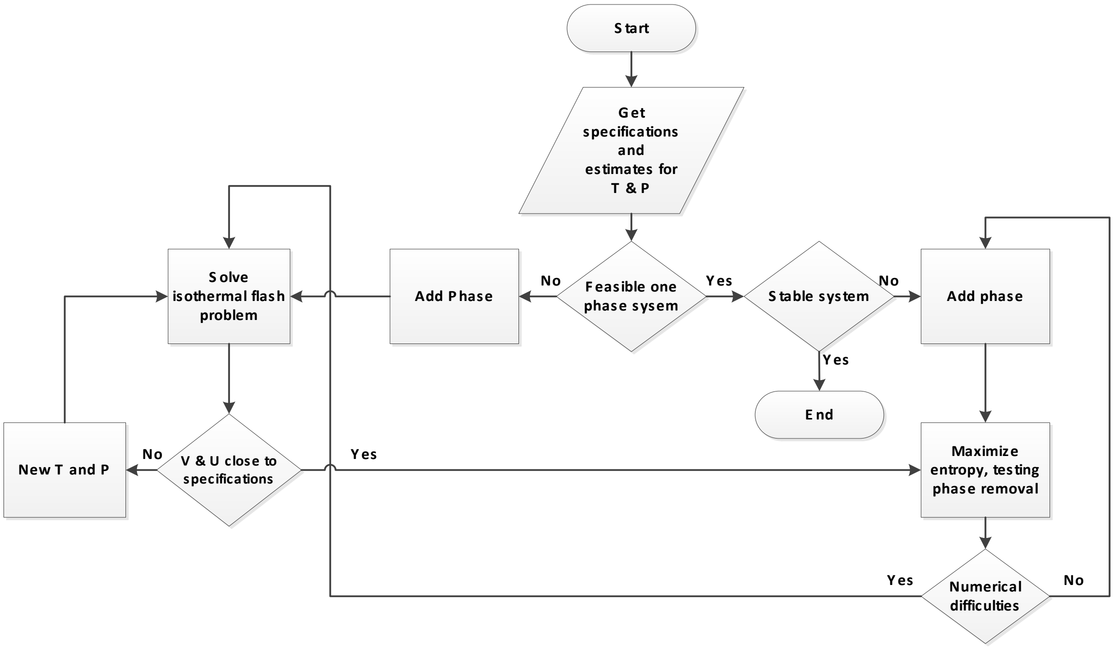

Figure 14. Flowchart of UVN procedure algorithm as suggested by Castier (2009) [110].

The algorithm is capable of solving phase equilibria problems with two or three phases, either at low or high pressures, including near-critical conditions, with some numerical instabilities under certain conditions. It was also integrated with a dynamic simulator than handles a pre-defined leak flow rate.

Castier [95] then investigated the use of the thermodynamic speed of sound in multiphase systems to simulate accidental leaks from tanks. Changes in sound speed can be used to detect the choking state of the fluid being discharged from a vessel. His work presents a general derivation of the thermodynamic sound speed for multiphase systems. Basha implemented his proposed sound speed calculations, in the context of a leaking tank/vessel to the existing algorithm developed by Castier [111]. This was done by assuming that the leak point, is the throat of an adiabatic, converging nozzle that operates isentropically. Also, the leak point is a known vertical position, and the size of the leak remains constant throughout. The program was also improved to account for different tank geometries, different leak point geometries and positions, and variable leak flow rates [111].

First, the system needs to specify by providing information regarding the vessel geometry, initial conditions and fluid properties. Possible vessel geometries include spherical, vertical and horizontal cylinders, as well as a horizontal cylinder with hemispherical caps. From the height and the diameter information provided, the vessel volume is computed. The initial temperature and number of moles of each component should also be provided. Finally, critical properties such as critical temperature, T_c, critical pressure, P_c, acentric factor of each component, ω_i, their binary interaction parameters for the PR EOS, and the coefficients of a polynomial expression for the molar heat capacity at constant pressure, in the ideal gas state, C_P^{ig}. Then, solving a *TVn* flash can determine the state of the fluid within the vessel, by computing the number of phases present, j, their volumes, V_j, the amount of each component in each phase, n_{ij}, and the internal energy of the fluid, U_{tot}. Next, the variables that define the dynamics of the leaking process need to be specified. This first includes the number of input streams and their conditions, the number of output streams and their conditions. Accidental leaks are considered output streams, and the leak point geometry and position are required inputs. The program algorithm can also handle controller actions, and heat loads. [111]

After all these specifications have been provided, the final step is to execute the dynamic simulations algorithm. At each time step, the numerical integrator first solves a *UVn* flash problem to determine the state of the fluid within the vessel to find variables j, n_{ij}, T, P and V_j. Then, the level of the interface(s) and the leaking phase(s) can be determined using information about j and vessel and leak point geometry. The leaking phase flow rate is calculated assuming that (i) the leaking point forms a hypothetical steady-state converging nozzle; (ii) this nozzle operates adiabatically and isentropically; (iii) the velocity of the fluid inside the vessel is negligible; (iv) the velocity of the fluid at the exit point is not zero; and (v) the exiting fluid may have more than one phase.[111]

The fluid at the exit point is assumed to leave at P_{atm}. Its velocity is determined using the leak area, the solution to the mass and energy balances, as well as the isentropic conditions in the nozzle. This velocity is compared to the sound speed at exit, to check for choking conditions. If the flow is found to be subsonic, the integrator proceeds to the next time step. If the flow is supersonic however, the velocity of the fluid is imposed as sonic, and the leak flow rate is recalculated.

A flow chart of the sound speed calculations developed are shown in Figure 15 [111]. A complete flow chart of the calculations developed by Basha and Castier is show in Figure 16.

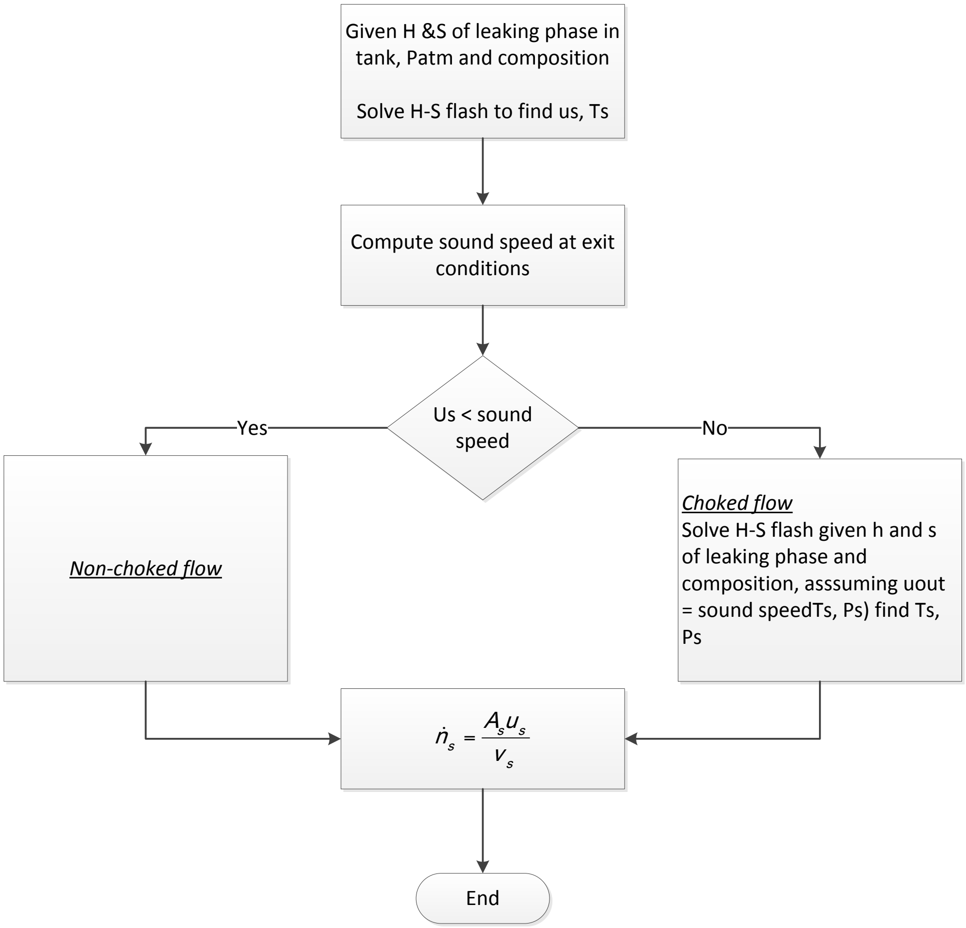

Figure 15. Sound speed calculations at exit point. Adapted from [111].

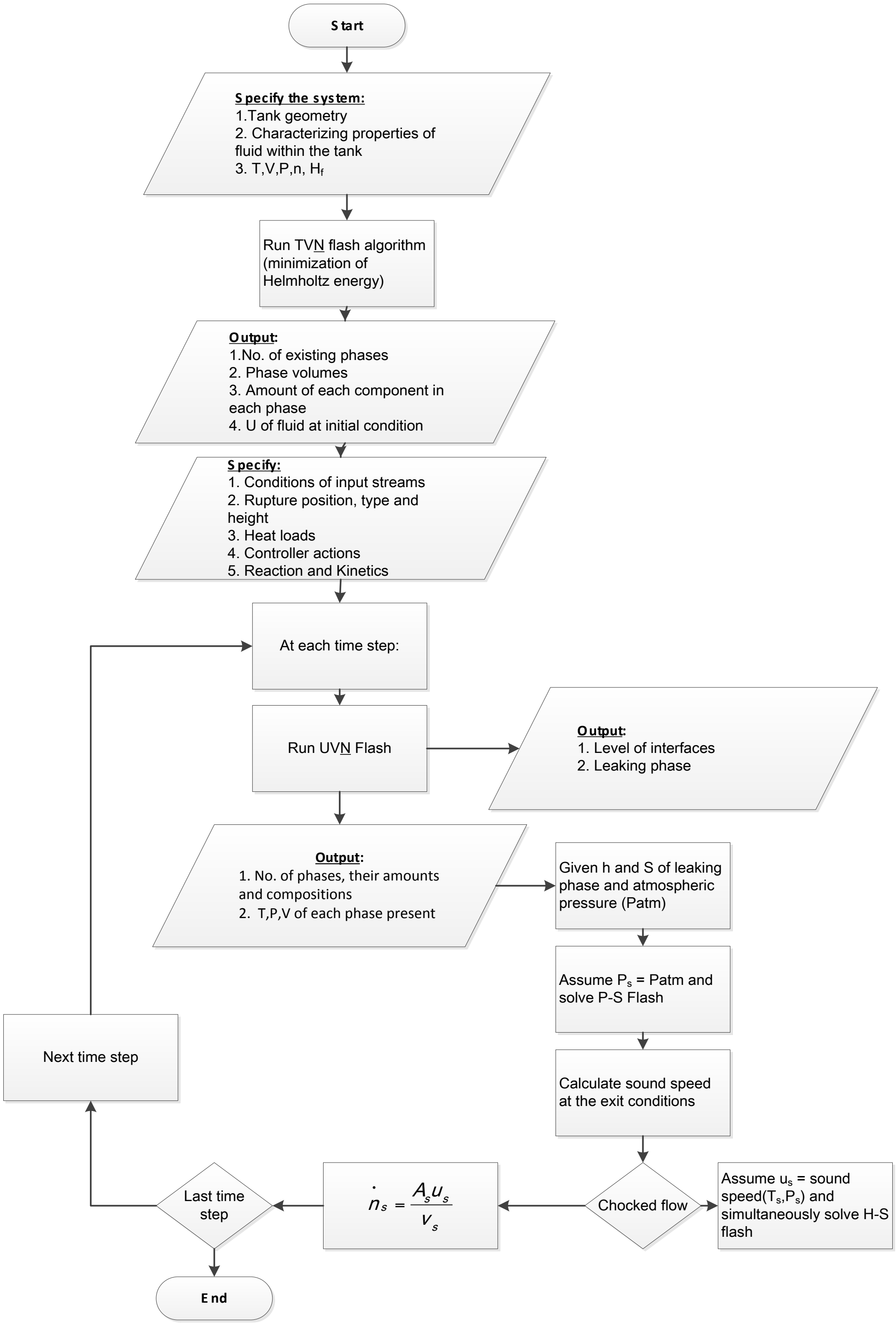

Figure 16. Overall flow calculations for dynamic vessel simulation with a leaking point. Adapted from [111].

4.5.2.1. Model validation

The model proposed by Basha [112] and Castier [106], [108], [110], [113] been validated against experimental data by Norris and Puls for leaking non-reactive systems [90], [114] and Raimondi's simulation of the Viareggio Railway station accident [115]. The validation against the experimental data by Norris and Puls [90] will be shown here. Details on the Viareggio Railway accident validation can be found in Basha's work [112].

In the first case, the vessel was modeled as a horizontal cylinder with diameter and length equal to 0.2052 m and 1.524 m, respectively, giving an internal volume of 0.0504 m^3. The initial condition is the presence of 210.936 moles of nitrogen, 56.448 moles of oxygen, and 2.701 moles of argon (mole fractions equal to 0.781, 0.209, and 0.010, respectively) at a temperature of 313.15 K. At these conditions, the fluid has a single phase at an absolute pressure of 13.91 MPa. These specifications match the initial conditions of the experiments reported in the literature by Norris and Puls [90].

The hole in the vessel, is 0.20 m above the bottom, and open from the start of the simulation, emulating a leak from a vessel, whose thermal insulation is assumed to be perfect. The hole height is high enough to guarantee that only vapor enters through it, in all the simulated cases, although partial condensation may occur as the fluid leaves the vessel, as the results will show. Simulations were performed for three different circular hole diameters: 1.5875×10^{-3} m, 4.7625×10^{-3} m , and 1.0211×10^{-2} m, to allow comparisons to the experimental results and previous simulations [90].

Figure 17 shows the release rate, in kg/s, as function of time for three hole diameters. The experimental data were obtained from a similar plot available in the work of Norris and Puls [90]. The simulations of this work predict the existence of a vapor phase, sonic discharge from the exit point during the time intervals of the experimental measurements of Norris and Puls [90]. These are also the time intervals that Norris and Puls [90] simulated with their FRICUP program. Their simulations and those of this work are in very good agreement and both exhibit similar deviations from the experimental data.

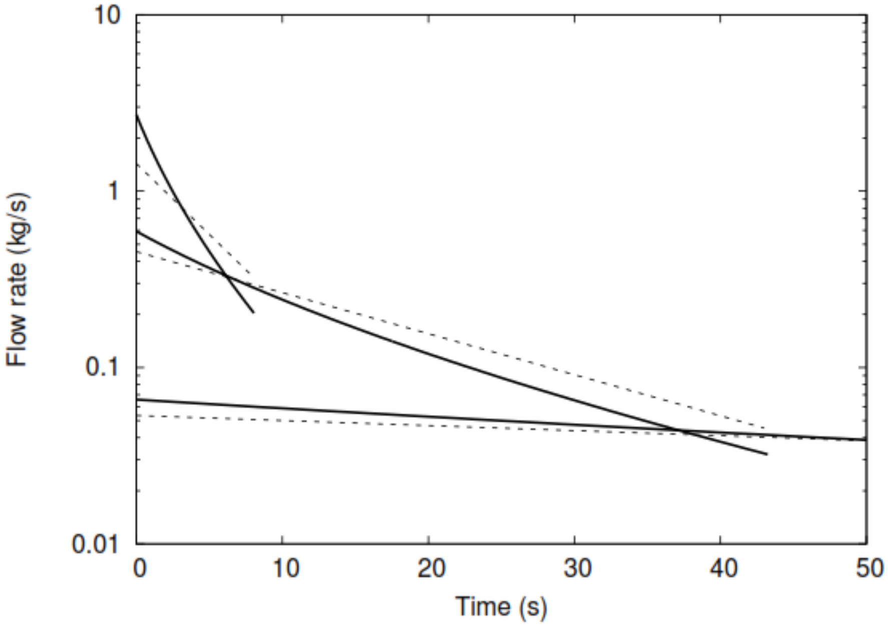

Figure 17. Release of air from an insulated vessel: exit flow rates for diameters equal to 1.5875 $\times 10^{-3}$ m (lower lines), 4.7625 $\times 10^{-3}$ m (middle lines) , and 1.0211 $\times 10^{-2}$ (upper lines). Dotted lines: experimental results [90] solid lines: simulations.

CHAPTER V

SCOPE OF WORK

Runaway reactions result from a loss of temperature control within a vessel containing a reactive mixture. This leads to a build-up of pressure, especially in the case of high vapor/gas generation, which may damage the structural integrity of the vessel, and lead to its explosion. Emergency Relief Systems (ERS), when properly designed, act as a last line of defense against explosion, by relieving the vessel pressure.

In the early 1980's by the Design Institute for Emergency Relief Systems (DIERS) developed ERS sizing methodologies for reactive systems based on the use of laboratory scale adiabatic calorimetry for the evaluation of the gas / vapor production rate under runaway conditions and the use of single-phase or two-phase flow models for the calculations of the vented flux through the ERS. These methods include simplifying and conservative assumptions with respect to the vessel behavior during venting (including reaction kinetics after the ERS opening, liquid level swell, type of the vented flow (single or two-phase), and homogeneous equilibrium flow through ERS). While the current user-friendly methodologies proposed by DIERS provide acceptable ERS sizes for chemical systems that produce vapor during the runaway (*vapor systems*), they tend to be oversizing for gas producing chemical systems (*untempered hybrid and gassy systems*) leading to unpractical and unrealistic ERS sizes. The improvement of ERS design for such reactive systems requires a deeper understanding of the phenomena governing the depressurization of a vessel containing a reactive mixture under runaway conditions.

This work proposes the development of a model that simulates the dynamic behavior of a reactor vessel containing a gas producing reactive mixture (peroxide decomposition) under runaway conditions before and after the opening of an ERS. This model aims to accurately predict the vessel temperature and pressure profiles, reactants/product mass inventory in the vessel, the vented flux, and the number of phases present and their compositions. The model also provides information on the conditions of the fluid at the ERS exit point. Such a model can then be used to improve upon the design of pressure relief systems that protect reactor vessels from thermal explosions.

To achieve this, the study has been divided into five sections:

1. Experimental study of the reactive system using differential and adiabatic calorimetry*: For this work, the decomposition reaction of 20 wt% solution of di-tert-butyl peroxide (DTBP) in toluene (a hybrid system) under runaway condition was chosen. Laboratory scale tests were conducted using Differential Scanning Calorimetry (DSC) and adiabatic calorimetry (PHI-TEC II) to experimentally characterize the nature of the runaway of this chemical system.*
2. Determination of the kinetic rate expression for the reactive system: *the experimental results of the calorimetric tests were used to determine the appropriate thermo-kinetic parameters for the decomposition reaction of 20% DTBP and develop a global kinetic rate expression.*

3. Formulation of dynamic model*: The dynamic model developed in this work was built upon a previous model by Castier [116] and Basha [111] that simulates leaks from high pressure vessels containing non-reactive systems*. *This model was previously validated against Norris and Pulls [90] experimental data for the blowdown simulation of air from a horizontal vessel (0.0504 m^3) at high pressure (13.8 MPa) and Raimondi's [115] modeling of the Viareggio Railway station accident that took place on June 29, 2009 as a result of LPG release. For the purpose of this work, Castier's model was modified and extended with the capability to simulate the opening of an ERS system at a given pressure and the capability to handle chemical reactions in the vessel.*

4. Dynamic simulations of a closed vessel and experimental validation*: the model was used to simulate the runaway of a 20% DTBP solution in a closed vessel. The parameters chosen for this simulation were similar to the conditions of the runaway experiment performed in closed cell configuration using adiabatic calorimetry. The comparison model/experiments allows a partial validation of the model (with no ERS).*

5. Sensitivity analysis of the effects of ERS area and ERS set pressure on vessel behavior after venting*: Several simulation of the venting of 20% DTBP under runaway condition was carried out to study the sensitivity of the model predictions to the ERS area and the ERS opening pressure.*

CHAPTER VI

EXPERIMENTAL KINETIC STUDY OF THE DECOMPOSITION OF DI-TERT-BUTYL PEROXIDE IN TOLUENE

6.1 Précis

The thermal decomposition of peroxides in liquid state or in non-protonic solvent proceeds by a first order reaction in which dissociation of the weak oxygen-oxygen bond is both a first-order unimolecular and a rate-determining step [117]. Peroxide decompositions reactions are studied extensively because of their highly exothermic and extreme self-heating rate, as well as their ability to form hot gaseous products that can altogether lead to a thermal runaway [118]. Thus, special safe handling of these chemicals is required during storage and transportation. In his work, AlDeeb presents a systematic approach for evaluating reactive systems, and their thermal stability [119].

The decomposition of 20 wt% DTBP solution in toluene was selected as the reactive system of study for this work. In this chapter, a review of literature on the decomposition kinetics of DTBP in toluene will be given. Also, the experimental analysis of the data collected using calorimetric techniques will be presented. Finally, a kinetic model will be developed using methods discussed in Chapter 2.

6.2 Decomposition of di-tert-butyl peroxide in toluene

Di-tert-butyl peroxide (DTBP) is one of the most used dialkyl peroxides for the generation of free radicals [119]. It is widely used as a modifier and cross-linking agent as well as polymerization initiator. DTBP can also be used to increase the cetane number of diesel fuels, since it readily decomposes for free-radicals. This in turn increases the rate of initiation. It is comparable to the 2-ethylhexyl nitrate, EHN, the current commercially used cetane improver, and more effective at reducing NOx emissions since it does not contain nitrogen. At typical fuel system temperatures, DTBP has proven to be thermally and oxidatively stable [120]. It must be noted DTBP is used as a calibration standard sample in adiabatic calorimeters such as the ARC (accelerating rate calorimeter) and PHI-TEC to check that the guard heaters and pressure compensation system work under extreme conditions [121], [122]. The molecular structure and physical properties of DTBP are presented below [123].

Table 1.Molecular structure and physical properties of DTBP from Knovel Dippr 108 Project [123]

Molecular Structure	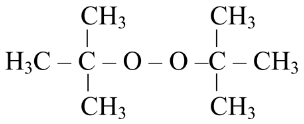 $H_3C-\overset{CH_3}{\underset{CH_3}{C}}-O-O-\overset{CH_3}{\underset{CH_3}{C}}-CH_3$
Molecular formula	$C_8H_{18}O_2$
Molar mass	146.2 g/mol
Boiling point	111 °C
Specific gravity	-40°C
Solubility in water	None
Vapor pressure at 20°C	2.6 kPa
Flash point	20°C

Various studies have been conducted to determine the pathway for the decomposition of DTBP in toluene [119]. In his work, AlDeeb identifies the six suggested pathways in literature and proves that they are all thermodynamically feasible their calculated Gibbs free energy is less than zero. All the proposed reactions pathways are shown in Figure 18. However, he predicts that Pathway I is the more dominant reaction pathway based on activation energy calculations of the elementary reactions [119]. Thus, it is assumed that DTBP decomposes into two moles of acetone and one mole ethane as such:

$$
\begin{aligned}
&(\mathrm{CH_3})_3\mathrm{COOC}(\mathrm{CH_3})_3 \rightarrow 2(\mathrm{CH_3})_3\mathrm{CO}\cdot \\
&(\mathrm{CH_3})_3\mathrm{CO}\cdot \rightarrow 2\mathrm{CH_3}(\mathrm{CO})\mathrm{CH_3} + \mathrm{CH_3}\cdot \\
&2\mathrm{CH_3}\cdot \rightarrow \mathrm{C_2H_6}
\end{aligned}
$$

$$
\begin{aligned}
&\text{Pathway I: } (\mathrm{CH_3})_3\mathrm{COOC}(\mathrm{CH_3})_3 \rightarrow 2\mathrm{CH_3}(\mathrm{CO})\mathrm{CH_3} + \mathrm{C_2H_6} \\
&\text{Pathway II: } (\mathrm{CH_3})_3\mathrm{COOC}(\mathrm{CH_3})_3 + 2\mathrm{CH_3}\cdot \rightarrow 2\mathrm{CH_4} + 2\mathrm{CH_3}(\mathrm{CO})\mathrm{CH_2CH_3} \\
&\text{Pathway III: } 2(\mathrm{C_6H_5})\mathrm{CH_3} + 2\mathrm{CH_3}\cdot \rightarrow 2\mathrm{CH_4} + 2(\mathrm{C_6H_5})\mathrm{C_2H_4}(\mathrm{C_6H_5}) \\
&\text{Pathway IV: } 2(\mathrm{C_6H_5})\mathrm{CH_3} + 4\mathrm{CH_3}\cdot \rightarrow 2\mathrm{CH_4} + 2(\mathrm{C_6H_5})\mathrm{CH_2CH_3} \\
&\text{Pathway V: } (\mathrm{CH_3})_3\mathrm{COOC}(\mathrm{CH_3})_3 + 2(\mathrm{C_6H_5})\mathrm{CH_3} \rightarrow 2(\mathrm{CH_3})_3\mathrm{COH} + (\mathrm{C_6H_5})\mathrm{C_2H_4}(\mathrm{C_6H_5}) \\
&\text{Pathway VI: } (\mathrm{CH_3})_3\mathrm{COOC}(\mathrm{CH_3})_3 + 2(\mathrm{C_6H_5})\mathrm{CH_3} + 2\mathrm{CH_3}\cdot \rightarrow 2(\mathrm{CH_3})_3\mathrm{COH} + 2(\mathrm{C_6H_5})\mathrm{CH_2CH_3}
\end{aligned}
$$

Figure 18. Possible identified pathways for the decomposition of DTBP in toluene. Adapted from AlDeeb [119]

The HEL PHI-TEC II Operating Manual [122] provides measured experimental rate and heat of reaction data, temperature, and pressure for 20 wt% DTBP in solution conducted in a closed, thermally insulated vessel, in the presence of nitrogen, which act as inert compounds and attenuate the temperature changes. As this exothermic reaction proceeds, the system temperature increases. Its pressure also increases, as consequence of the increase in temperature and of the additional moles present in the system because of the stoichiometry of the decomposition reaction. The results reported by HEL are shown in Table 2.

Table 2. HEL PHI-TEC II manual results for 20wt% DTBP in toluene decomposition [122]

Onset Temperature (K)	383.15 – 403.15
Final Temperature (K)	493.15- 513.15
Maximum Self-Heat Rate (K/min)	323 – 393 (493 K $< T_f <$ 503 K) 363 – 200 (503 K $< T_f <$ 513 K)
Enthalpy of Reaction (J/g)	210-300
Activation Energy (kJ/mol)	150-170
Order of fit	First order

The values reported by HEL are simply just ranges of acceptable kinetic and safety parameters. Thus, more literature was reviewed in order to see more specific measurements for the system under study. Oxley et al. conducted a study that yield kinetic information on solution phase decomposition of fuel combustion additives such as DTBP, with varying mechanistic pathways [124]. They also reported activation energies that varied from 138 to 167 kJ/mol. Iizuka and Surianaray made the first attempt to study the adiabatic decomposition of DTBP using ARC experiments, taking into account both chemical and physical transformations simultaneously [125]. For 20 wt% DTBP in toluene, they reported an onset temperature toluene ranging from 383.8 – 393.8 K, activation energy values ranging from 158.4 – 165.5 kJ/mol and pre-exponential factors ranging from 1.032×10^{17} – 1.149×10^{18} s^{-1}. Kimura and Otsuka [126] also studied the decomposition of DTBP using adiabatic experiments in ARC. The resulting thermal curves from their work are shown in Figure 19.

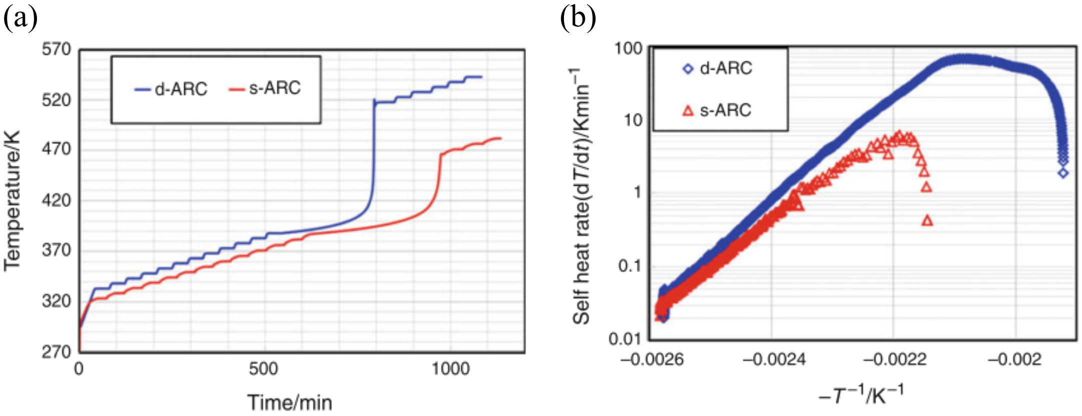

Figure 19. (a) Thermal behavior and (b) self-heating rateof 20 wt% of DTBP mixture measured by two types of ARC. Adapted from Kimura and Otsuka [126]

From the curves in Figure 19, it can be seen that the s-ARC is a calorimeter with a low adiabaticity (high phi factor), and the d-AR is highly adiabatic calorimeter (low phi factor). Kimura and Otsuka reported an onset temperature of 387.3 K for s-ARC and 388.2 K for d-ARC, as well as a maximum self-heat rate of 6.13 K/min for s-ARC and

67.2 K/min for d-ARC. The activation energy was calculated as 156 kJ/mol with s-ARC and 157 kJ/mol with d-ARC, while the pre-exponential factor was found to be $4.5\times10^{15} - 5.5\times10^{15}$ s^{-1}.

Jaiyu et al. studied the thermodynamics and kinetic parameters using both TSu (thermal screening unit) and ARC. Ramp tests were conducted in the TSu with 5g of 20 wt % DTBP in toluene, a heating rate of 2 K/min and a temperature range 298-573K. In the ARC, ramp tests were performed for a temperature range of 298 – 773 K and same heating rate, using the heat wait and search method. The onset temperature, T_o, based on the criteria dT/dt > 1 K/min, was found to be around 423 K. Also, the noted that the maximum pressure developed by the pure DTBP is 38 bar, whereas the maximum pressure developed by 20 wt% solution is 43 bar. This difference in pressure is mainly due to the fact that boiling point of toluene is 383 K, which is lower than onset temperature of the 20 wt% DTBP solution, and thus solvent evaporation brings the whole system to a higher pressure. If this solvent evaporation pressure contributed is subtracted, Jaiyu et al. noted that the pressure generated by 1 g DTBP in toluene was less than 1 g pure DTBP. This result indicates that the stable diluents can help reduce hazards caused by DTBP under runaway conditions. Toluene, being a low boiling point solvent makes it a less applicable alternative. [127]

For the thermal decomposition analysis by ARC using heat wait and search, Jaiyu et al. were able to obtain thermokinetic parameters for both pure DTBP and DTBP solution as show in Table 3. The reaction was assumed to be of first order based on theoretical analysis. Based on the tabulated results obtained for A and Q, pure DTBP will have higher reaction rates.

Table 3. Thermokinetic parameters for DTBP and 20wt% DTBP in toluene [127]

Samples	Q (J/g)	n	E (kJ/mol)	A (s^{-1})
DTBP	463.64	1	170.61	1.06×10^{20}
20% DTBP	251.77	1	164.32	4.33×10^{18}

Duh et al., using an ARC, found the exothermic onset temperature of 20 wt% DTBP, [128] in toluene to be 110.6 ˚C. This onset point was determined using the temperature rise rate criterion of dT/dt > 1 ˚C/min. For pure DTBP, various onset temperatures, determined by TSu, were presented, using different criteria, as listed in Table 4 below. It can be seen that the onset temperatures are detected earlier on when selecting the pressure and pressure rise rate criterions [129].

Table 4. Onset temperatures of pure DTBP determined by TSU using different criteria. [129]

Onset temperature (˚C)	Criteria
73.5	Ponset > 1.5 bar
99.3	Ponset > 2 bar
122.4	dP/dT > 1psi/min
137.5	dT/dt > 1 ˚C/min

Duh et al. conducted studies on the thermal decomposition and subsequently the thermokinetic parameters of DTBP and several other compounds using DSC analysis [130]. According to their work, the onset temperature was found to be around 124.4 ˚C, and the heat of reaction, the integral of their DSC curve, was found to be 1534.5 J/g. For the activation energy, they reported a value of 161 kJ/mol, and a pre-exponential factor of 3.98×10^{14} s^{-1}.

6.3 Experimental analysis

The estimation of safety parameters with respect to reactive chemical hazards are based on experimental analysis after theoretical computational methods have been used to determine the most favorable reaction pathway. Following a review of the literature, the experimental analysis consists of a screening stage performed using differential scanning calorimetry. In this case, the PerkinElmer DSC 8500 Hyper-enabled Double-Furnace Differential Scanning Calorimeter was used. This is usually followed by detailed thermal analyses using adiabatic calorimeters, such as the PHI-TEC II. In this section, the results of both types of experimental tests are presented.

6.3.1. Materials and apparatus

98% DTBP provided by Sigma Aldrich, and 99.99 % analytical grade Toluene provided by Fisher Scientific were used to prepare 20 wt% DTBP in toluene solutions. The solutions were prepared the same day the tests were conducted, and no additional purification of the chemical used was performed. With the PHI-TEC II tests, compressed nitrogen was used for the pressure compensation system that helps maintain the integrity of the cell.

Thermal analysis of the samples was performed using the PerkinElmer DSC 8500 Hyper-enabled Double-Furnace Differential Scanning Calorimeter, followed by the PHI-TEC II adiabatic calorimeter. These instruments are described in detail in Appendix A.1 and B.1, respectively. Time-temperature data was collected using DSC, while time-temperature-pressure data was collected using adiabatic calorimetry.

6.3.2. DSC thermal analysis

Samples of 10 μL were tested in high-pressure Stainless Steel O-ring pans provided by Perkin Elmer. The Stainless Steel pans with O-rings, are designed to suppress the vaporization of a solvent or a volatile reaction product, thus eliminating the any effects of the heat of vaporization. These capsules can withstand an internal pressure of 40 atm, have a volume of 60 μL, and are to be operated between 233.15 K to 673 K. Scanning runs were performed for a temperature interval of 303.15 – 573.15 K/min. Multiple heating rates are required, as described in section 4 of chapter 3. In this work, the heating rates chosen used were 5 K/min, 7.5 K/min, 10 K/min, 12.5 K/min, and 15 K/min.

In terms of its calorimetric performance, the DSC has a dynamic range of ±1300 mW, which allows for applications with high-energy thermal transitions to be measured. The instruments accuracy for heat flow measurements is <±0.2% while its precision is <±0.03%. The temperature measurements are performed using platinum resistance thermometers, which are more accurate and linear over a wider temperature range than thermocouples. The calorimeter can operate within a wide temperature range of 93.15 K to 1023.15 K with an excellent accuracy of <±0.05°C and a precision of <±0.008°C [131]. Since the resulting uncertainties (a maximum of ± 0.0051 mW) associated with the data will be smaller than the thickness of the line of the curves, they were not shown in the resulting thermograms in Figure 20.

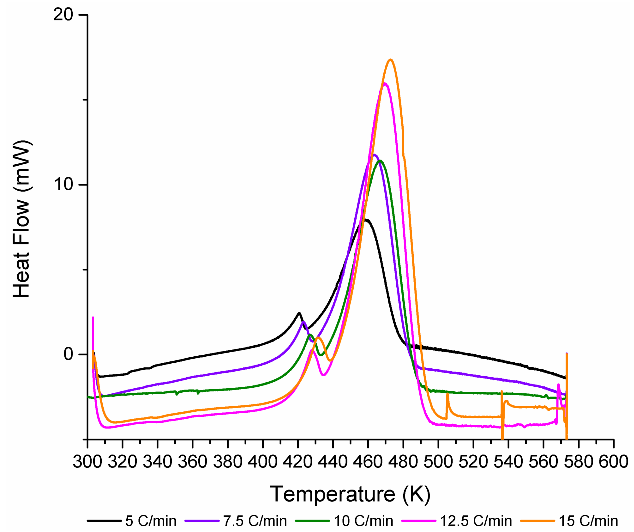

Figure 20. DSC heat flow profile of the decomposition of 20wt% DTBP in Toluene at different heating rates.

In terms of its calorimetric performance, the DSC has a dynamic range of ±1300 mW, which allows for applications with high-energy thermal transitions to be measured. The instruments accuracy for heat flow measurements is <±0.2% while its precision is <±0.03%. Also, it can operate within a wide temperature range of 93.15 K to 1023.15 K. Its accuracy with respect to temperature performance is <±0.05% while its precision is

<±0.008% [131]. Since the resulting uncertainties associated with the data are smaller than the thickness of the line of the curves, they were not shown in the resulting thermograms in Figure 20.

Exothermic heat flow, wherein energy is transferred from the system, is selected to be positive, and thus the curves are all have positive heat flow. The curves presented in Figure 20 have two peaks, indicating an earlier side reaction, which takes place, along with a major secondary reaction. These two peak heat flow curves are consistent with those presented by Duh e al. [130]. Since the predominant reaction is simply the decomposition of DTBP into acetone and ethane, any secondary reaction was ignored for the purpose of this work, and a first order reaction was assumed. These curves were treated as single curve peaks, and the smaller first peak was neglected as its influence in comparison to the larger peak is quite small.

From these thermograms, an average value of the onset temperature and the heat of reaction can be calculated. The onset temperature is calculated by finding the intersection between the slope of the heat flow curve before the curvature starts (deviation from baseline) and just after. This is done using the Pyris ™ Software for the PE 8500 DSC. The integration of the curve, to obtain the heat of reaction, is also computed by the software. Tabulate values from each thermogram can be found in Table 5. The average onset was found to be 397K and the average heat of reaction, ΔH_{rxn} was found to be -355 J/g. This is in agreement with values presented by HEL [122]. The onset temperature and reaction energy provide screening values, which give preliminary values.

Table 5. Onset temperatures and heat of reaction energies for DSC thermograms with 20wt% DTBP in toluene.

Heating rate (K/min)	T_{onset} (K)	ΔH_{rxn} (J/g)
5.0	401.0	-393.3
7.5	386.7	-371.7
10.0	407.5	-347.6
12.5	390.8	-335.8
15.0	402.7	-325.7
Average Values:	397.7	-354.8

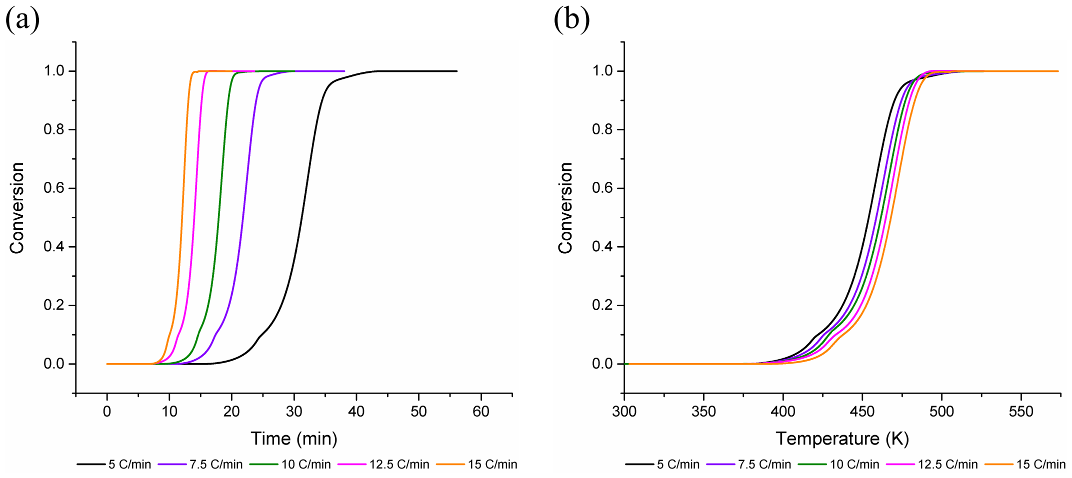

Figure 21. DSC (a) Conversion-time and (b) conversion-temperature curves for 20wt% DTBP in toluene.

The heat flow at each point of time in proportion to the total heat flow, which is the ΔH_{rxn} gives the conversion. The conversion as function of both time and temperature, respectively, is shown in Figure 21. As the heating rate increases, the reaction reaches completion faster, which is expected.

The conversion curves can be further analyzed to extract the activation energy and pre-exponential factors of the kinetic expression. This will be performed in section 6.4 according to the isoconversional methods described in section 4 of chapter 3.

6.3.3. PHI-TEC II thermal analysis

Experimental analysis of the 20 wt% DTBP in toluene systems was performed using adiabatic calorimetry with the PHI-TEC II. Samples of 12.25 g of DTBP in 48.98g of toluene were prepared and injected into 1.1×10^{-4} m^3 thin-walled cell. The fill level for these experiments was calculated to be 55%. Three trials were conducted; resulting time-temperature-pressure data curves were collected for each one and are presented in Figure 22. For the purpose of this work, the results are acceptable with respect to reproducibility. However, in the future, more tests should be performed to confirm a more accurate onset temperature range. Temperature data was collected using a K-type Omega thermocouple, with an uncertainty of ± 1.1 ˚C[132]. Due to the large quantity of data collected, error bars were not included.

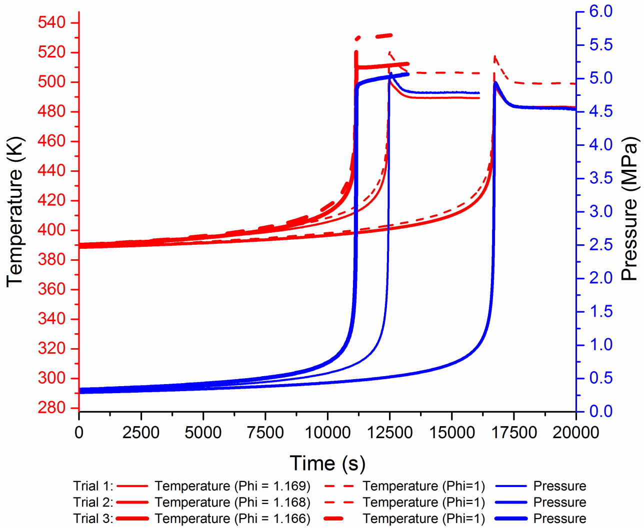

Figure 22. PHI-TEC II time-temperature-pressure and corrected temperature profiles of the decomposition of 20wt% DTBP in Toluene.

The self-heating rate, or the temperature rise rate of each curve, plotted against -1000/T(K) was used to determine the activation energy, E_a. The slope of the section of the curve before the curvature, where the conversion is zero or low, is equivalent to average value of –Ea/R. This is shown for each trial in Figure 23. This is an approximate value which will be later confirmed through analysis of DSC data.

This was then used to correct each temperature profile, and consequently self-heating rate profile as described in Appendix B.4, for Phi-factor of 1 according to the method proposed by Fisher et al (1992) as part of the DIERS vent sizing project [19]. This method is described in detail in Appendix APPENDIX B. The corrected data can then be compared to large scale simulations, since the adiabaticity of unity reflects that the heat capacity of the vessel is negligible compared to that of the fluid inside it. A revised onset is another result of this correction.

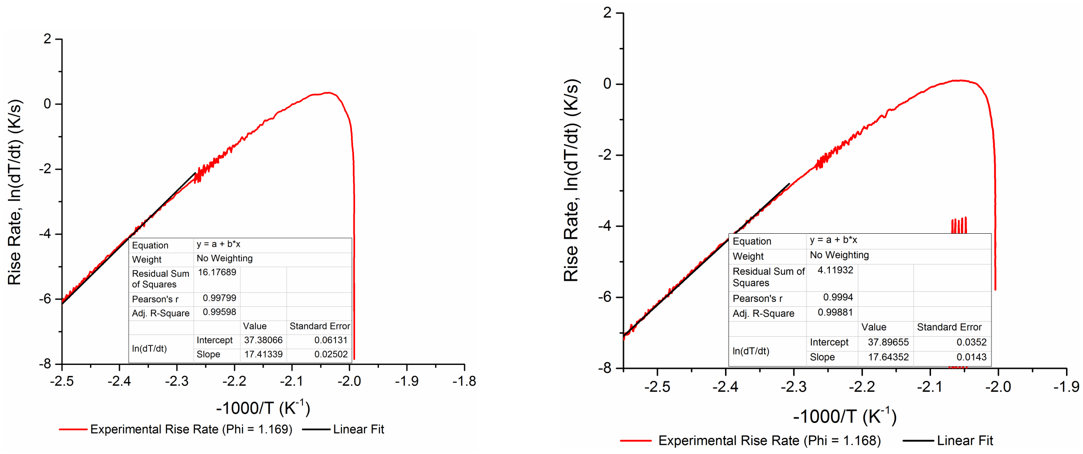

(a)Trial 1

(b) Trial 2

Equation	y = a + b*x		
Weight	No Weighting		
Residual Sum of Squares	16.17689		
Pearson's r	0.99799		
Adj. R-Square	0.99598		
		Value	Standard Error
ln(dT/dt)	Intercept	37.38066	0.06131
	Slope	17.41339	0.02502

Equation	y = a + b*x		
Weight	No Weighting		
Residual Sum of Squares	4.11932		
Pearson's r	0.9994		
Adj. R-Square	0.99881		
		Value	Standard Error
ln(dT/dt)	Intercept	37.89655	0.0352
	Slope	17.64352	0.0143

(c) Trial 3

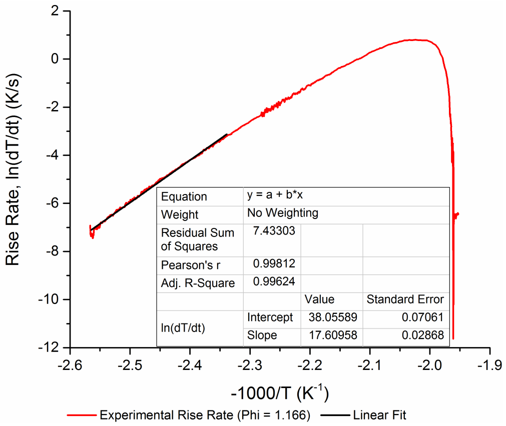

Equation	y = a + b*x		
Weight	No Weighting		
Residual Sum of Squares	7.43303		
Pearson's r	0.99812		
Adj. R-Square	0.99624		
		Value	Standard Error
ln(dT/dt)	Intercept	38.05589	0.07061
	Slope	17.60958	0.02868

Trial No.	Ea (kJ/mol)
1	144.79
2	146.77
3	146.41
Average	145.99

Figure 23. PHI-TEC II uncorrected temperature rise rate profiles, and extracted activation energy values for the decomposition of 20wt% DTBP in Toluene.

Both the temperature and pressure data have been smoothed, a technique used for reducing/cancelling the random variation inherent in large data collected over time. Averaging methods are most commonly used to reduce errors, especially in derivatives of data points [133]. For each moving average calculation (based on the mathematical method proposed by Savitzky–Golay [134], [135]) 50 points were used to obtain the slope of the central point. This reduces the error significantly.

These curves were corrected for Phi-factor of 1 according to the methodology described in Appendix B.4. The corrected curves for temperature and pressure are also depicted in the dashed lines in Figure 24 (a). As can be seen, the final temperature is higher for the corrected curve, as well as the fact that onset of the runaway takes place much earlier than with the raw uncorrected data. Also, the corrected curves for the temperature and pressure rise rates can be seen in Figure 24 (b). On the logarithmic scale it can be seen that maximum temperature rise rate corrected values can be up to 4 times larger than those obtained with uncorrected data.

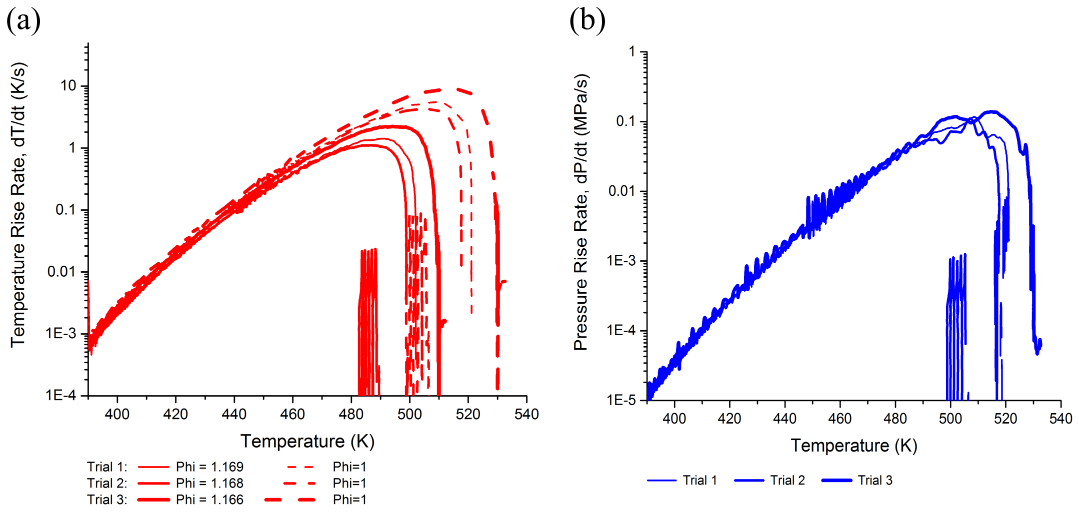

Figure 24. PHI-TEC II corrected temperature rise rate profiles, and pressure rise rate profiles for the decomposition of 20 wt% DTBP in Toluene

A comparison of relevant safety parameters between the uncorrected raw data and the corrected data can be found in Table 6. The onset temperature is predicted to be much earlier when using data corrected for a phi factor of 1. Using the raw data under predicts the onset, and basing any emergency relief scenarios on these results would lead to catastrophic events taking place, like a thermal explosion.

Table 6. Relevant safety parameters extracted from PHI-TEC II data.

	Trial 1		Trial 2		Trial 3	
	Phi = 1.169	Phi = 1	Phi = 1.168	Phi = 1	Phi = 1.166	Phi = 1
T_{max} (K)	502.1	520.9	498.9	517.3	512.4	533.0
$(dT/dt)_{max}$ (K/s)	1.4	5.4	1.1	4.2	2.2	8.8
T @$(dT/dt)_{max}$ (K)	502.0	508.0	498.9	502.8	512.3	513.1
Pmax (MPa)	5.1	5.1	4.9	4.9	5.1	5.1
$(dP/dt)_{max}$ (MPa/s)	0.1	0.1	0.1	0.1	0.1	0.1
T_{onset} (K)	390.6	389.2	388.4	387.1	389.9	388.6
P_{max}/P_i	4.5	4.5	3.8	3.8	5.1	5.1
$P_{max} - P_i$	5.0	5.0	4.8	4.8	5.0	5.0
T @ $(dP/dt)_{max}$ (K)	490.6	507.5	489.7	506.5	496.6	514.5
P @ $(dP/dt)_{max}$ (MPa)	4.1	4.1	4.1	4.1	4.0	4.0
(dT/dt) @ $(dP/dt)_{max}$ (K/s)	1.4	5.4	1.1	4.1	2.2	8.8

Also, both the maximum temperatures, and rates are affected by a phi-factor correction, while the pressure data remains unaffected. The maximum temperature increases by roughly 20 degrees in each case, while the maximum rise rates, as can be seen increase by a factor of 4. When performing a safety analysis, it is important to know the correct self-heating rate at large scale, in order to be able to adequately identify the critical regions of the runaway, and the extent of the hazard that they pose.

6.4 Kinetic modeling of the decomposition rate of DTBP in toluene

In order to define the rate of the decomposition reaction, thermokinetic parameters like the order, the activation energy, and the pre-exponential factor, also known as the kinetic triplet, all need to be defined. In this section, the experimental data from DSC and PHI-TEC II will be used in order to get the kinetic triplet characteristics of the system under study.

6.4.1. Extracting activation energy using the Friedman isoconversional method

Based on the review of the literature, isoconversional model free methods, described in section 4 of chapter 3 can be used to extract this kinetic triplet from scanning data, like that from DSC analysis. These methods are derived based on the principle that a fixed conversion, the reaction rate becomes only temperature dependent [29]. The most common of these methods is the Friedman method, wherein, for each heating rate, at any given X, the value of E_a is found from the slope of a plot of $\ln\left(\beta dX/dt\right)$ versus 1/T (see Eq.(26)). Based on ICTAC recommendations [29], E_a values were determined at conversions of 0.01-0.95 in order to be able to accurately determine the dependence of E_a on X. Discrete values of conversion from 0.1 -0.9 were chosen, with 0.1 intervals, were chosen to construct the isoconversional lines seen in Figure 25

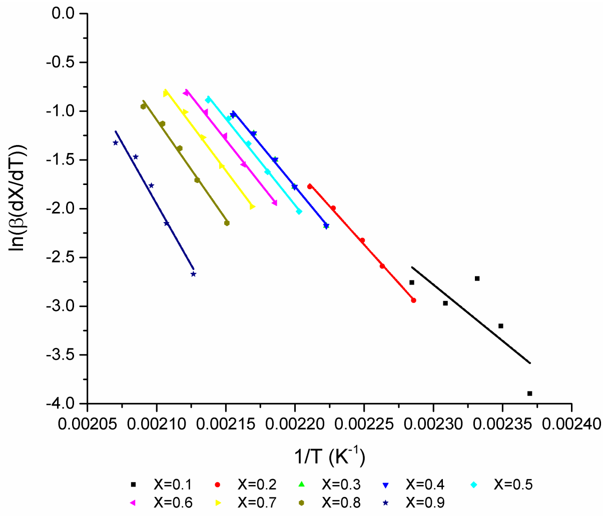

Figure 25. Friedman analysis plot for the decomposition of 20wt% DTBP in Toluene in DSC.

There are five data points on each isoconversional line, each corresponding to a specific heating rate. There is a good agreement between the data and each of their corresponding linear fits. At low conversion, typically 0.1, the non-linearity is expected since this is typically the region where the first smaller peak is located in the DSC thermograms in Figure 25. The slope, equivalent to $–E_a/RT$, the intercept, equivalent to $\ln[k_0 f(X)]$, and the R-square values are given in Table 7.

The average activation energy value calculated was 149 kJ/mol, which is within the range suggested by HEL [122], as well as the values predicted by the PHI-TEC II data in section 6.3.3. While the effect of the smaller first peak in the heat flow curve not clearly modeled, it was taken into account when calculating the average activation energy. The intercept value requires knowledge the mechanism model, and thus cannot be fully extracted without it. This limits the use of the Friedman method to only providing a reliable activation energy value, model free.

Table 7. Linear fit parameters for isoconversional lines using Friedman analysis and DSC data.

X	Slope, -Ea/R	Ea (kJ/mol)	Intercept, $\ln[k_o(X)]$	R-Square
0.100	-11533	95.888	23.75	0.519
0.200	-15773	131.137	33.12	0.997
0.300	-16955	140.966	35.66	0.994
0.400	-17194	142.954	36.05	0.994
0.500	-17725	147.369	37.03	0.994
0.600	-17935	149.112	37.27	0.994
0.700	-18941	157.478	39.11	0.993
0.800	-20369	169.352	41.69	0.986
0.900	-25065	208.393	50.69	0.959
Average		149.183	38.82	

6.4.2. Extracting the pre-exponential factor using a least square parameters fit

Based on the review of literature presented in section 6.2, the decomposition of 20 wt% DTBP was found to be of the first order. Thus, the reaction mechanism model , *f(X),* was given by a simplified Šesták and Berggren [34] expression (Eq. (19)), wherein parameters $m=0$, $n=1$ and=0 yielding an expression for the rate of conversion as

$$\frac{dX}{dt} = K_k\left(1 - X\right) \tag{40}$$

whereby K_k is defined according to the Arrhenius law, and X is the conversion.

Given the different methods discussed in section 4.2 in chapter 3 for obtaining the pre-exponential factor, a least parameter square fit was deemed the most inclusive of all the experimental data collected. Thus, the rate of reaction expression given by Eq. (40) was used and the DSC as well as PHI-TEC II experimental data were used to determine the best square fit for pre-exponential factor, given the order and the activation energy obtained in section 6.4.1The resulting value of the pre-exponential factor obtained was 5.6×10^{-14} s^{-1}.

A model based on Eq. (21), was constructed with an activation energy value of 149183 J/mol, a pre-exponential factor of 5.6×10^{-14} s^{-1}, and a reaction order of 1. Temperature DSC data, as well as initial values of conversion (at t=0) were fed to the model in order to determine the rate of conversion, dX/dt, profiles. These profiles were then integrated using a simple Euler relation to determine the X profile. Then, the resulting dX/dt and X curves were compared to their experimental counterparts for each heating rate. These are shown in Figure 26. Overall, there is good agreement between the model and the experimental DSC data, expect near the first smaller peak, which was neglected for the purpose of this work.

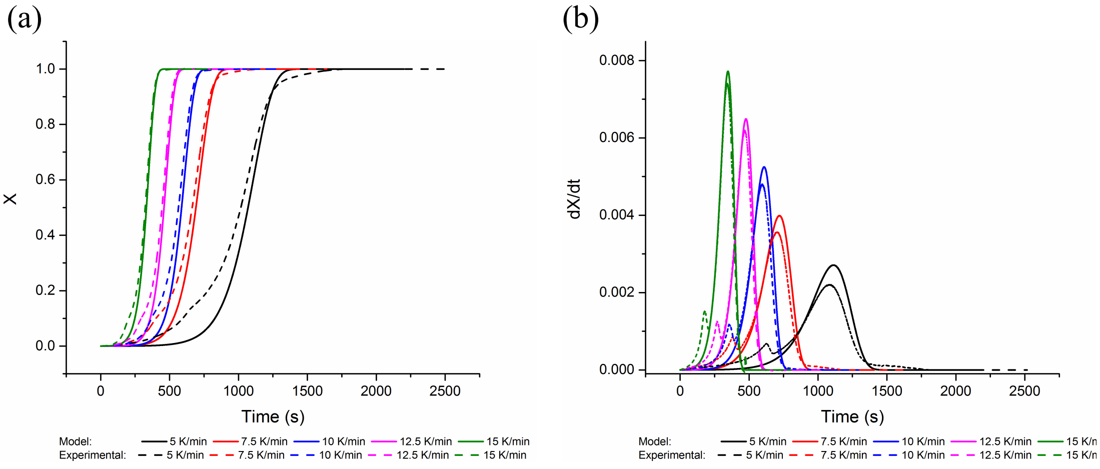

Figure 26. Least Square Parameters fit for value of pre-exponential factor using DSC tests of the decomposition of 20wt% DTBP in Toluene: (a) conversion profiles, (b) rate of conversion profiles.

For adiabatic data on the other hand, it was also more important to fit the rate of temperature rise, dT/dt. In order to do this, the experimental conversion was calculated as

$$X = \frac{T - T_{onset}}{T_{\max} - T_{onset}} \tag{41}$$

where T_{onset} is the corrected onset temperature for each run, and T_{max} is corrected value. A comparison of the relevant safety parameters between the uncorrected raw data and the corrected data can be found in Table 6. The profile for dX/dt was again calculated using Eq. (40). The adiabatic balance, given by Eq. (22) was used to obtain dT/dt. The temperature profile was determined through a simple Euler integration of dT/dt. These are shown in Figure 27, which also shows good the agreement between the model, and the corrected PHI-TEC II data with respect to the temperature rise profile.

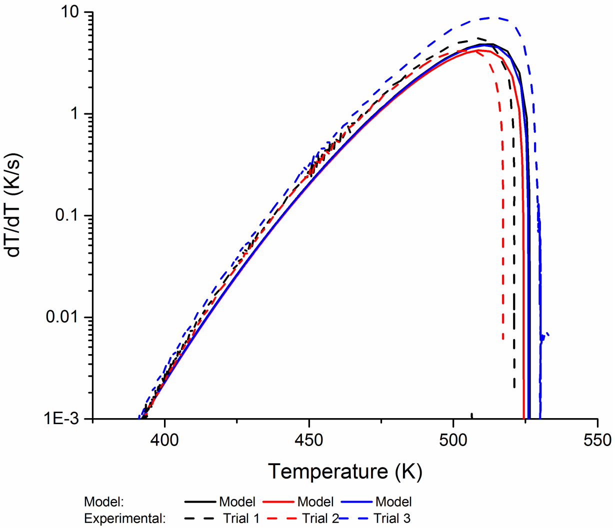

Figure 27. Least Square Parameters fit for value of pre-exponential factor using PHI-TECII tests of the decomposition of 20wt% DTBP in Toluene; a comparison of rate of temperature rise.

However, it can be seen from Figure 27, that the prediction of the maximum rate is not fully captured. This is related to the simplicity of the kinetic rate expression. Also, since both DSC and PHI-TEC II data was used for the fit, it is expected that the parameter value is not all a perfect fit for every single curve. Moreover, simplified kinetics, with respect to considering a single reaction pathway, and an order of exactly 1, will result in slightly less representative model expressions.

CHAPTER VII

DEVELOPMENT OF THE SIMULATOR FOR REACTOR VESSEL VENTING

7.1 Précis

The model developed by Castier [106], [108], [110], [113] and Basha [112] was described in detail in Chapter 3. It consists of a series of differential and algebraic equations. The differential equations were amended to include a trivial differential equation for time, a mass balance that is able to handle reactive systems, as well as equations for cumulative amounts of each component that enter or leave the vessels through each stream. The energy balance was not modified, the only difference, in this formulation, is in the way the enthalpies are calculated, which now includes the formation properties. The system was treated as 'lumped', wherein the dependent variables of interest are a function of time alone [105].

In this chapter, the modifications made to this model so that it can handle the depressurization of a vessel containing reactive systems through an ERS system are discussed. These include the assumptions made, the vessel set up, any changes to the model equations, and changes to the implementation and numerical methods used to solve the system.

7.2 Assumptions

The necessary modifications to the model were made with the following assumptions:

- the vessel is rigid and its volume is defined;

- the heat capacity of the vessel's construction material is neglected;
- the fluid in the vessel is in phase equilibrium at all times;
- there is complete and instantaneous disengagement of the phases; as consequence, liquid phase swelling caused by bubbles is neglected;
- the leak or venting occurs through one or more holes at known vertical position(s);
- the size of the hole(s) remains constant;
- the region around a leaking or venting point behaves as a hypothetical adiabatic converging nozzle that operates isentropically;
- there may be chemical reactions;
- level swell is neglected ;
- when chemical reactions occur, their rates are used to compute the changes in amounts of reactants and products within the vessel. In other words, the assumption of instantaneous chemical equilibrium is not used;
- changes in the potential energy of the fluid are negligible inside the vessel and in the input and output streams;
- the kinetic energy of the fluid within the vessel and in the input streams is negligible compared to the kinetic energy of the fluid at the exit point of a leak or ERS;
- system is treated as ‘lumped’, wherein the dependent variables of interest are a function of time alone [105].

7.3 Vessel setup for reactive systems

The general formulation for a vessel equipped with an ERS device, containing a chemical system includes making changes to and mass balances in order to include the heat released or evolved, as well as the generation and consumption terms, respectively. Also, the ERS is an orifice that is activated at a certain set pressure, and is located very close to the top of the vessel. This can be seen in Figure 28.

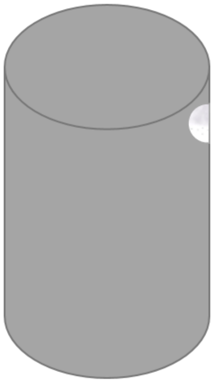

Figure 28. Vessel set up for reactive system

7.4 Physical properties

The simulations carried out in this work require several thermodynamic properties, such as fugacities (for phase equilibrium calculations), enthalpies and internal energies (for energy balances), and entropies (for exit flow conditions and sound speed calculations), and their derivatives with respect to mole numbers, volume, and internal energy or temperature. Enthalpies, internal energies, and entropies were calculated by adding the formation properties in the ideal gas state at 298.15 K and 1.0132×10^5 Pa to the ideal gas and residual contributions.

The heat capacities at constant pressure in the ideal gas state were considered as third degree polynomials in absolute temperature [136]. The residual contributions were obtained from an equation of state. Analytical expressions for all properties and derivatives were used, obtained via computer algebra [106]. The procedure is general and should work with any equation of state capable of predicting the properties of liquid and vapor phases. In this work, the Peng-Robinson equation of state (EOS) [137], widely used by the oil, gas, and petrochemical industries, was used. All binary interaction parameters were set to zero in the examples of this paper. The Knovel DIPPR Project 108 [123] was used to obtain critical properties, formation properties, and heat capacity coefficients.

7.5 Formulation

7.5.1. Mass and energy balance

The mass balance of component *i* within a vessel is now given by

$$\frac{dn_i}{dt} = \sum_{m=1}^{ns_{in}} \dot{n}_{im}^{in} - \sum_{m=1}^{ns_{out}} \dot{n}_{im}^{out} + \dot{R}_i + \qquad (42)$$

where t is the time, n_i denotes the number of moles of component $\underline{i}$ in the vessel, m is the subscript that refers to the streams, $\dot{n}_{im}^{in}$ and $\dot{n}_{im}^{out}$ refer to the molar flow rates of component i in stream m. These flow rates can result from input streams, denotes by ns_{in}, or output streams, which include ERS venting and leaking flow conditions, denoted ns_{out}.

In order to account for reactive systems, the term $\dot{R}_i$ is used to represent the rate of formation of component *i*. This value is set to zero for non-reactive systems as well as inert compounds. The rate of formation is calculated by taking into account the contribution of the n_r reactions that take place within the vessel, and is defined as follows

$$\dot{R}_i = \sum_{k=1}^{n_r} \frac{\nu_{ik}}{\nu_{I_k k}} \dot{r}_k \tag{43}$$

where $\dot{r}_k$ is the rate of reaction *k*, referred to component I_k, with a stoichiometric coefficient of $\nu_{I_k k}$.The stoichiometric coefficients of components *i* in reaction *k* are given as ν_{ik}. The rate of reaction *k* is negative if component I_k is a reactant and positive if it is a product.

The rate expression for $\dot{r}_k$ is dependent on the kinetic data available, and the kinetic model used. For this work, two options have been implemented. The first options, adapted from the work of Castier et al. on reactive distillation [102], gives a reaction expression as

$$\dot{r}_k = \pm K_k \sum_{j=1}^{n_p} V_j \prod_{i=1}^{n_c} \left(\frac{x_{ij}}{v_j} \right)^{\zeta_{ik}} \tag{44}$$

where K_k is the rate constant of reaction k, V_j and v_j are the volume and molar volume of phase j, respectively, x_{ij} is mole fraction of components i in phase j, and ξ_{ik} is the order of components i in reaction k. The ratio x_{ij}/v_j is molar concentration of components i in phase j within the vessel. Here, the number of components and fluid phases are represented by n_c and n_p, respectively.

The second option is to use conversion, X, to express the global reaction rateexpressed as in Eq. (14), and assuming that $f(X)$ is given by a simplified Šesták and Berggren [34] expression (Eq. (19), wherein parameters $m=0$, $n=1$ and=0, as determined by DSC studies in section 3.2 in chapter 6 (Eq. (40)).

Conversion based kinetics, which depends on the heat released by a reaction, can easily be associated with change in number of amounts by defining X to be

$$n_i = n_{i0}\left(1 - X_i\right) \Rightarrow X_i = 1 - \frac{n_i}{n_{i0}} \tag{45}$$

Combining Eqs. (40) and (45) gives

$$\frac{dX_i}{dt} = K_k \frac{n_i}{n_{i0}} \tag{46}$$

Knowing that the rate of change of component i in reaction k is given by the differential of Eq. (45)

$$\frac{dn_i}{dt} = n_{i0} \frac{dn_i}{dt} \tag{47}$$

Combining Eqs. (46) and (47) gives

$$\frac{dN_i}{dt} = -K_k n_i \tag{48}$$

For the purpose of this work, the reaction rate is then represented as

$$\dot{r}_k = -K_k n_{I_k} \tag{49}$$

where I_k is the reactant taken as a reference for expression that of reaction *k*.

For either option used to define the reaction rate, the rate of consumption or generation within the vessel is given by Eq. (49). Also, the rate constant is always defined by the Arrhenius law as described in Eq.(13). What should be noted is that there exists the option to input a minimum density in order to control in which phase the reaction takes place. For the purpose of this work, with the use of global kinetics, a very small minimum density was used.

The energy balance within the vessel is now given by

$$\frac{dU}{dt} = \sum_{m=1}^{ns_{in}} \dot{n}_m^{in} h_m^{in} - \sum_{m=1}^{ns_{out}} \dot{n}_m^{out} \left(h_m^{out} + M_m^{out} \frac{\left(u_m^{out}\right)^2}{2} \right) + \dot{Q} \tag{50}$$

where U is the internal energy of the fluid within the vessel, and $\dot{Q}$ represents the heat transferred to the vessel. Quantities $\dot{n}_m^{in}$ and h_m^{in} represent the molar flow rate and molar enthalpy of each input stream, while superscript *out* represent analogous quantities in the output streams. The molar mass of the fluid passing through the exit point and its velocity are respectively denoted as M_m^{out} and u_m^{out}. The heats of reaction do not appear explicitly in Eq. (50) because the thermal effects of the reactions are considered by using the formation properties in the evaluation of internal energies and enthalpies, as explained in the following section.

In addition to the mass and energy balances, a trivial differential equation for time was included, given by

$$\frac{dt}{dt} = 1 \tag{51}$$

The main purpose behind this was to prevent numerical difficulties during the integration of the differential equations, when the integration variable is different from time. This is discussed in more detail in section 7.6.2

7.5.2. Cumulative amounts

In the case of fluid release to the environment, it is important to know the instantaneous release rate of each component *i* through each release point *m*, which is represented by $\dot{n}_{im}^{out}$ in Eq. (50). It is also essential to evaluate the cumulative amounts released. Together these quantities can provide useful insight when assessing the risks associated with the fluid being released, as well as mitigation/control techniques in the case of loss of primary containment scenarios.

Since the current formulation allows for chemical reactions and the possible existence of input streams to the vessel during the simulated period, the cumulative releases cannot simply be calculated as the difference in the amounts inside the vessel at a given time and at the beginning of the simulation. To compute them, ODEs were included to represent the cumulative release of component *i* through each release point *m*, among the ns_{out} exit points that exist in the vessel.

This was given by

$$\frac{dn_{im}^{out}}{dt} = \dot{n}_{im}^{out} \tag{52}$$

Likewise, it is possible to compute the cumulative amounts that enter the vessel through the ns_{in} input streams, if any, during the simulated period by including differential equations of the form

$$\frac{dn_{im}^{in}}{dt} = \dot{n}_{im}^{in} \tag{53}$$

The evaluation of cumulative amounts adds $n_c\left(ns_{in} + ns_{out}\right)$ ODEs to the system. Despite their number, their computational load is small because the effort is dominated by the evaluation of thermodynamic properties, which have to be calculated anyway in order to solve the mass and energy balances, and their accompanying algebraic equations.

7.5.3. Position of the phase interface within the vessel

During the numerical ODE integration, it was necessary to determine the position of the phase interfaces within the vessel. They dictate the phase, or phases, that will leak or vent through a hole or exit stream, depending on its position. Figure 29 is a schematic of an exit point wherein exists a simultaneous discharge from the liquid and vapor phases because of the interface position.

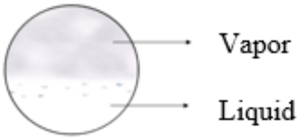

Figure 29. Schematic of a circular exit point wherein there is two-phase flow.

The solution of the algebraic equations of the model at each time step provides the values of several properties, among which the phase volumes. Given these phase volumes and the vessel shape, it is possible to find the interface levels. The upper interface of a phase depends on its own volume and of on the volumes of the phases below it inside the vessel, i.e., the phases with mass densities larger than that of the phase under consideration. Assuming the phases are ordered in decreasing mass density order, the upper interface of a phase *j* depends on the stacked volume, V_j* defined as

$$V_j^* = \sum_{m=1}^{j} V_m \tag{54}$$

where V_m is the volume of the phase *m*.

Four vessel geometries were considered in this work, namely: vertical cylinders, horizontal cylinders, spheres, and horizontal cylinders with hemispherical caps. For this purpose of this work, a vertical cylinder was used and thus this will be described. More detail can be found on the remaining geometries in Basha's work [112]. For vertical cylinders, determining the interface positions for given phase volumes is simple. Taking the bottom of the tank as reference, the position of the upper interface of phase *j*, denoted by h_j, occurs at:

$$h_j = \frac{V_j^*}{\pi r^2} \tag{55}$$

where r is the vessel radius.

7.5.4. Shape and location of fluid exits

Two simple geometries for the exit point are considered: rectangular and circular. Both geometries are assumed to be on the lateral vessel wall, whose curvature is neglected, and thus the hole has no considerable effect on the vessel volume. The model and its computational implementation account for the possibility of multiple exit points (holes) but in the work that follows, no index was assigned to the variables denoting the holes, in order to alleviate the notation.

The hole is also assumed to be of fixed size and its central position is known. A given hole may be exposed to a certain fluid phase throughout the simulated period as in the case of a vapor phase leaking from a hole located at a position high on the vessel wall. In other situations, the leaking phase exposed to the exit point can change due to movement of the interface during vessel discharge.

If such is the case, more than one phase may be exposed to the hole; the simplest case being that with two phases. The instantaneous composition of a leaking fluid with multiple phases is assumed to be the area-averaged composition. To apply this assumption, it is necessary to find the area of the hole in contact with each phase.

7.5.4.1. Rectangular holes

For each phase j partially or totally exposed to a rectangular hole, the area of the hole exposed to that phase, A_j is given by

$$A_j = w\left(\min\left(h_T, h_j\right) - \max\left(h_L, h_{j-1}\right)\right) \tag{56}$$

where w is the width of the rectangular hole and h_T and h_L are the levels of the top and bottom of the hole, respectively. As defined in section 7.5.3 , h_j stands for the level of the interface between phase j and (j+1). By definition, $h_0 = H_B$ and $h_{np} = H_T$, where h_0 is the bottom of the vessel, and h_1 is the level of the interface between the densest and the second densest phases, until h_{np}, which coincides with the top of the vessel. H_B and H_T, represent the level of the bottom and top of the vessel, respectively.

7.5.4.2. Circular holes

For each phase j partially or totally exposed to a circular hole, the area of the hole exposed to that phase, A_j , is evaluated as the difference between the areas of two circular segments, A_{j1} and A_{j2} such that

$$A_j = A_{j2} - A_{j1} \tag{57}$$

The values of A_{j1} and A_{j2} are calculated using

$$A_{j1} = \left(r^2 \cos^{-1}\left(1 - \frac{h_{j1}}{r}\right) + \sqrt{-h_{j1}\left(h_{j1} - 2r\right)}\left(h_{j1} - r\right)\right) \tag{58}$$

$$A_{j2} = \left(r^2 \cos^{-1}\left(1 - \frac{h_{j2}}{r}\right) + \sqrt{-h_{j2}\left(h_{j2} - 2r\right)}\left(h_{j2} - r\right)\right) \tag{59}$$

where r is the radius of the circular hole and h_{j1} and h_{j2} are given by:

$$h_{j1} = \max\left(\left(h_{j-1} - h_L\right), 0\right) \tag{60}$$

$$h_{j2} = \min\left(\left(h_j - h_L\right), \left(h_T - h_L\right)\right) \tag{61}$$

where h_j, h_T and h_L retain the same definition as in section 7.5.3.

7.5.5. Flow velocity at the fluid exits

The region around each hole is treated as a hypothetical converging nozzle that operates adiabatically and isentropically. In a converging nozzle, the maximum fluid speed possible at the throat (location of minimum diameter) is the sound speed of the fluid at the local conditions, in what is called choked flow. Determining whether the flow is choked involves a series of steps, as outlined in this section.

The composition of the fluid that passes through the nozzle will generally change because of the global dynamics of the vessel. Therefore, the conditions of the stream that enters the hypothetical nozzle are different at each integration step. However, the size of the hypothetical nozzle region is assumed very small compared to the volume of the whole vessel. Thus, accumulation effects are neglected and the hypothetical nozzle is assumed to operate at steady-state. The consequence of this assumption, as applied to the mass balances, is that the compositions and molar flow rates of the fluids entering and leaving the nozzle at a given time are equal. In addition, it is assumed that the fluid velocity inside the vessel and at the entrance of the hypothetical nozzle is negligible, compared to its velocity at the exit point. The energy balance around a hypothetical nozzle located at exit point *m* is given by

$$\left(h_m^{out} + M_m^{out} \frac{\left(u_m^{out}\right)^2}{2} \right) - h_m^z = 0 \tag{62}$$

where h_m^z is the molar enthalpy of the fluid that enters the nozzle with negligible speed. More specifically, it is the molar enthalpy *inside the vessel* of the exiting fluid. Using analogous symbols for the entropies, the isentropic operation condition imposes that:

$$s_m^{out} - s_m^z = 0 \tag{63}$$

The calculation proceeds by initially assuming that the fluid pressure at the nozzle's exit plane is equal to the backpressure. This backpressure is the pressure away from the vessel, assumed to be equal to atmospheric pressure (P_m^{out}=1.01325×10^5 Pa). Using this assumption, the fluid pressure, molar entropy, and molar composition are known, allowing the formulation of a flash problem under these specifications, referred here as a *PSn* flash problem. This flash is solved using an internal loop in which an isothermal flash problem (*TPn* flash) [107], [109] is solved and an external loop that changes the temperature in order to satisfy Eq. (63).

After solving the *PSn* flash, the fluid speed, u_m^{out} , is calculated using Eq (62). The thermodynamic sound speed, *a*, is calculated at the same conditions using a rigorous procedure that takes into account the existence of multiple phases and deviations from ideal gas behavior [95]. If $u_m^{out} > a$, the problem specification is impossible because the fluid velocity cannot be higher than the sonic speed at the exit of a converging nozzle. The consequence is that the pressure at the exit plane is higher than the backpressure. In this case, the previous solution is discarded and the energy balance is rewritten as

$$\left(h_m^{out} + M_m^{out} \frac{\left(a\left(T_m^{out}, P_m^{out} \right) \right)^2}{2} \right) - h_m^z = 0 \tag{64}$$

Eq. (63) and (64) provide the specification of a flash problem at given values of molar enthalpy, molar entropy, and molar composition, i.e., an *HSn* flash problem, which is solved as the *PSn* flash with an additional external loop in which the pressure is modified in order to satisfy Eq. (64). A schematic of the two nested loops *PSn and HSn* flash problems can be seen in Figure 30.

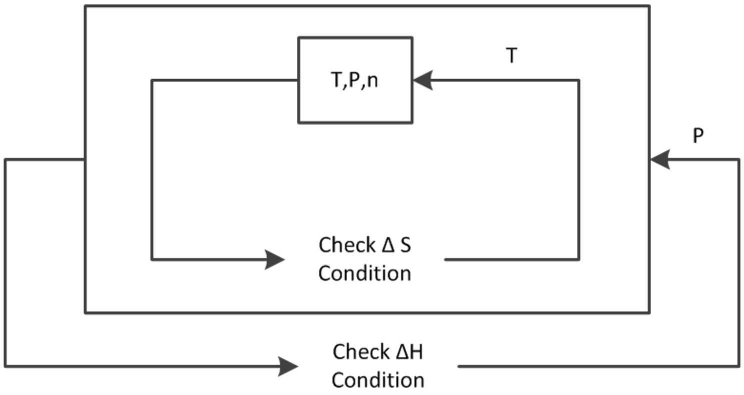

Figure 30. Schematic of nested loops *PSn and HSn* flash problems.

The solution of this flash problem provides the values of temperature, pressure, and molar volume at the exit plane and, therefore, the flow is sonic, and the velocity is given by

$$u_m^{out} = a\left(T_m^{out}, P_m^{out} \right) \tag{65}$$

The molar flow rate of each component *i* through the hole, $\dot{n}_{im}^{out}$, is given by

$$\dot{n}_{im}^{out} = \frac{z_{im}^{out}}{v_m^{out}} A u_m^{out} \tag{66}$$

where *A* is the area of the hole, v_m^{out} is the molar volume at the exit plane, and z_{im}^{out} is the mole fraction of component *i* in the leaking or venting stream. It is important to note that the fluid at the exit plane may have one or more phases. Thus, the *PSn* and *HSn* flashes need to be complete procedures that automatically determine the number of phases present and their thermodynamic properties. In addition, the method used to compute the sound speed at the exit conditions needs to consider the possible existence of multiple phases. Few rigorous algorithms exist [94], [95], [138] for such calculations. The procedure proposed by Castier [95] is used in this work.

7.6 Implementation and numerical methods

The mathematical model described in the previous sections is a modified version of the system of differential-algebraic equations (DAE) described in section 5.2 of chapter 4. The simulated period is split into events, some of which are physical events and others are events linked to numerical convenience or difficulties.

Physical events may either occur at specified times or be triggered by conditions such the appearance or disappearance of phases within the vessel. Their common feature is to cause an abrupt change in the right-hand side of at least one of the differential equations of the model. Numerical events may occur at any time and are detected during the simulation. The various types of events, their category, occurrence, and testing frequency are summarized in Table 8 below.

Table 8. Simulation events

Event	Category	Occurrence	Testing Frequency
Programmed valve opening/closing	Physical	Specified times	End of each time step
Vessel rupture	Physical	Specified times	End of each time step
Opening of ERS	Physical	Detected	End of each time step
Phase appearance within vessel	Physical	Detected	End of each time step
Phase disappearance within vessel	Physical	Detected	End of each time step
Phase appearance in exit flow	Physical	Detected	End and middle of each time step
Phase disappearance in exit flow	Physical	Detected	End and middle of each time step
Change of integration variable	Physical	Detected	End of each time step
Non-convergence of algebraic equations	Physical	Detected	End and middle of each time step

7.6.1. Relief valves

To account for the programmed opening or closing of input or output valves at set times, the numerical integration of the differential equations is split into time segments between the set times for opening or closing. In this way, the transition from one time segment to the next coincides with one of these physical events. The model does not include equations for the mechanical resistance of the vessel and, for this reason, ruptures that cause leaks are treated like events that occur at set times, as done with the opening and closing of valves at set times.

The opening of an ERS or burst disk, on the other hand, is a physical event that is modeled to occur once the pressure of the fluid within the vessel reaches a specified threshold. Therefore, it needs to be detected and the moment it will occur is unknown at the beginning of the simulation. Many numerical procedures for ODE integration move back and forth in the independent variable during a step, but the values at the end of the step are those that represent a physical point of the solution trajectory. As the check happens at the end of the step, it may happen that the pressure is slightly higher than the pressure set for opening the valve, but this was neglected because the opening delay is of, at most, one integration step. Once it is detected that the valve should open, the integration is interrupted and automatically restarted with the valve open.

7.6.2. Change of the integration variable

The change of integration variable is also treated as a numerical event in which preemptive action is taken to prevent numerical difficulties. During reaction runways and venting, large changes in component amounts in the vessel occur during small time intervals. A step too large in time may lead to unphysical specifications for the algebraic equations during the subsequent time step, preventing the numerical convergence to their solution. Therefore, the choice of time as independent variable of the ODE system in all integration steps is inconvenient. The strategy is to choose, at the end of each integration step, the variable that will be considered as independent during the subsequent integration step. The ODE set comprises of Eqs. (42) and (50)-(53). However, only Eqs. (42), (50)- and (51) are directly related to the conditions inside the vessel as the other two differential equations serve for documentation purposes only. In addition, the selection of internal energy as independent variable led to numerical instabilities in our implementation. Therefore, the criterion to select independent variables is as follows:

$$\max\left(\left|\frac{1}{n_1}\frac{dn_1}{dt}\right|,\left|\frac{1}{n_2}\frac{dn_2}{dt}\right|,\ldots,\left|\frac{1}{n_{n_c}}\frac{dn_{n_c}}{dt}\right|,\frac{1}{t}\right) \tag{67}$$

In this expression, the last term, *1/t,* represents the term that contains the derivative of time. Without additional conditions, this criterion tends to favor the selection of components present in very small amounts, which occasionally cause numerical difficulties as the independent variable for numerical integration. As an empirical additional condition, components with mole fraction less than 0.01 are considered ineligible to be the independent variable. Using *y* to represent the selected independent variable, the set of differential equations used at each time step becomes:

$$\frac{dn_i}{dy} = \frac{dn_i}{dt}\bigg/\frac{dy}{dt} \tag{68}$$

$$\frac{dU}{dy} = \frac{dU}{dt}\bigg/\frac{dy}{dt} \tag{69}$$

$$\frac{dt}{dy} = 1\bigg/\frac{dy}{dt} \tag{70}$$

$$\frac{dn_{im}^{in}}{dy} = \frac{dn_{im}^{in}}{dt} \bigg/ \frac{dy}{dt} \tag{71}$$

$$\frac{dn_{im}^{out}}{dy} = \frac{dn_{im}^{out}}{dt} \bigg/ \frac{dy}{dt} \tag{72}$$

where the time derivatives are calculated using Eqs. (42) - (50)

7.6.3. Initial estimates for UVn flash problem

In addition to the proper selection of independent variable of the ODE system, the converged results of the four most recent solutions for each unknown of the *UVn* flash problem are used to fit a linear function of the current independent variable of the ODE system. Thus, the generation of the initial estimate for each unknown of the *UV* flash problem is obtained by linear extrapolation. With these precautions and the automatic step size selection of the Bulirsch–Stoer method [104] used for ODE integration, the solution of the algebraic equations is usually successful. However, lack of convergence occasionally occurs and is treated as numerical event, which may be detected at several points during a time step, but especially during the solution of the *UVn* and *HSn* flashes. If it is detected, the calculation of the given step is interrupted, the procedure steps back to the beginning of the time step, and retries it with subsequently smaller values of step size until the successful completion of the time step.

7.6.4. Stability test for phase insertion and removal

The stability test for possible phase insertion [109] and the phase removal [107] test could be executed inside a step but a phase addition or removal cause an abrupt change in the differential equations, which would force a restart of the ODE integration.

For this reason, these tests are executed only at the end of each integration step. In this way, during a time step, the number of phases inside the vessel and at each exit point, remains constant.

If the amount of an inert (non-reactive) component falls below a specified threshold and the derivative of its amount with time is negative, the derivative is arbitrarily set to zero. The threshold was arbitrarily set to 4×10^{-4} moles, but simulations of systems much bigger or much smaller than the examples of this thesis may require bigger or smaller thresholds, respectively. The consequence of this approximation is that the amount of this component within the vessel remains a fixed small amount. It mainly serves to avoid phase equilibrium calculations with components in tiny amounts, which may give origin to numerical difficulties. However, it should be noted that the decision of whether to set the derivative to zero is taken at every time step and can be reversed. For example, if an input valve opens allowing a certain component to enter the vessel, the derivative of its amount with time becomes positive and is used as calculated, changing the amount of the component within the vessel.

7.6.5. Dynamic simulator set-up

The dynamic simulator algorithm consists of several parts. Figure 31 shows the updated simulator and its capabilities, tailored to encompass the objectives of this work. A list of inputs are provided, regarding the tank specifications, the tank components and their properties, as well as the initial condition of the tank. This input data is used for to perform a non-reactive *TVn* flash (the formation properties are simply stored and passed on to the rest of the program) which determines the initial conditions within the tank.

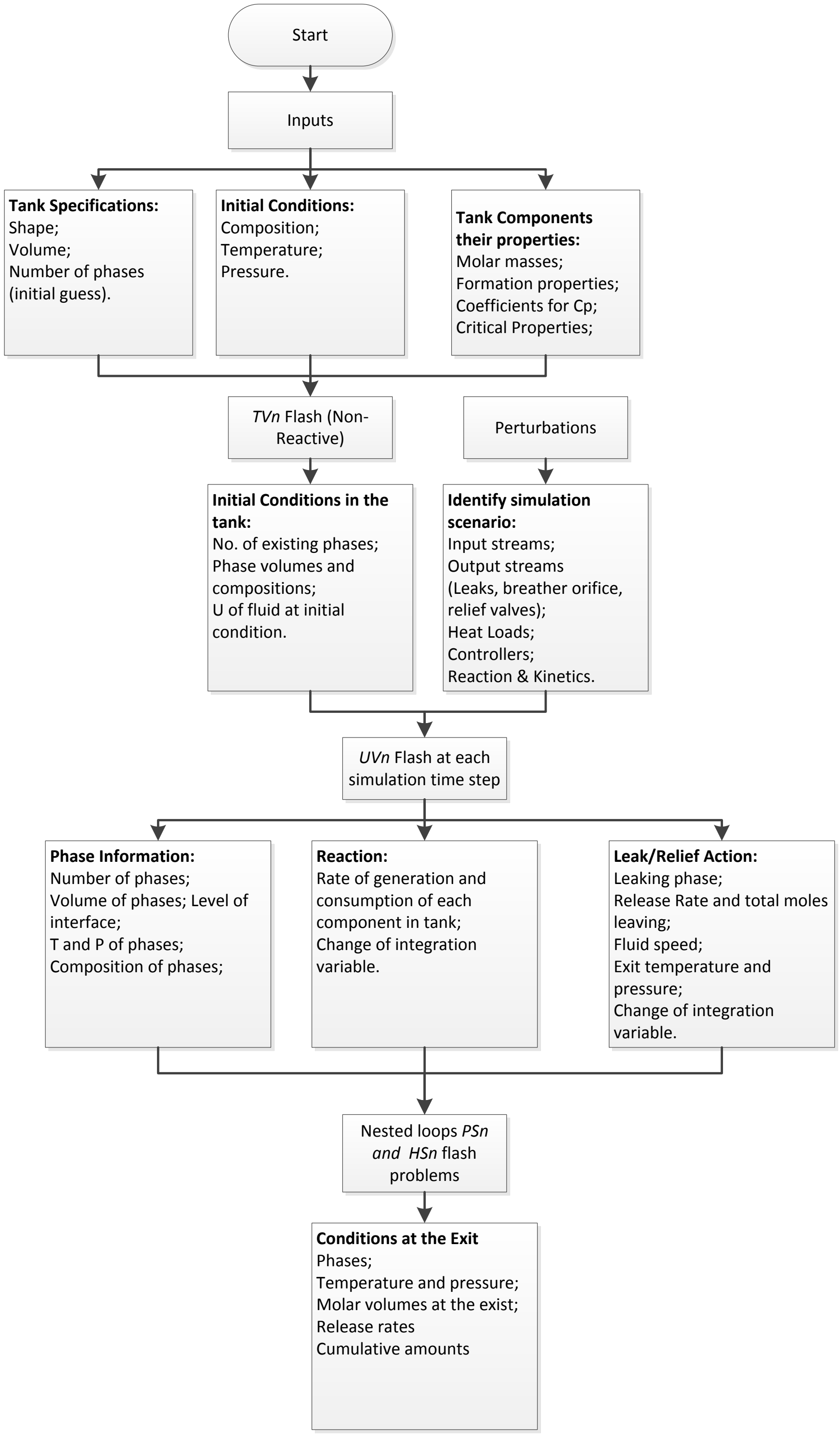

Figure 31. Dynamic simulator set-up

Next, a perturbation file is created that stores any perturbations made to the system. This includes input stream information, output stream information, controller action, heat loads and reactions. Sudden leaks, an ERS, and breather orifices are treated as output streams. However, they are specified by a type with a variable that can be used to differentiate how the program treats them. Details of reaction kinetics inputs can be found in chapter 6. Both, the results of the *TVn* flash and the perturbation data are then used to perform a *UVn* flash at each simulation time step.

The *UVn* flash provides information about the conditions of the vessel at all times. For closed systems, the outputs include information about the volume of the phases, the distribution of the components in these phases, as well as a complete temperature and pressure profile of the vessel fluid. If an event like a leak is triggered, either instantaneously, or based on a specified pressure rating like with an ERS, there is a separate output file that stores information such as cumulative amounts that have exited the vessel, the release rates, which could be useful in the future for dispersion modeling when analyzing possible release scenarios and their consequences, as well as the speed of the fluid and sound speed at the exit.

CHAPTER VIII

SIMULATION RESULTS AND SENSITIVITY ANALYSIS

8.1 Précis

This chapter displays the results of the simulations obtained by the modified simulator from chapter 6. The simulations presented here are for a vertical cylindrical vessel with diameter and height equal to 0.21204 m and 0.28320 m, respectively, resulting in an internal volume of 0.010 m^3. The vessel's load for the simulations consists of 0.32450 moles of nitrogen, 6.42514 moles of DTBP, 40.7878 moles of toluene, and small initial amounts of acetone and ethane, equal to 10^{-8} moles each, to prevent numerical problems in the calculation of thermodynamic properties. For the closed vessel simulations, the initial conditions were 390.61 K and 0.30569 MPa, as per the initial experimental conditions of adiabatic trial 1 in chapter 5. This allows for partial validation. For the reference simulation, and the sensitivity analysis, the initial temperature was 389.33 K, and 0.3007 MPa. This is very close to average values of adiabatic experimental onsets and their corresponding pressures as seen in Table 6.

The simulation of all the cases presented in this section started from these initial conditions, which were chosen to match adiabatic test data conditions. Despite the difference in size with the experimental setup, the simulation conditions are consistent with the values of the intensive properties (such as temperature, pressure, densities, and mole fractions). Therefore, comparisons of intensive properties are justifiable. Also, validation of the model against experimental data when performing a closed vessel test simulation is possible.

In all the cases presented, the vessel has perfect thermal insulation, no external heat loads, and no controller action. The cases also illustrate situations with phase addition or removal and with the transition from the sonic to subsonic flow regime at the exit point. Also, the initial time step was equal to 1/500 of the simulation time step specified for each case, which was around 20,000 seconds. However, if the algorithm cannot overcome some numerical difficulties for certain runs, the time step was decreased accordingly to either 1/1000 or 1/1500.

8.2 Closed vessel simulation and experimental validation

At present, there are very few experimental data available on the behavior of untempered gassy systems in particular under runaway conditions [20], [24]–[28]. Thus, large scale experimental data cannot be used to validate simulation results. The next best available experimental data is that obtained using adiabatic calorimetry, as those presented in chapter 5.

For the purpose of partial validation, a closed vessel containing 20 wt% DTBP in toluene was simulated to observe the decomposition reaction. For this run, there were no input streams and no output streams. The thermal effects due to the reaction were calculated based on the use of formation properties as one of the contributions (along with the ideal gas and residual contributions) that comprise the evaluation of internal energies and enthalpies in the simulation program. Figure 32 shows the evolution of temperature and pressure in an insulated closed vessel until the depletion of DTBP with the implemented kinetics.

As can be seen there is good agreement between the simulated and experimental curve, which are represented by the red and black line, respectively. The simulated temperature curve is sharper than the corrected temperature curve (black dotted line). This is to be expected according to Kossoy et al [139], who recognize that Fisher's correction does not take into account the fact that the reaction will be faster at lower phi-factor. This is because, under adiabatic conditions, the same heat release will give way to a higher self-heating. This in turn accelerates the reaction kinetics and, thus, the reaction will reach completion much earlier, leading to a sharper temperature profile overall.

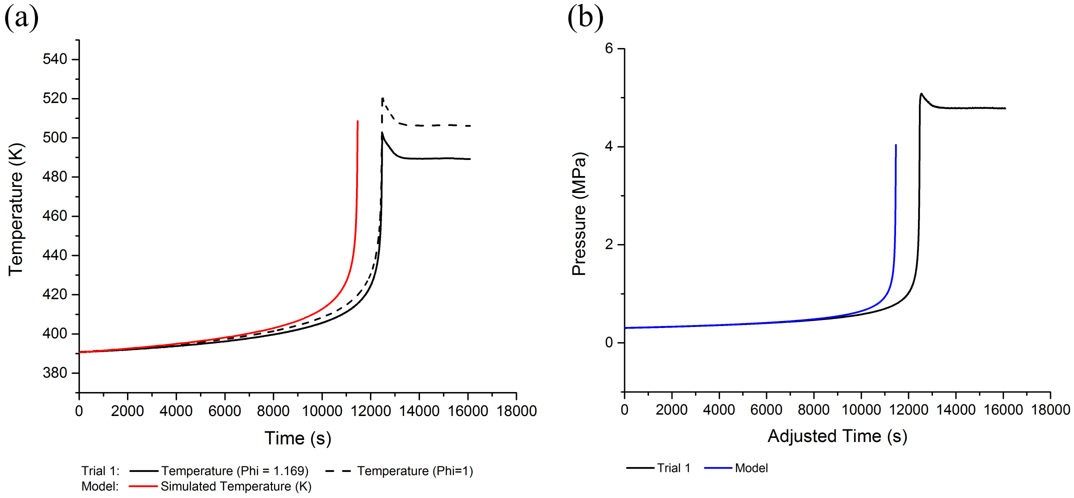

Figure 32. Temperature and pressure profile of the decomposition of 20 wt% DTBP in Toluene in a closed vessel validated against experimental trial 1.

The maximum temperature predicted by the simulation is 507.5 K, and the maximum pressure evolved in the vessel is 4 MPa. The maximum temperature is higher than that given by the experimental adiabatic trial, but lower than the corrected curve for a phi-factor of 1. The simulated pressure is highly dependent on the simulated temperature and both peak before their experimental counterparts. This could be because of side reactions, which were not considered in the model. Anyway, the maximum calculated pressure value of 4 MPa for this reactive system is similar to experimental measurements of other authors for similar situations [125], [126].

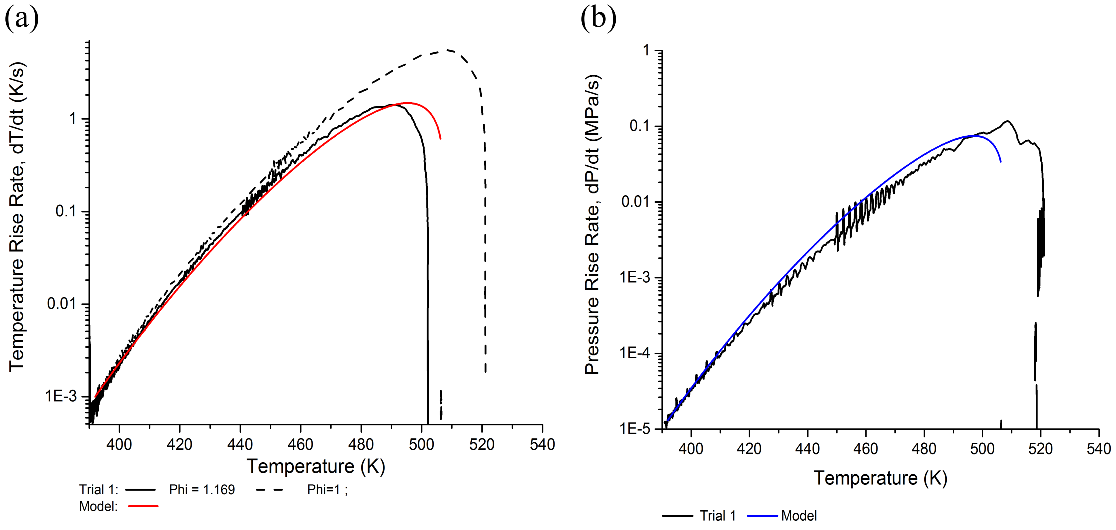

Figure 33. (a) Temperature rise (self-heating) rate and (b) pressure rise rate of the decomposition of 20wt% DTBP in Toluene in a closed vessel.

Still, the rate of temperature rise profile, and not the temperature profile, is the better basis for comparison when it comes to thermal runaway conditions. Thus, Figure 33 shows the temperature rise (self-heating) rate and pressure rise rates for both the experimental and simulation curves. Since the simulation ends, for some numerical reason, when there are around 0.05 moles of DTBP in the vessel, which is just shy of complete depletion, the full self-heat rise rate profile is not developed. The maximum self-heat rise rate for the simulated case, which is perfectly adiabatic, was 1.39 K/s. This is similar to the uncorrected experimental data but substantially smaller than the corrected experimental self-heat rise rate.

This deviation could be due to the simplicity of the phi-correction in general, which neglects the effect of the phase changes that occur within the vessel It is based on the initial fluid (taken to be just the initial liquid mass) heat capacity, and this changes as the reaction proceeds and vapor/gas form. Another reason could simply be the EOS chosen. While PR-EOS provides good results for the oil and gas industry, it may not be the best EOS to use for reactive systems that contain polar compounds. A change in the EOS will also impact the sound speed calculations.

A definitive limitation however, is that resulting from a simplified global kinetic expression. A small sensitivity analysis was performed on the effect of the pre-exponential factor, and the activation energy on the simulation results. Their separate effects on temperature are shown in Figure 34. While a 5% change in the pre-exponential factor still brings a horizontal shift in the temperature curves, a 5% change in the activation energy plays a major role in defining the speed of the reaction.

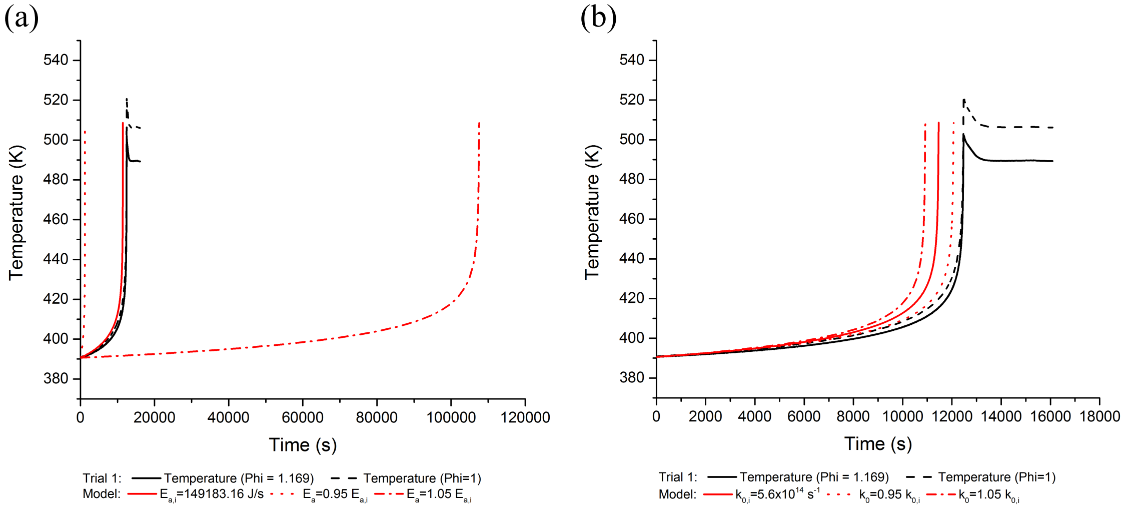

Figure 34. Temperature profile for varying (a) activation energy and (b) pre-exponential factor for the decomposition of 20 wt% DTBP in Toluene in a closed vessel.

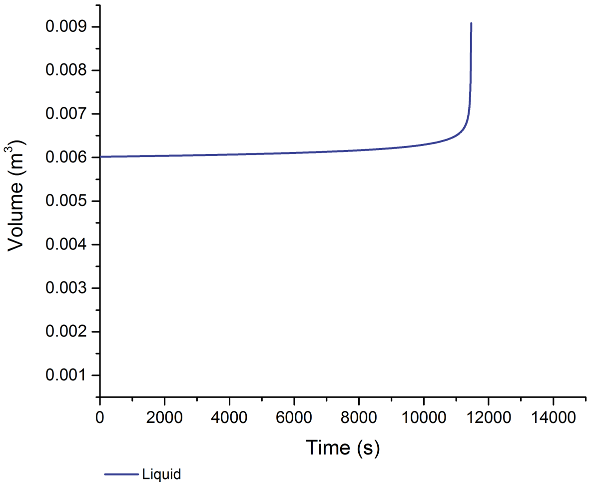

Figure 35. Liquid phase volume of the decomposition of 20wt% DTBP in Toluene in a closed vessel.

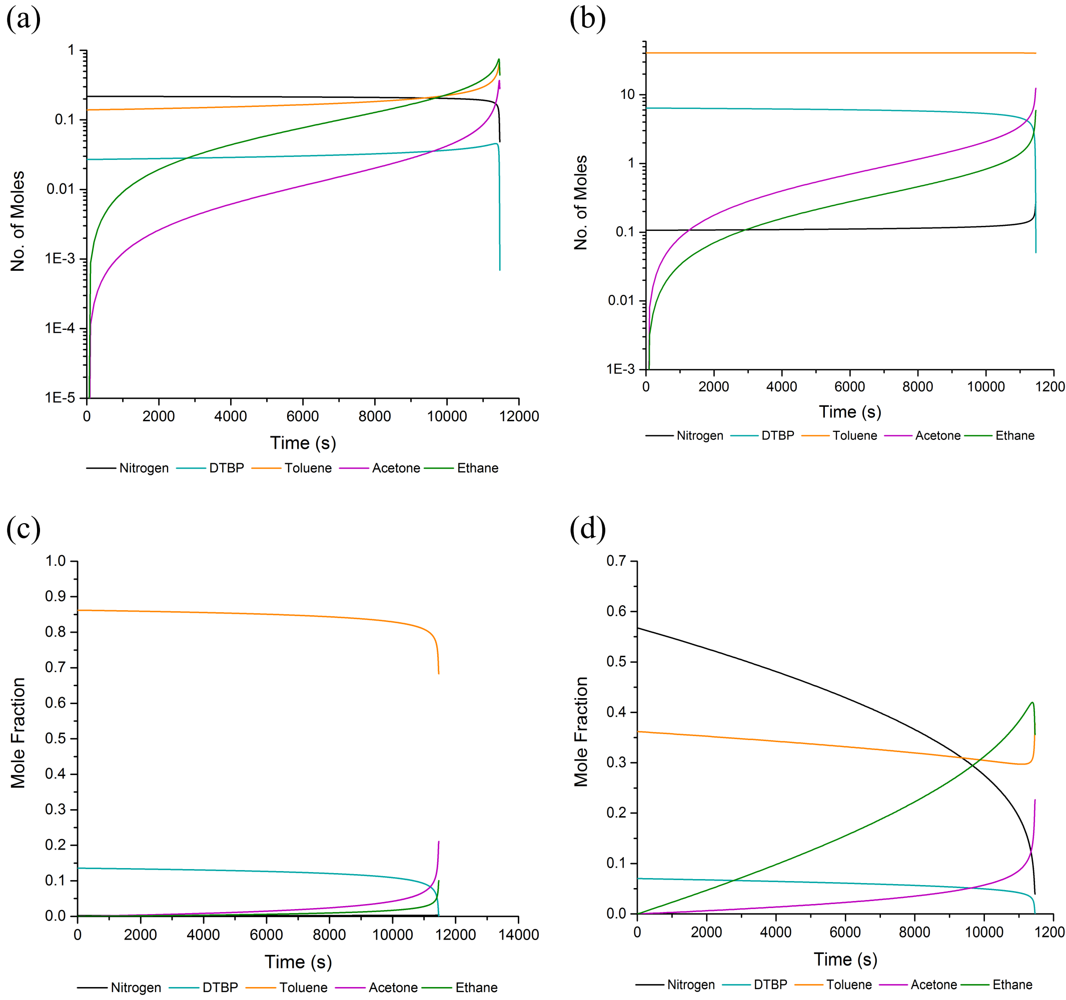

Figure 36. Profiles of (a) vapor component amounts, (b) liquid component amounts, (c) vapor phase mole fractions, (d) liquid phase mole fractions of the decomposition of 20wt% DTBP in Toluene in a closed vessel.

The simulation output also provides a history of the phase volumes within the vessel. The phase volumes at all times should add up to the total volume of the vessel, which was defined to be 0.01 m^3. This was observed at all times in all the test cases reported in this chapter. The liquid volume increases over time because for every mole of DTBP that decomposes two moles of acetone are generated, and thus the liquid phase becomes more acetone rich. This is shown in Figure 35.

The simulation results also provide information regarding the amounts of the components within the vessel as the reaction takes place in each phase, as shown Figure 35(a) – (b). The liquid phase is initially rich in DTBP and toluene, while the vapor phase is rich in nitrogen. The products, acetone and toluene, increase in a stoichiometric fashion, as the reaction evolves. Ethane, being the more volatile product has a larger presence in the vapor phase when looking at the mole fractions in Figure 35 (c) –(d). When looking just at the mole numbers, because of the high system pressure, the results show that ethane has a non-negligible liquid phase mole fraction.

8.3 Reference ERS venting simulation

Next, the vessel was simulated with an ERS device located on the lateral wall, at 0.264 m above the bottom of the tank. At such a high position and with no liquid surge, as assumed in this work, the vented fluid was always from the vapor phase within the vessel in the cases presented here. The reference ERS venting simulation case was chosen to be when the set pressure, P_{set} was 0.4MPa, and the area of the ERS, A_{ERS} was 1×10^{-4} m^2. This selection was based on previous work done by Casson et al [140].

The temperature and pressure profiles are given in Figure 36. The sharp and fast decrease of the temperature of the fluid in the vessel is captured, as a result of the sharp depressurization of the vessel at the set pressure of 0.4MPa. The maximum temperature reached is 410K. A vessel with an A_{ERS} of 1×10^{-4} m^2 allows for the system to behave in a tempered manner with the temperature following the pressure curve, confirming that general classification that DTBP in toluene is a tempered system.

Since the depressurization occurs over a small period of time, the integration variable here is not time, but a rapidly changing component within the vessel at this point due to venting. Figure 37 shows the temperature and pressure profiles, after the ERS opens, for both the vessel and at the ERS exit. Also, the tempering effect is quite clearly captured as the temperature and pressure within the vessel both decrease. When the pressure reaches atmospheric pressure, after which the simulation comes to an end. The temperature on the other hand drops by approximately 16 K. For this case, it takes about 14 seconds to depressurize the vessel.

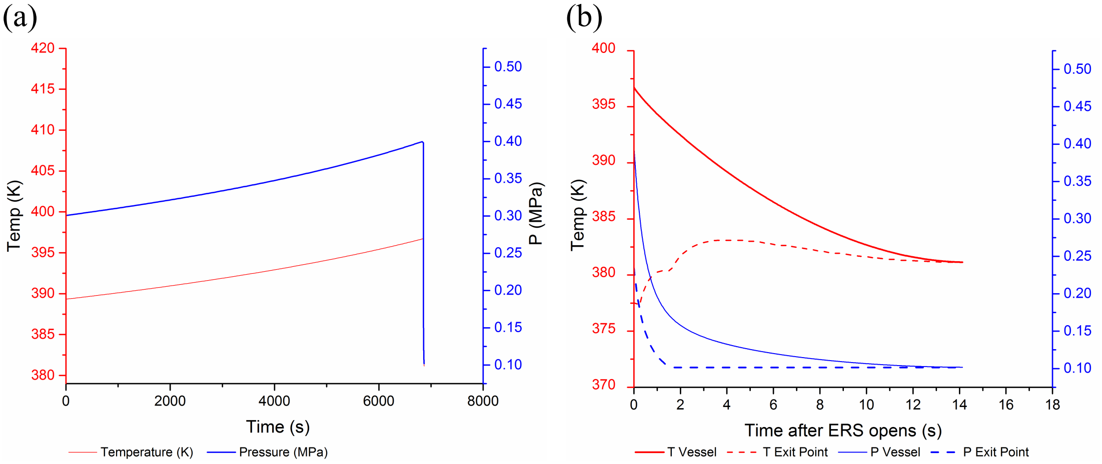

Figure 37. Temperature and pressure profiles of the decomposition of 20wt% DTBP in Toluene in a vessel equipped with an ERS with $A_{ERS} = 1\times10^{-4}$ m^2 and $P_{set} = 0.4MPa$: (a) full simulation time and (b) after ERS opens.

From Figure 37 it can be seen that the exit temperature and pressure are initially much lower than those within the vessel, with a value of 371 K for the exit temperature and 0.23 MPa for the exit pressure, which is expected. Despite complex parallel phenomena occurring during depressurization, the behavior at the ERS exit can be explained by the phase profiles as well as the fluid speed and sound speed profiles presented in Figure 38.

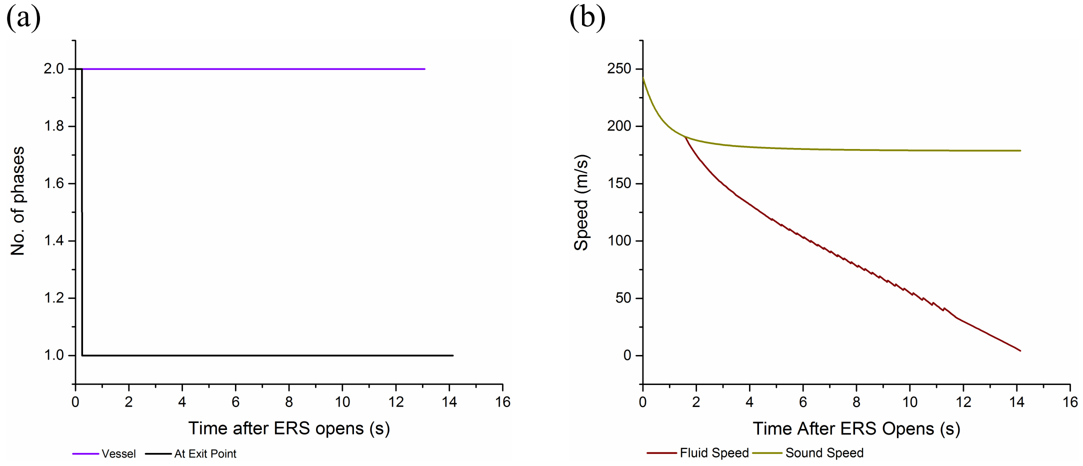

Figure 38. Profiles at the ERS exit of (a) number of phases (b) fluid and sound speeds for a vessel containing the decomposition of 20wt% DTBP in Toluene and equipped with an ERS with $A_{ERS} = 1\times10^{-4}$ m^2 and $P_{set} = 0.4$MPa.

As can be seen, the simulation predicts two-phase flow for about 0.2 seconds at the exit and then eliminates the second phase, so that there is only all vapor venting, while the vessel maintains two phases at all times. An independent flash problem was used to simulate the conditions at the exit point, confirming the transition from the two to the one-phase regime at about 0.2 seconds. Since the fluid is released at such a high pressure, partial condensation is a reasonable outcome.

Also, from Figure 38 , the fluid speed is initially sonic. At about 2 seconds, it becomes subsonic and the fluid temperature increases to compensate for the decrease in kinetic energy. As the pressure within the tank decreases, as seen in Figure 37, the pressure ratio moves away from the chocking ratio, and the fluid experiences a transition from sonic to subsonic flow. As the velocity suddenly decreases, this is compensated by an increase in enthalpy in order to satisfy the energy balance, thus explaining the second temperature increase at the ERS exit in Figure 37. There are some oscillations in the fluid speed curve during the time interval 7 – 15 seconds, which can be attributed to numerical instability. However, they do not hinder the overall trend of a decreasing fluid speed as the vessel depressurization is complete, reaching atmospheric pressure.

Also part of the output results, are the generation rates within the vessel. These rates are shown in Figure 39. The rates of toluene and nitrogen overlap, at zero, which is expected since they do not take part in the decomposition reaction. Also, the rate at which DTBP decomposes is the same as that which ethane forms as seen by the turquoise and green lines. The rate of acetone generation, shown in purple, is twice that of ethane.

These values agree with the stoichiometry of the reaction expression for the decomposition of DTBP used in these simulations. As the pressure in the vessel decreases due to venting, and as the DTBP amount within the vessel decreases, the generation rates approach zero.

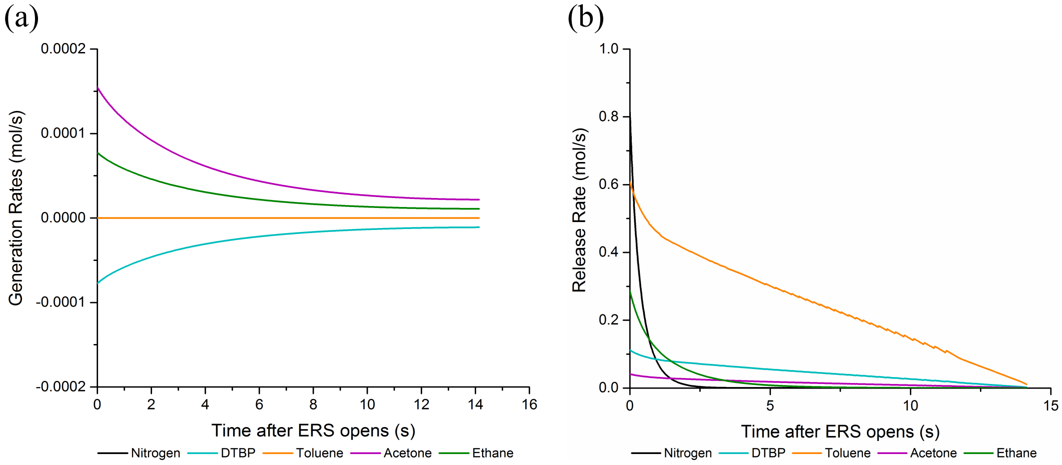

Figure 39. Profiles at the ERS exit of (a) generation rates (b) instantaneous release rate for a vessel containing the decomposition of 20wt% DTBP in Toluene and equipped with an ERS with $A_{ERS} = 1\times10^{-4}$ m^2 and $P_{set} = 0.4$MPa.

The instantaneous release rates and amounts are also given in Figure 39. The release rates are very high as soon as the ERS opens, which is expected. Then, at about 2 seconds, the time after which the fluid transitions to a subsonic speed, and with decreases in vessel pressure, the release rates are much slower. The release rate of nitrogen is the highest, since it is an inert and concentrates in the vapor phase, where the discharge takes place. All the other components experience similar rapid discharges until around 2 seconds, where the sonic-to-subsonic transition takes place, after which the rates approach zero. The sole exception is toluene, which experiences a rapidly decreasing release rate event after the transition. This could be due to the fact that it is also an inert, not taking part in the reaction. Despite the fact that toluene is an inert, it is the most plentiful component in the system, by far. Thus, even if its volatility is not that high at the problem conditions, there is so much of it that there is always a sizeable amount of it in the vapor.

This can further confirmed by looking at Figure 40, which shows the amounts released to the atmosphere as are result of the venting phenomena. The highest released amount is toluene, followed by DTBP. This is again attributed to the temperatures both in the vessel and at the exit point being close to their respective boiling points. The released amounts of nitrogen and ethane remain relatively constant after the transition to subsonic flow, and acetone experiences the least release. This is supported by its low release rate.

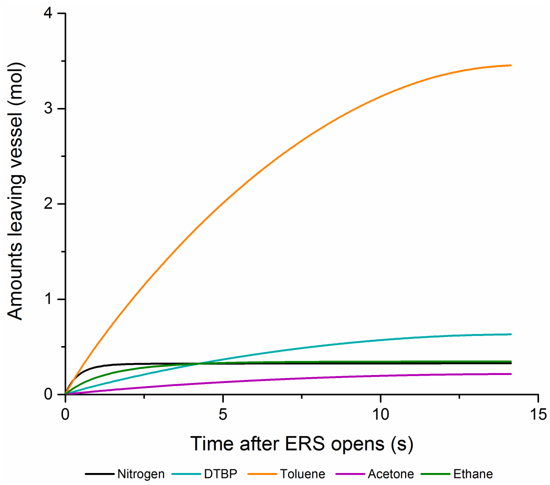

Figure 40. Released amounts profiles at the ERS exit of a vessel containing the decomposition of 20wt% DTBP in Toluene and equipped with an ERS with $A_{ERS} = 1\times10^{-4}$ m^2 and $P_{set} = 0.4MPa$.

8.4 Sensitivity of dynamic simulator to ERS relief area

8.4.1. Large ERS areas

The results and observations presented in the previous section were for a P_{set} of 0.4MPa, and an A_{ERS} of 1×10^{-4} m^2. In order to assess the effect of A_{ERS}, a sensitivity analysis was performed. For a constant P_{set} of 0.4MPa, simulations were run for the following values of the ERS area: 5×10^{-5}, 1×10^{-4}, 1.25×10^{-4}, 1.50×10^{-4}, 2×10^{-4} and 2.5×10^{-4} m^2. Their corresponding diameters are shown in Table 9

Table 9. List of simulated ERS areas and their corresponding diameters

Area of ERS (m^2)	Diameter of ERS (m)
0.00005	0.00798
0.00010	0.01128
0.00015	0.01382
0.00020	0.01596
0.00025	0.01784

Since the temperature and pressure developed within the vessel before the ERS opens is the same as those presented in section 8.2 for the closed vessel, only the time interval after the ERS opens is considered for analysis purposes. The collective temperature and pressure profiles for the depressurization of the vessel with varying ERS areas are shown in Figure 41. The first thing to note that is that because the set pressure is constant, the starting and end points for all the curves with respect to temperature and pressure are the same. The only differing factor is the time: as the area increases, the resulting temperature and pressure drop with in the vessel is much faster. For an A_{ERS} of 5×10^{-5} m^2, the time for vessel depressurize to atmospheric pressure is about 30 s.

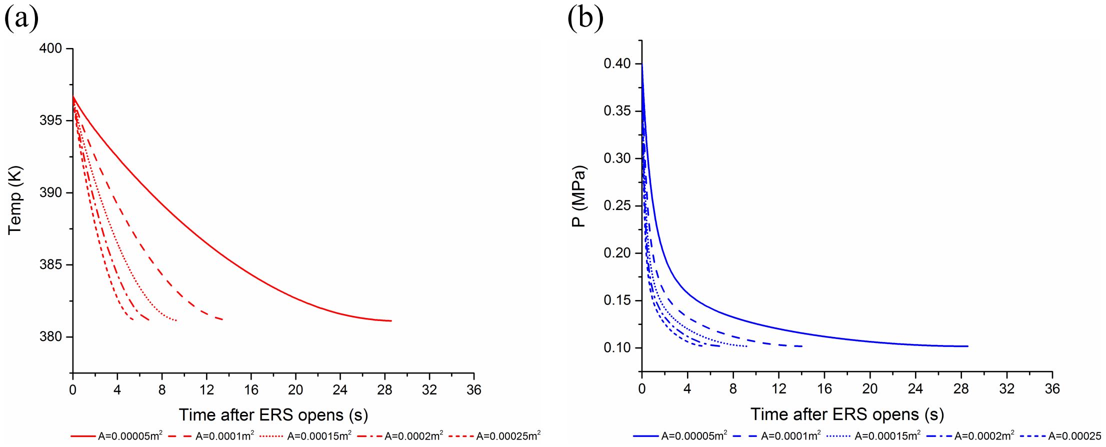

Figure 41. Profiles of (a) temperature and (b) pressure during depressurization of a vessel containing the decomposition of 20wt% DTBP in Toluene and equipped with an ERS with P_{set} = 0.4MPa.

When A_{ERS} is increased by a factor of 5, the vessel depressurize time is around 6 seconds. This means that as the A_{ERS} is increased by a factor of 5, the time it takes to depressurize the vessel to atmospheric pressure decreases by a factor of 5. Thus, the depressurization time is inversely proportional to the A_{ERS}. This is expected because the flow rate is linearly proportional to the ERS area in the model.

The effect of the ERS area can also be extended to the exit point conditions, whose temperature and pressure profiles are shown in Figure 42. The smaller the A_{ERS} is, the longer it takes for the temperature and pressure of the exiting fluid to drop. The time it takes for the temperature to drop at these exit and within the vessel is relatively the same for all areas. This is mainly due to the transition from sonic to subsonic flow, which is shown in Figure 42 for all ERS areas.

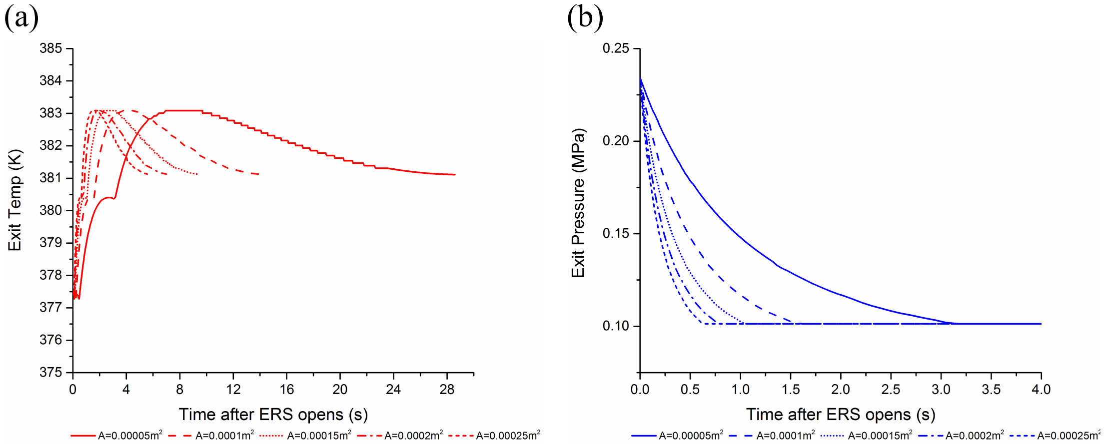

Figure 42. Profiles of ERS exit (a) temperature and (b) pressure during depressurization of a vessel containing the decomposition of 20wt% DTBP in Toluene and equipped with an ERS with $P_{set} = 0.4$MPa.

During this transition, the fluid velocity decreases, inducing an increase in enthalpy in order to satisfy the energy balance. The longer it takes for the flow to become subsonic, such as is the case for an A_{ERS} of 5×10^{-5} m^2, the less sharp the jump in temperature is. For larger values, like an A_{ERS} of 2.5×10^{-4} m^2, the pressure decrease of the exit stream (Figure 42) is so rapid (~ 0.5s), and therefore the transition from choked to non-choked (Figure 43) flow is equally rapid, the resulting temperature increase is sharp (Figure 42).

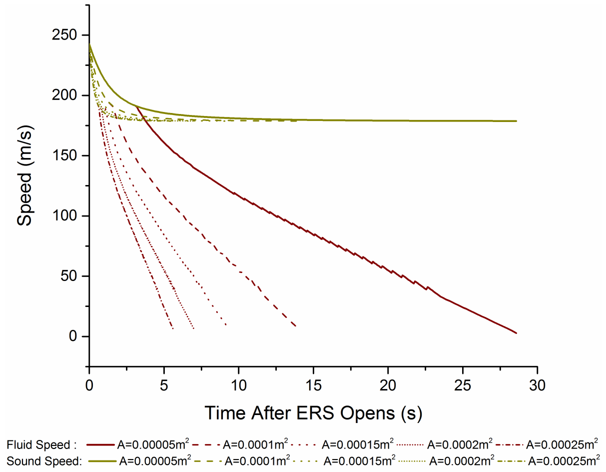

Figure 43. ERS exit fluid and sound speed profiles for depressurization of a vessel containing the decomposition of 20wt% DTBP in Toluene and equipped with an ERS with P_{set} = 0.4MPa.

8.4.2. Intermediate and small ERS areas

Perhaps what is more interesting to note is that for all the ERS areas used, the system remains tempered, with the temperature and pressure decreasing at the same time. This means that all the ERS areas used for this sensitivity analysis can fully depressurize the vessel, and act as adequate relief. Thus, more simulations were run with much smaller values of A_{ERS} using the same vessel specifications. The areas chosen and their corresponding diameters are shown in Table 10

Table 10. List of simulated ERS areas and their corresponding diameters

Area of ERS (m^2)	Diameter of ERS (m)
9.62113×10^{-8}	0.00035
7.06858×10^{-8}	0.00030
4.90874×10^{-8}	0.00025
3.14159×10^{-8}	0.00020

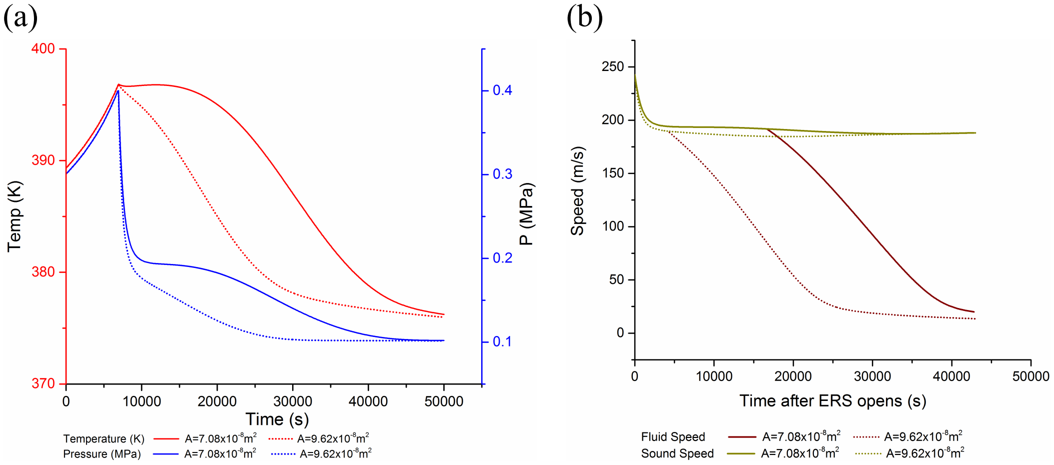

Figure 44. Profiles of (a) temperature and pressure (b) fluid and sound speed during depressurization of a vessel containing the decomposition of 20wt% DTBP in Toluene and equipped an ERS with P_{set} = 0.4MPa and intermediate ERS areas.

The analysis of the areas will be coupled such that the results for ERS areas of 9.62×10^{-8} m^2 and 7.07×10^{-8} m^2 (intermediate areas) will be discussed together, and 4.91×10^{-8} m^2 and 3.14×10^{-8} m^2 (small areas) will also be discussed together. The temperature and pressure profiles in the vessel with for the intermediate ERS areas are given in Figure 44 (a). For both areas, the pressure drops at the set pressure of 0.4 MPa at about 10,000 seconds.

For an A_{ERS} of 9.62×10^{-8} m^2 the resulting pressure drop is not enough to depressurize the vessel to atmospheric pressure, but only to 0.2 MPa right after the ERS opening. Then, there is a significant change in the slope of pressure profile, where by it takes the vessel about 20,000 seconds in order for the vessel pressure to reach atmospheric pressure after the ERS opens. The temperature profile does not exactly follow the pressure profile, in that there is no drastic temperature decrease because of the ERS opening. Rather, the temperature drops at a more or less constant rate throughout (about 20 K over a period of 20,000 seconds), until the vessel pressure becomes equivalent to atmospheric, and the simulations ends.

Similarly, for an A_{ERS} of 7.07×10^{-8} m^2 the resulting pressure drop is not enough to depressurize the vessel to atmospheric pressure, but only to 0.2 MPa right after the ERS opening. Then, the pressure passes through a minimum value and increases afterwards, only to decrease once again. The temperature however does not follow the pressure curve. It experiences a very small dip at the opening of the ERS, slowly starts to increase, then passes through a maximum, after which it decreases again. The increase comes about because the ERS area has no lasting effect on the temperature, and thus cannot override the governing decomposition reaction kinetics. There is also a small increase in pressure due to gas generation, but because of constant venting through the now open ERS, the pressure decreases to atmospheric once again. This result indicates that a system cannot be classified as ‘tempered’ solely based on the chemicals involved, as the area of the ERS plays an important role in drawing the line between tempered and untempered behavior.

The fluid and sound speed of the exit streams are shown in Figure 44 (b). The transition from sonic to subsonic or chocked to non-choked flow is much delayed when using a smaller ERS area, which is acceptable because the pressure in the vessel drops much slower when the ERS area decreases. Figure 46 shows the exit temperature and pressure profiles, the amounts leaving the vessel, as well as the amounts remaining within the vessel for both intermediate areas. The temperature experiences a maximum, and then starts to decrease at the same rate that the temperature in the vessel is also decreasing. For an ERS area A_{ERS} of 7.07×10^{-8} m^2, it takes much longer for the exit temperature to decrease than for an ERS area of 9.62×10^{-8} m^2. At the transition regions between choked to non-choked flow, there is a small increase again in temperature, but not as significant as with the larger areas. This is explained by the fact that high fluid flow speeds are associated with low temperatures in order to maintain the energy balance, and vice versa. The pressure takes 15000 seconds longer to reach atmospheric pressure with an A_{ERS} of 7.07×10^{-8} m^2 and, thus, more mass is vented with the smaller area, as seen in Figure 46. Also, when looking at the amounts remaining within the vessel, or more particularly ethane as it is the more volatile of the two products, it decreases as the ERS area increases. It can also be seen that all the nitrogen was vented out, with the smaller ERS area taking longer to vent out the same nitrogen quantity.

The temperature and pressure profiles, as well as the fluid speed profiles in the vessel with for the small ERS areas are given in Figure 47. For both areas, the pressure drops at the set pressure of 0.4 MPa at about 7,000 seconds. When the ERS area is 4.91×10^{-8} m^2, the effect of the ERS opening is more pronounced on the temperature and pressure curves, such that there is a defined dip in both properties. The property curves experience a second pressure peak at 2.5 MPa as a result of the temperature increase to 490K.

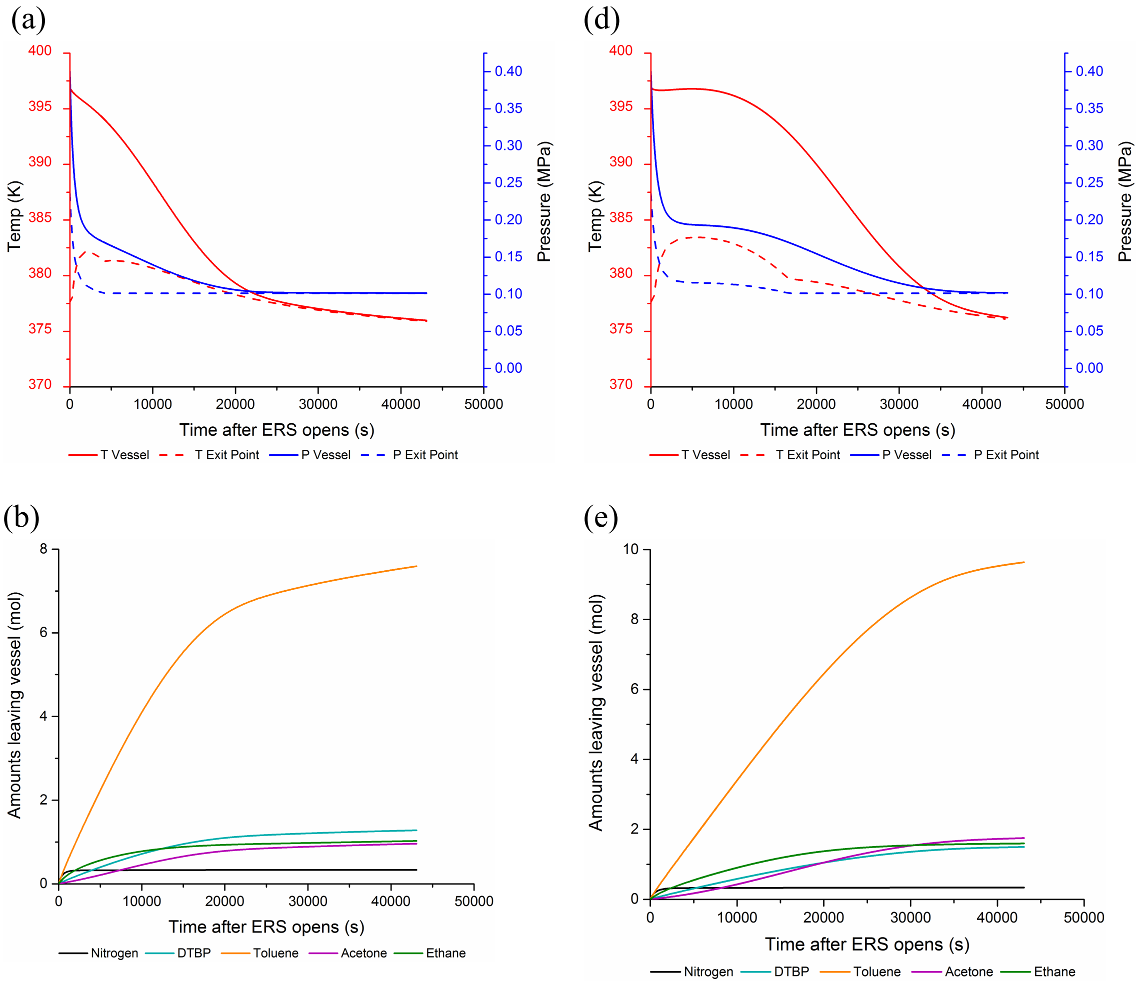

Figure 45. Vessel containing the decomposition of 20 wt% DTBP in Toluene and equipped with an ERS with $P_{set} = 0.4$MPa. For an A_{ERS} of 9.62×10^{-8} m^2 : (a) ERS exit temperature and pressure profiles, (b) profile of amounts leaving, and (c) total amounts in the vessel. For an A_{ERS} of 7.07×10^{-8} m^2: (d) ERS exit temperature and pressure profiles, (e) profile of amounts leaving, and (f) total amounts in the vessel.

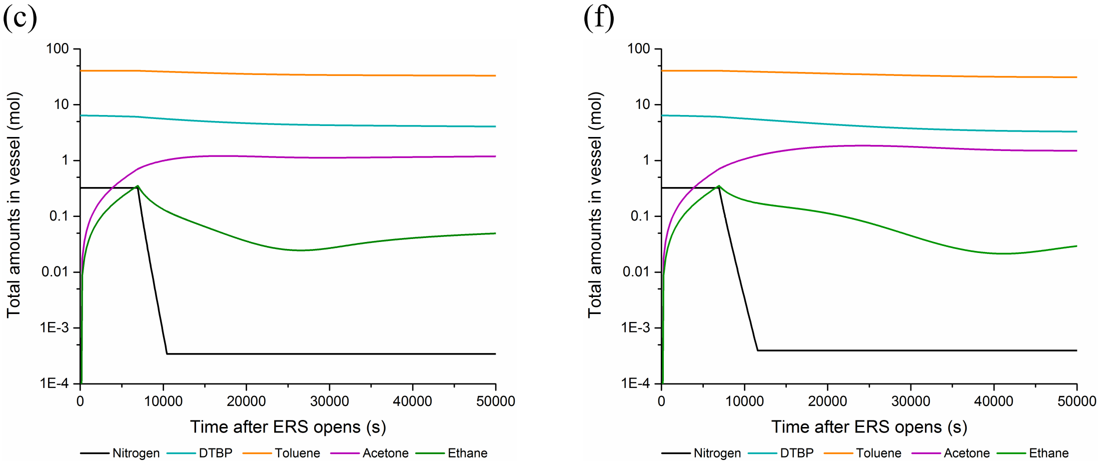

Figure 46. Vessel containing the decomposition of 20 wt% DTBP in Toluene and equipped with an ERS with P_{set} = 0.4MPa. For an A_{ERS} of 9.62×10^{-8} m^2 : (a) ERS exit temperature and pressure profiles, (b) profile of amounts leaving, and (c) total amounts in the vessel. For an A_{ERS} of 7.07×10^{-8} m^2: (d) ERS exit temperature and pressure profiles, (e) profile of amounts leaving, and (f) total amounts in the vessel.

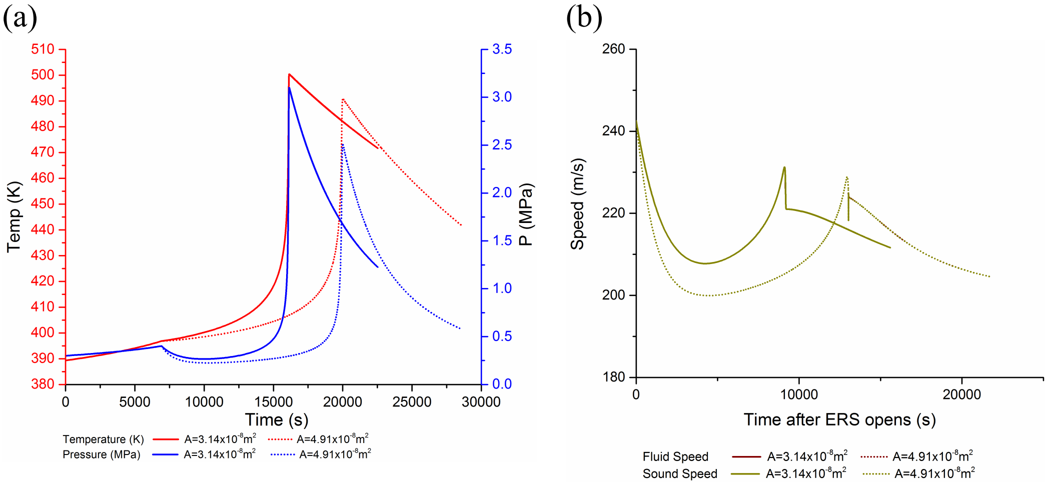

Figure 47. Profiles of the (a) temperature and pressure (b) fluid and sound speed during depressurization of a vessel containing the decomposition of 20wt% DTBP in Toluene and equipped an ERS with P_{set} = 0.4MPa and small ERS areas.

In the case of an ERS area of 3.14×10^{-8} m^2, the act of venting drops the pressure only slightly because it builds up again. This is because the venting had almost no impact on the temperature, which increases due to the kinetics of the reaction, generating a sharp temperature increase to 500 K, and a corresponding second pressure peak at 3.25MPa. It can thus be concluded that the smaller the area, the larger and the faster the temperature and pressure increase.

To better understand the fluid and sound speed profiles, the phase change profiles for the small ERS areas are shown in Figure 48. The flow throughout the simulated time period is sonic, as the fluid speed curve in maroon overlaps the sound speed curve in olive green. Both curves experience a minimum at around the time where the ERS opens. The smaller ERS area of 3.14×10^{-8} m^2 experiences much higher velocities, because its temperature and pressure starts to build up much earlier due to inadequate venting. The sharp peaks in both fluid speed curves can be explained by the phase changes that occur at those times.

Initially the sound speed starts to decrease because the pressure in the tank is decreasing, albeit at a slow rate. The temperature however is still increasing, and thus the reaction is generating gaseous products that cause the pressure within the vessel to increase once again. The fluid and sound speeds increase again, and only experience a sudden drop when a second phase appears at around 9,000 seconds for an area of 3.14×10^{-8} m^2 and at around 13,000s for an area of 4.91×10^{-8} m^2. This result is expected as phase addition can cause abrupt changes in sound speeds. Single phase discharge immediately followed by two-phase flow during reactor top venting, for a short time is normal, and is attributed to liquid entrainment of droplets or condensation of vapors in the nozzle [141]. Since the model does not account for liquid entrainment, condensation is the most likely cause for two-phase flow discharge. Also, it should be noted that the two phase flow region after single phase venting cannot be attributed to numerical inaccuracy/anomaly, and is indeed a sustained result as there were enough sampled points.

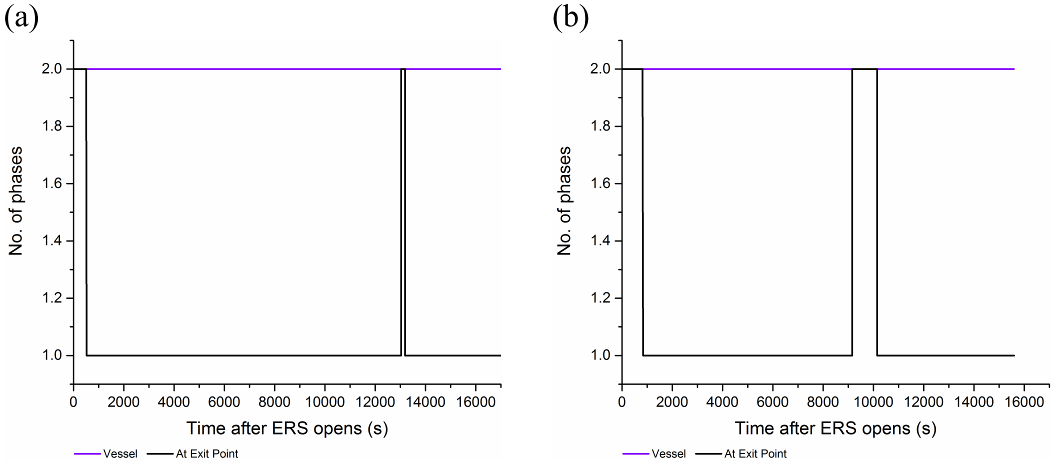

Figure 48. Vessel and ERS exit phase change profiles for depressurization of a vessel containing the decomposition of 20wt% DTBP in Toluene and equipped with an ERS with P_{set} = 0.4MPa and (a) A_{ERS} of 4.91×10^{-8} m^2 (b) A_{ERS} of 3.14×10^{-8} m^2

Figure 50 shows the exit temperature and pressure profiles, the amounts leaving the vessel, as well as the amounts remaining within the vessel for both intermediate areas. A larger ERS area means a large release to the atmosphere. Also, it should be noted that the change in slope of the exit temperatures (at around 1000s for A_{ERS} =

3.14×10^{-8} m^2 and at about 500s for $A_{ERS} = 4.91 \times 10^{-8}$ m^2) is due to the appearance of a second phase at the same aforementioned times.

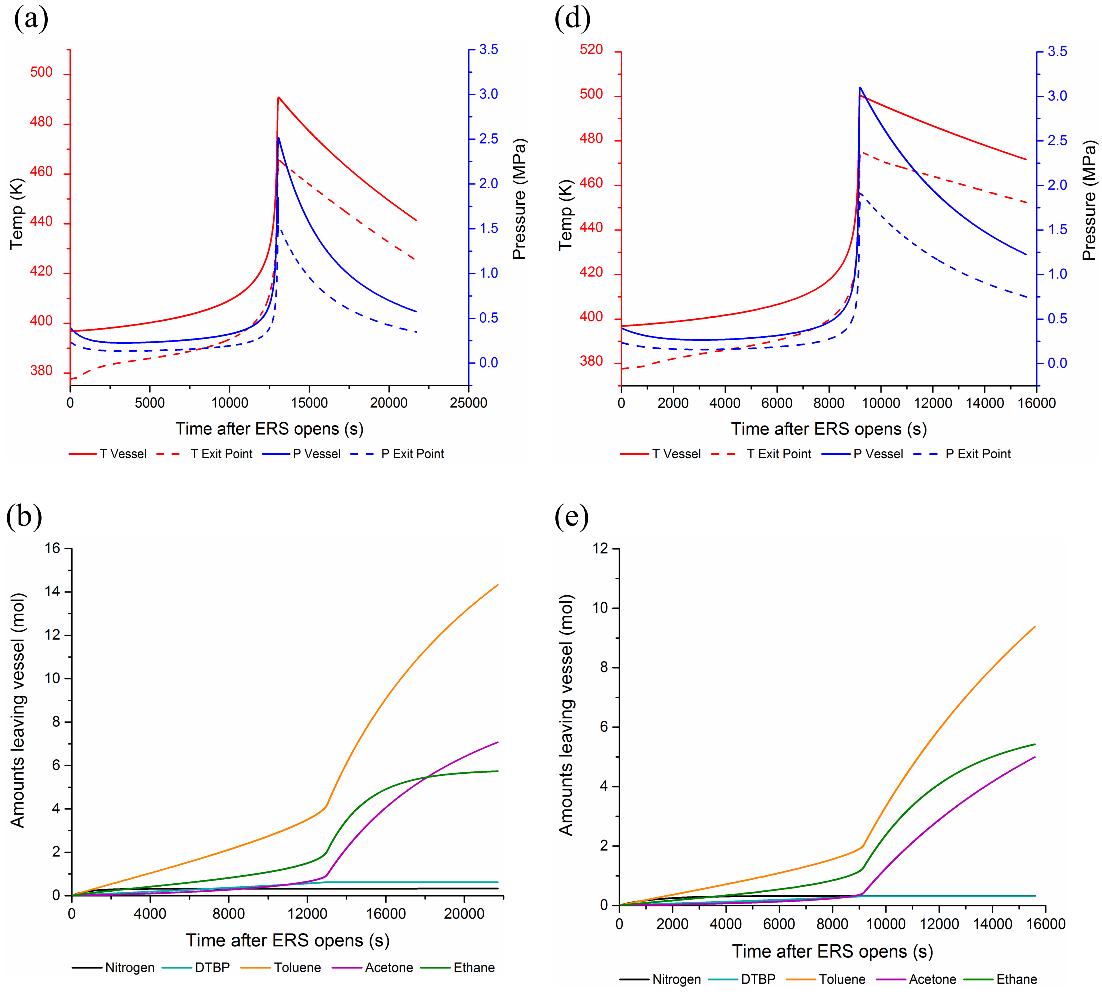

Figure 49. Vessel containing the decomposition of 20wt% DTBP in Toluene and equipped with an ERS with $P_{set} = 0.4$MPa. For an A_{ERS} of 4.91×10^{-8} m^2 : (a) ERS exit temperature and pressure profiles, (b) profile of amounts leaving, and (c) total amounts in the vessel. For an A_{ERS} of 3.14×10^{-8} m^2 : (d) ERS exit temperature and pressure profiles, (e) profile of amounts leaving, and (f) total amounts in the vessel.

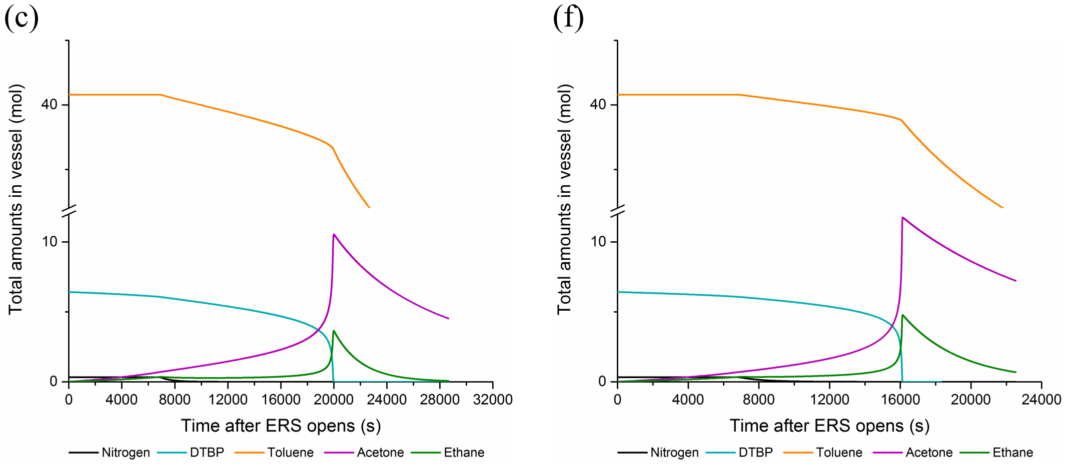

Figure 50. Vessel containing the decomposition of 20wt% DTBP in Toluene and equipped with an ERS with $P_{set} = 0.4MPa$. For an A_{ERS} of 4.91×10^{-8} m^2 : (a) ERS exit temperature and pressure profiles, (b) profile of amounts leaving, and (c) total amounts in the vessel. For an A_{ERS} of 3.14×10^{-8} m^2 : (d) ERS exit temperature and pressure profiles, (e) profile of amounts leaving, and (f) total amounts in the vessel.

When looking at the released amounts and the amounts remaining within the vessel, the amount of DTBP that is released with the smaller ERS area is very minute, as most of it is involved in the reaction within the vessel. When the amount of DTBP has been fully depleted, the reaction is complete. Thus, the remaining components experience a change of slope, resulting from no more generation, to counter the amount being vented. As the reaction comes to completion, for both areas, it can be seen that the temperature and pressures start to decrease as shown in Figure 50.

8.4.3. Sensitivity of dynamic simulations to ERS set pressure

The results and observations presented thus far show the predicted effect of the relief valve diameter on the resulting temperature and pressure of the fluid within the vessel. In order to predict the effect of different set pressures, P_{set}, of the ERS, a sensitivity analysis was performed with a fixed A_{ERS} of 1×10^{-4} m^2. Since the starting pressure within the vessel was already at 0.3 MPa, the chosen ERS set pressures were 0.4 MPa, 0.5 MPa and 0.6 MPa.

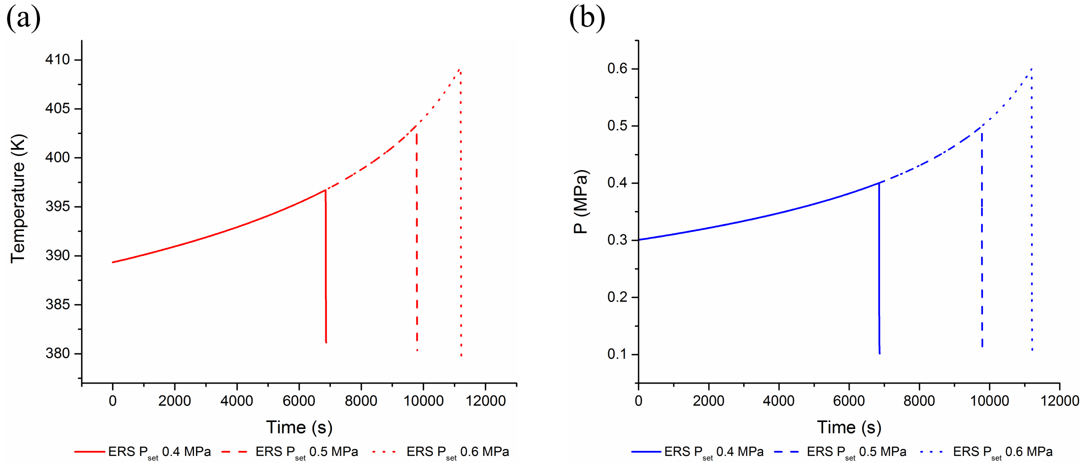

Figure 51. Profiles of the (a) temperature and (b) pressure during the decomposition of 20wt% DTBP in Toluene in a vessel equipped with an ERS with $A_{ERS} = 1\times10^{-4}$ m^2 and varying P_{set}.

Figure 51 shows the resulting temperature and pressure profiles, respectively, as P_{set} increases. It can be seen that the earlier the vent opens, the less developed the temperature and pressure profiles are. As can be seen, the time it takes for the pressure to reach 0.4 MPa is around 7,000 seconds, for 0.5MPa the time is around 9,800 seconds and for 0.6MPa the time is 11,000 seconds. This decrease in time intervals between one set pressure to a higher one is due to the exponential nature of the increase in temperature.

Figure 53 shows that changes in vessel temperatures and pressures during depressurization, as well changes in ERS exit point temperature and pressure profiles as the set pressure increases. With higher set pressures, it naturally takes longer for the vessel pressure to reach atmospheric conditions, and thus the vessel temperature profile at higher pressures cools down much slower. In fact, for a P_{set} of 0.4 MPa it takes 14 seconds for the vessel to depressurize, while for a P_{set} of 0.5 MPa it takes 17 seconds, and for a P_{set} of 0.6 MPa it takes 19 seconds.

When looking at the exit conditions, the temperature experiences a small drop because there is a change from a two phase flow regime to single phase at roughly 0.3 seconds or so for each curve as shown in the phase profiles in Figure 53 (f). As the sound speed experiences a minimum, the temperature experiences a maximum and starts to decrease. At the point where the flow changes from choked to non-choked, there is a sudden drop from sonic velocity to subsonic velocity. This is compensated by an increase in enthalpy in order to satisfy the energy balance, and thus a second spike in the fluid temperature.

Figure 54 shows the amounts leaving the vessel at the ERS exit. The curves are presented using a logarithmic scale in order to be able to fully capture all the components. Nitrogen, which exists mostly in the vapor phase is released at the beginning, then the cumulative amount remains constant because it is not released anymore. However, at higher pressures and subsequently temperatures, it takes longer for the pressure to reach atmospheric conditions, and thus there is more time for material to flow from the vessel. The dotted lines, signifying a P_{set} of 0.6 MPa are always higher than the remaining curves. At higher temperatures, more acetone and ethane can be vented as well.

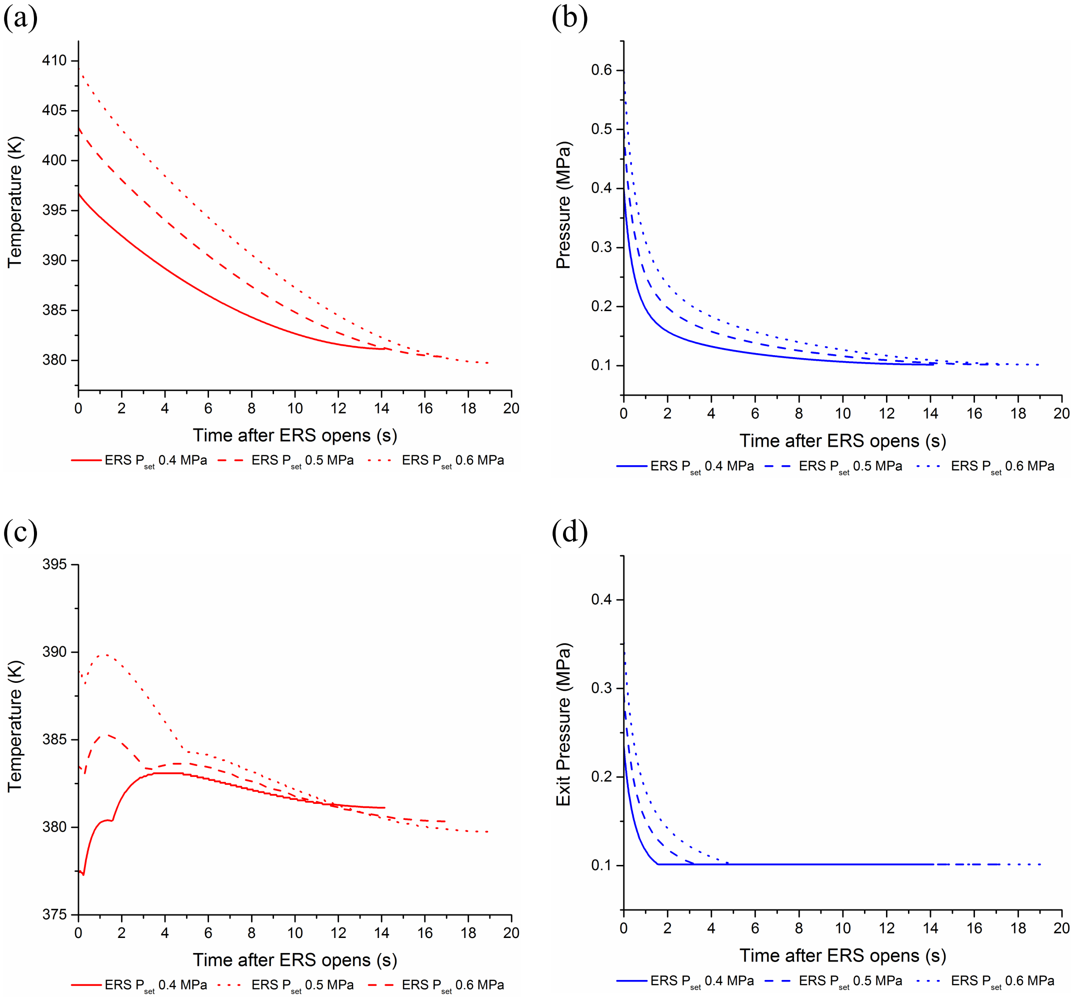

Figure 52. Vessel containing the decomposition of 20wt% DTBP in Toluene and equipped with an ERS with $A_{ERS} = 1\times10^{-4}$ m^2 and varying P_{set}: (a) vessel temperature profiles; (b) vessel pressure profiles; (c) ERS exit temperature profiles; (d) ERS exit pressure profiles; (e) fluid and sound speeds; (f) phase profiles in the vessel and at the ERS exit.

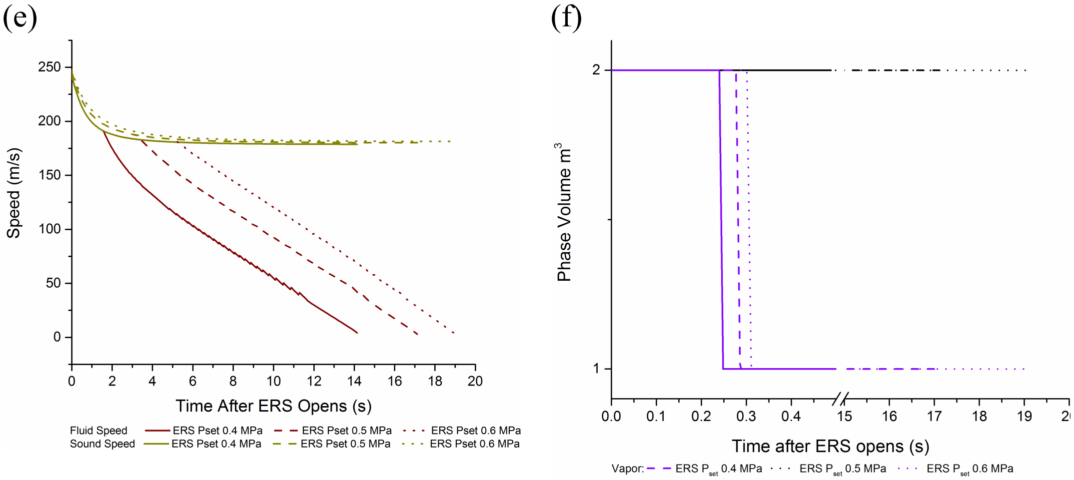

(e)

(f)

Figure 53. Vessel containing the decomposition of 20wt% DTBP in Toluene and equipped with an ERS with $A_{ERS} = 1\times10^{-4}$ m^2 and varying P_{set}: (a) vessel temperature profiles; (b) vessel pressure profiles; (c) ERS exit temperature profiles; (d) ERS exit pressure profiles; (e) fluid and sound speeds; (f) phase profiles in the vessel and at the ERS exit.

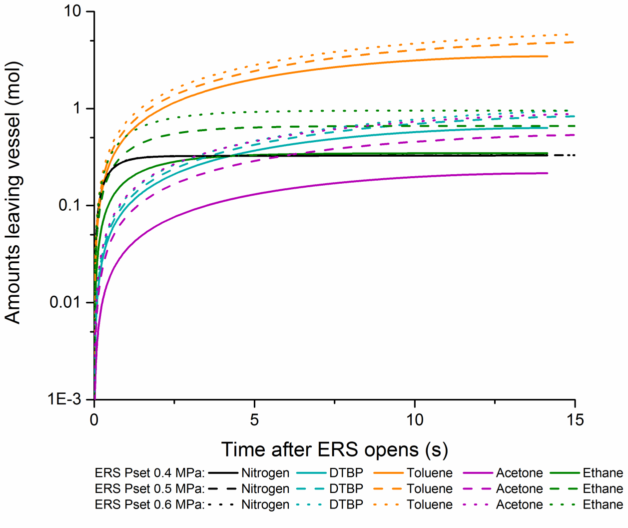

Figure 54. Amounts leaving the vessel at the ERS exit profiles of the decomposition of 20wt% DTBP in Toluene inside a vessel equipped with an ERS with $A_{ERS} = 1\times10^{-4}$ m^2 and varying P_{set}.

8.5 Key observations

A full sensitivity analysis conducted was done for all the large diameters and set pressures discussed in this section. Due to similar trends and behaviors, not all the results were shown, since the results presented are enough to illustrate several points.

The first of which is the fact these simulations results are based on a simplified global kinetic expression that does not include any side reaction. This presents limitations in the full developed of the temperature and pressure profiles.

Despite this, they provide a good description of vessel behavior and depressurization phenomena. For large ERS areas, the simulated system remains tempered all times, with the decrease in vessel pressure subsequently inducing a decrease in temperature in a matter of seconds. Also, there exist intermediate areas wherein the system temperature will not experience a sharp drop, but rather stagnate and gradually drop at a very slow pace. In this case, the time it takes for the temperature to lower is in the order of hours. This may or may not be acceptable depending on many aspects, such as the process used and the risks it poses. At small areas, a second pressure peak could be observed, and the temperature continues to run away.

When the ERS set pressure was changed, it was observed that the higher the set pressure, the higher the resulting temperature in the vessel. Thus, it takes longer for the pressure to reach atmospheric conditions, and thus there is more time for material to flow from the vessel. This is a problem if the material is hazardous, or if the critical runaway temperature is reached.

CHAPTER IX

CONCLUSIONS

The need for more information on emergency relief system sizing for reactive systems was identified over 20 years ago [142]. Since then, a considerable amount of research has been carried out on the subject, particularly in the US by the Design Institute for Emergency Relief Systems (DIERS). However, there is still a need for more information on the design methods, particularly given the limitation of current models, and their tendency to oversize ERS, particularly for gassy/hybrid systems. These limitations give rise to the need for dynamic models that utilize: (i) rigorous thermodynamics to evaluate component and mixture properties, (ii) adiabatic calorimetric data for model validation with respect to temperature and pressure profiles; (iii) a kinetic model that describes the evolution of the reaction; (iv) a level swell model that describes the rise of bubbles, and swell of the liquid-vapor interface; and (v) a two-phase flow model.

The procedure proposed in this study uses rigorous evaluations of the thermodynamics properties of fluids inside the vessel and at the exit points, a simplified global kinetic expression to describe the reaction progression with parameters (i.e. the activation energy, pre-exponential factor and reaction order) based on experimental data, and a two phase model based on sound speed calculations in multiphase systems to establish the number of phases and choking conditions. Level swell, however, was not considered in this work. Also, due to an overall simplified kinetic expression, side reactions were not included.

The output of the proposed model quantifies several properties of the fluid inside the vessel and at each exit point. The properties of the fluid in the vessel computed during the simulations include the temperature, pressure, number of phases, and phase volumes, amounts, and compositions. The properties of the fluids at each exit point include the local temperature and pressure, number of phases, molar volume, instantaneous flow rates of each component, and cumulative amounts that enter or leave the vessel through each input or output stream. This information allow for a detailed assessment of the vessel behavior during relief venting and provides valuable information about the source term in simulations of the environmental dispersion of chemicals. The results of this work can be used to enhance ERS design methods, and in the planning for emergencies that involve the release of hazardous chemicals.

The closed vessel simulations show a relatively good agreement with closed vessel adiabatic experimental data. It should be noted that the simulated pressure and temperature profiles are not as fully developed as the experimental curves. This is due to the use of simplified kinetics, which does not allow for the consideration of side reactions that may contribute to increased gas generation, and some numerical instability that stops the simulations just shy of completion. The source of such numerical instability can be attributed to various reasons. Perhaps the most influential of which is that there is no general criteria for choosing the limiting amount of a component, such that it can no longer become a viable integration variable. An arbitrary cut-off was chosen for the simulations in this work. Thus, together, these limitations do not allow for a ‘perfect’ comparison with experimental profiles. However, for the purpose of this work, the results are acceptable.

Sensitivity studies, when no experimental data were available for comparison, showed numerical results that follow meaningful qualitative trends. The main parameters studied in this work, were the effect of the ERS area and the ERS set pressure on the depressurization of the vessel, and exit point conditions. Also, the results shed light on the intrinsic classification of ‘tempering’ based on the chemical reaction involved.

For large ERS areas, the simulated system remains tempered all times, with sharp decreases in vessel pressure to atmospheric pressure in the order of seconds. As a result, the vessel temperature also experiences a sharp drop. For intermediate ERS areas, the system pressure experiences a sharp drop, but the vessel pressure does reach atmospheric pressure. This is because the sudden drop in pressure does not induce a sharp drop in temperature, allowing the reaction to continue at high temperature. This increases the gas production rate, and contributes to the total vessel pressure, despite depressurization via ERS. Depending on the intermediate ERS area, the temperature either experiences a small increase or stagnates before gradually drop at a very slow pace. In this case, the time it takes for the temperature to decrease is in the order of hours. This may or may not be acceptable depending on many aspects, such as the process used and the risks associated. At small ERS areas, a second pressure peak was observed, and the temperature experiences a small change in slope during relief action, but since this is inadequate, the runaway occurs. This leads to the conclusion that it is not the nature of the chemical system, but in fact, the ERS area that governs whether a system behaves in a tempered or untempered manner.

When the ERS set pressure was changed, it was observed that the higher the pressure, the higher the temperature in the vessel. Thus, it takes longer for the pressure to reach atmospheric conditions, and thus there is more time for material to flow from the vessel. This is a problem if the material is hazardous or if the critical runaway temperature is reached.

Experience accumulated throughout this study has demonstrated that the program runs well for several cases, however, it should be noted that the most time consuming element of these simulations was the evaluation of component flow rates during choked (sonic) releases. This computation requires the solution of a flash problem with specified values of enthalpy and entropy, which is solved using nested loops in the current version of the simulator.

The numerical and scientific limitations of this model give possibility for future developments, outlined in the next section.

CHAPTER X

FUTURE WORK

In order to reduce numerical instability arising from the nested loops in the flash calculations with specified values of enthalpy and entropy, it recommended that single loop be used, with the nested loops acting as a back-up method in the cases of slow or non-convergence. This is the way the isochoric-isoenergetic (UV$\underline{N}$) flash is currently implemented, and it leads to much faster numerical calculations. It should be noted that this is currently under development. Also, a more global criterion of selecting limiting quantities of component, for it to be a viable integration variable should be considered. This could reduce instability and allow for the reaction in the simulations to reach completion.

From the simulations carried out and the results obtained, it is clear that there is a need to test other parameters besides the ERS area and set pressure. This includes utilizing the ability of the model to accommodate different vessel shapes (spherical, horizontal, etc) as well as the study of the effect of secondary venting system represented by a permanent orifice. The current model has not been tested with two exit points, but, in principle, should be able to handle such cases. Moreover, the effect of the fill level can be studied. Of course, this would require a more comprehensive experimental study, in order to validate the results obtained, and obtain good reproducibility, especially at the adiabatic stage. In additions, the effect of an external fire should also be tested, as the model is equipped to handle such cases as well. It is also recommended that different chemical systems should be studied in order to confirm the results of this study.

Furthermore, a more comprehensive kinetic study is required in order to be able to model what takes place experimentally. This requires the use of thermogravimetric analysis (TGA) in order to be able to confirm reaction products. Then based on these studies, the inclusion of secondary side reactions that may contribute to the overall gas production rate should be considered. Also, further studies need to be conducted to predict the order of the reaction. In this work, and in much of discussed literature, this value was simply taken to be 1, based on the global behavior of the system.

Finally, the addition of level swell phenomena, which was overlooked in this study, will provide deeper insight into the behavior of the hydrodynamics of the vessel, and the occurrence of two-phase flow. This will greatly affect the choice of size for the ERS system in place.

REFERENCES

[1] J. Barton and R. Rogers, *Chemical Reaction Hazards*, 2nd ed. Wiltshire: Gulf Professional Publishing, 1997.

[2] D. A. Crowl and J. F. Louvar, *Chemical Process Safety: Fundamentals with Applications*, Third Edit. 2011.

[3] J. Etchells and J. Wilday, *Workbook for Chemical Reactor Relief System Sizing*. HSE,Health & Safety Executive, 1998.

[4] HSE, "HSE: Information about health and safety at work." [Online]. Available: http://www.hse.gov.uk/. [Accessed: 20-Aug-2013].

[5] J. C. Leung, "Venting of Runaway Reactions with Gas Generation," *AIChe J.*, vol. 38, no. 5, pp. 723–732, 1992.

[6] H. K. Fauske, "Revisiting DIERS' two-phase methodology for reactive systems twenty years later," *Process Saf. Prog.*, vol. 25, no. 3, pp. 180–188, 2006.

[7] G. B. Wallis, *One-dimensional two-phase flow*. McGraw-Hill, 1969.

[8] L. Raimondi, "Rigorous Calculation of Critical Flow Conditions for Pressure Safety Devices," *Process Saf. Environ. Prot.*, vol. 85, no. 4, pp. 277–288, 2007.

[9] J. Vilchez, S. Sevilla, H. Montiel, and J. Casal, "Historical analysis of accidents in chemical plants and in the transportation of hazardous materials," *J. Loss Prev. Process Ind.*, vol. 8, no. 2, pp. 87–96, 1995.

[10] U.S. Chemical Safety And Hazard Investigation Board, "Investigation report - T2 Laboratories, Inc. - Runaway Reaction (Four Killed, 32 Injured) - Report No. 2008-3-I-FL," 2009.

[11] P. C. Bowes, *Self-heating: Evaluating and Controlling the Hazards*. Amsterdam: Elsevier, 1984.

[12] F. Fei and D. Liang, "Research progress and comparison of methods for testing self ignition materials," in *Procedia Engineering*, 2011, vol. 11, pp. 91–99.

[13] V. Casson-Moreno, "Analisi Della Decomposizione Di Perossidi Con Tecniche Di Screening Calorimetrico," Universita Delgi Studi Di Padova, 2008.

[14] D. A. Frank-Kamenetskii, *Diffusion and Heat Transfer in Chemical Kinetics*, 2nd Editio. Plenum Press, NY, 1969.

[15] J. C. Jones, “Calculation of the Frank–Kamenetskii critical parameter for a cubic reactant shape from experimental results on bituminous coals,” *Fuel*, vol. 78, no. 1, pp. 89–91, 1999.

[16] P. F. Beever, “Self-heating and spontaneous combustion,” in *SFPE Handbook of Fire Protection Engineering*, 2nd ed., P. J. DiNenno, Ed. Quincy, Mass.; Boston, Mass.: National Fire Protection Association ; Society of Fire Protection Engineers, 1995, pp. 180–189.

[17] HarsNet, *Safety Engineering in Practice Vol. 6: HarsBook, A technical guide for the assessment of highly reactive chemical systems.* Frankfurt: Dechema e.V, 2002.

[18] HarsNet, “HarsBook.” [Online]. Available: http://www.harsnet.net/harsbook/harsbook_02.htm.

[19] H. G. Fisher, H. S. Forrest, S. S. Grossel, J. E. Huff, A. R. Muller, J. A. Noronha, D. A. Shaw, and B. J. Tilley, *Emergency Relief System Design Using DIERS Technology: The Design Institute for Emergency Relief Systems (DIERS) Project Manual*. Design Institute for Physical Property Data/AIChE, 1992.

[20] L. Véchot, J.-P. Bigot, D. Testa, M. Kazmierczak, and P. Vicot, “Runaway reaction of non-tempered chemical systems: Development of a similarity vent-sizing tool at laboratory scale,” *J. Loss Prev. Process Ind.*, vol. 21, no. 4, pp. 359–366, Jul. 2008.

[21] H. K. Fauske, “Properly size vents for nonreactive and reactive chemicals,” *Chem. Eng. Prog.*, vol. 96, no. 2, pp. 17–28, 2000.

[22] L. Friedel and S. Korfmann, “Predictive accuracy of simplified vent area sizing methods for the case of thermal runaway reactions,” *J. Loss Prev. Process Ind.*, vol. 13, no. 2, pp. 125–152, Mar. 2000.

[23] L. Véchot, J. Kay, and J. Wilday, “Round robin vent sizing exercise on a gassy system: 40% dicumyl peroxide in butyrate solvent,” in *Proceeding of the Hazards XXII Conference, IChemE Symposium Series 156*, 2011, no. 156, pp. 278–286.

[24] S.-H. Wu, H.-C. Chou, R.-N. Pan, Y.-H. Huang, J.-J. Horng, J.-H. Chi, and C.-M. Shu, “Thermal hazard analyses of organic peroxides and inorganic peroxides by calorimetric approaches,” *J. Therm. Anal. Calorim.*, vol. 109, no. 1, pp. 355–364, Jun. 2012.

[25] S.-H. Wu, M.-L. Lin, and C.-M. Shu, “Thermal hazard evaluation of tert-butyl peroxide using non-isothermal and adiabatic calorimetric approaches,” *J. Therm. Anal. Calorim.*, vol. 109, no. 2, pp. 975–980, Jul. 2012.

[26] H.-Y. Hou, C.-H. Su, and C.-M. Shu, “Thermal risk analysis of cumene hydroperoxide in the presence of alkaline catalysts,” *J. Loss Prev. Process Ind.*, vol. 25, no. 1, pp. 176–180, Jan. 2012.

[27] L. Véchot, W. Minko, J.-P. Bigot, M. Kazmierczak, and P. Vicot, “Vent sizing: analysis of the blowdown of a hybrid non tempered system.,” *J. Hazard. Mater.*, vol. 191, no. 1–3, pp. 8–18, Jul. 2011.

[28] J.-H. Chi, S.-H. Wu, and C.-M. Shu, “Thermal explosion analysis of methyl ethyl ketone peroxide by non-isothermal and isothermal calorimetric applications.,” *J. Hazard. Mater.*, vol. 171, no. 1–3, pp. 1145–9, Nov. 2009.

[29] S. Vyazovkin, A. K. Burnham, J. M. Criado, L. a. Pérez-Maqueda, C. Popescu, and N. Sbirrazzuoli, “ICTAC Kinetics Committee recommendations for performing kinetic computations on thermal analysis data,” *Thermochim. Acta*, vol. 520, no. 1–2, pp. 1–19, Jun. 2011.

[30] H. S. Fogler, *Elements of Chemical Engineering*, Fourth. Massachusetts: Prentice Hall, 2006.

[31] M. Avrami, “Kinetics of Phase Change. I General Theory,” *J. Chem. Phys.*, vol. 7, no. 12, p. 1103, 1939.

[32] A. Ortega, L. P. Maqueda, and J. M. Criado, “The problem of discerning Avrami-Erofeev kinetic models from the new controlled rate thermal analysis with constant acceleration of the transformation,” *Thermochim. Acta*, vol. 254, pp. 147–152, Apr. 1995.

[33] A. K. Burnham, “Application of the Šesták-Berggren Equation to Organic and Inorganic Materials of Practical Interest,” *J. Therm. Anal. Calorim.*, vol. 60, no. 3, pp. 895–908, 2000.

[34] J. Šesták and G. Berggren, “Study of the kinetics of the mechanism of solid-state reactions at increasing temperatures,” *Thermochim. Acta*, vol. 3, no. 1, pp. 1–12, Oct. 1971.

[35] E. G. Prout and F. C. Tompkins, “The thermal decomposition of potassium permanganate,” *Trans. Faraday Soc.*, vol. 40, p. 488, 1944.

[36] A. Khawam and D. R. Flanagan, “Solid-state kinetic models: basics and mathematical fundamentals.,” *J. Phys. Chem. B*, vol. 110, no. 35, pp. 17315–28, Sep. 2006.

[37] P. Vallet, “Etude theorique de la decomposition des corps en temperatures linearirement croissantes,” *C. R. Hebd. Seances Acad. Sci.*, vol. 200, no. 2, pp. 315–317, 1935.

[38] S. Vyazovkin and C. A. Wight, “Isothermal and non-isothermal kinetics of thermally stimulated reactions of solids,” *Int. Rev. Phys. Chem.*, vol. 17, no. 3, pp. 407–433, Jul. 1998.

[39] G. O. Piloyan, I. D. Ryabchikov, and O. S. Novikova, “Determination of Activation Energies of Chemical Reactions by Differential Thermal Analysis,” *Nature*, vol. 212, no. 5067, p. 1229, Dec. 1966.

[40] T. Ozawa, “A New Method of Analyzing Thermogravimetric Data,” *Bull. Chem. Soc. Jpn.*, vol. 38, no. 11, pp. 1881–1886, 1965.

[41] J. H. Flynn and L. A. Wall, “General treatment of the thermogravimetry of polymers,” *J. Res. Natl. Bur. Stand. Sect. A Phys. Chem.*, vol. 70A, no. 6, p. 487, Nov. 1966.

[42] T. R. Ingraham and P. Marier, “Activation energy calculation from a linearly-increasing-temperature experiment,” *Can. J. Chem. Eng.*, vol. 42, no. 4, pp. 161–163, Aug. 1964.

[43] A. W. Coats and J. P. Redfern, “Kinetic Parameters from Thermogravimetric Data,” *Nature*, vol. 201, no. 4914, pp. 68–69, Jan. 1964.

[44] R. M. Fuoss, I. O. Salyer, and H. S. Wilson, “Evaluation of rate constants from thermogravimetric data,” *J. Polym. Sci. Part A Gen. Pap.*, vol. 2, no. 7, pp. 3147–3151, Jul. 1964.

[45] H. H. Horowitz and G. Metzger, “A New Analysis of Thermogravimetric Traces.,” *Anal. Chem.*, vol. 35, no. 10, pp. 1464–1468, Sep. 1963.

[46] L. Reich and D. W. Levi, “Thermal stability indices for polymeric materials based on energy considerations,” *Die Makromol. Chemie*, vol. 66, no. 1, pp. 102–113, Jan. 1963.

[47] C. D. Doyle, “Kinetic analysis of thermogravimetric data,” *J. Appl. Polym. Sci.*, vol. 5, no. 15, pp. 285–292, May 1961.

[48] E. S. Freeman and B. Carroll, “The Application of Thermoanalytical Techniques to Reaction Kinetics: The Thermogravimetric Evaluation of the Kinetics of the Decomposition of Calcium Oxalate Monohydrate,” *J. Phys. Chem.*, vol. 62, no. 4, pp. 394–397, Apr. 1958.

[49] H. J. Borchardt and F. Daniels, “The Application of Differential Thermal Analysis to the Study of Reaction Kinetics,” *J. Am. Chem. Soc.*, vol. 79, no. 1, pp. 41–46, Jan. 1957.

[50] J. Zsakó, “Kinetic analysis of thermogravimetric data,” *J. Therm. Anal.*, vol. 46, no. 6, pp. 1845–1864, Jun. 1995.

[51] R. H. Gore and W. W. Wendlandt, “The solid-state kinetics of the deaquation and anation of some [Co(NH3)5H2O]X3 complexes,” *Thermochim. Acta*, vol. 1, no. 5, pp. 491–494, Oct. 1970.

[52] M. McCarty, J. N. Maycock, and V. R. P. Verneker, “Thermal decomposition of lithium aluminum hydride,” *J. Phys. Chem.*, vol. 72, no. 12, pp. 4009–4014, Nov. 1968.

[53] J. N. Maycock and V. R. Pai Verneker, “Characterization of thermal and photosublimation of organic explosives by thermobarogravimetric techniques,” *Thermochim. Acta*, vol. 1, no. 2, pp. 191–198, May 1970.

[54] J. N. Maycock, “Thermal analysis of explosives and solid propellant ingredients,” *Thermochim. Acta*, vol. 1, no. 4, pp. 389–407, Aug. 1970.

[55] H. L. Friedman, “Kinetics of thermal degradation of char-forming plastics from thermogravimetry. Application to a phenolic plastic,” *J. Polym. Sci. Part C Polym. Symp.*, vol. 6, no. 1, pp. 183–195, Mar. 2007.

[56] N. Sbirrazzuoli, “Is the Friedman Method Applicable to Transformations with Temperature Dependent Reaction Heat?,” *Macromol. Chem. Phys.*, vol. 208, no. 14, pp. 1592–1597, Jul. 2007.

[57] M. . Starink, “The determination of activation energy from linear heating rate experiments: a comparison of the accuracy of isoconversion methods,” *Thermochim. Acta*, vol. 404, no. 1–2, pp. 163–176, Sep. 2003.

[58] J. H. Flynn, “A general differential technique for the determination of parameters for d(α)/dt=f(α)A exp (−E/RT),” *J. Therm. Anal.*, vol. 37, no. 2, pp. 293–305, 1991.

[59] J. Málek and J. Criado, "The shape of a thermoanalytical curve and its kinetic information content," *Thermochim. Acta*, vol. 164, pp. 199–209, 1990.

[60] J. Málek and J. Criado, "Empirical kinetic models in thermal analysis," *Thermochim. Acta*, vol. 203, pp. 25–30, 1992.

[61] J. Málek, "The kinetic analysis of non-isothermal data," *Thermochim. Acta*, vol. 200, pp. 257–269, Jul. 1992.

[62] G. I. Senum and R. T. Yang, "Rational approximations of the integral of the Arrhenius function," *J. Therm. Anal.*, vol. 11, no. 3, pp. 445–447, Jun. 1977.

[63] J. M. Criado, J. Málek, and A. Ortega, "Applicability of the master plots in kinetic analysis of non-isothermal data," *Thermochim. Acta*, vol. 147, no. 2, pp. 377–385, Jul. 1989.

[64] A. I. Lesnikovich and S. V. Levchik, "A method of finding invariant values of kinetic parameters," *J. Therm. Anal.*, vol. 27, no. 1, pp. 89–93, May 1983.

[65] R. K. Agrawal, "Kinetic analysis of complex reactions," *J. Therm. Anal.*, vol. 31, no. 6, pp. 1253–1262, Nov. 1986.

[66] S. . Vyazovkin and A. . Lesnikovich, "Estimation of the pre-exponential factor in the isoconversional calculation of effective kinetic parameters," *Thermochim. Acta*, vol. 128, pp. 297–300, Jun. 1988.

[67] S. V. Vyazovkin, V. I. Goryachko, and A. I. Lesnikovich, "An approach to the solution of the inverse kinetic problem in the case of complex processes. Part III. Parallel independent reactions," *Thermochim. Acta*, vol. 197, no. 1, pp. 41–51, Mar. 1992.

[68] S. Vyazovkin and W. Linert, "Kinetic analysis of reversible thermal decomposition of solids," *Int. J. Chem. Kinet.*, vol. 27, no. 1, pp. 73–84, Jan. 1995.

[69] S. Vyazovkin, "Conversion dependence of activation energy for model DSC curves of consecutive reactions," *Thermochim. Acta*, vol. 236, pp. 1–13, May 1994.

[70] S. Vyazovkin, "An approach to the solution of the inverse kinetic problem in the case of complex processes: Part 4. Chemical reaction complicated by diffusion," *Thermochim. Acta*, vol. 223, pp. 201–206, Aug. 1993.

[71] J. Lenclud and J. E. S. Venart, “Single and two-phase discharge from a pressurized vessel,” *Rev Gen Therm*, vol. 35, pp. 503–516, 1996.

[72] P. S. Cumber, “Predicting outflow from high pressure vessels,” *Inst. Chem. Eng.*, vol. 79, no. January, pp. 13–22, 2001.

[73] T. Hibiki and M. Ishii, “One-dimensional drift-flux model and constitutive equations for relative motion between phases in various two-phase flow regimes,” *Int. J. Heat Mass Transf.*, vol. 46, no. 25, pp. 4935–4948, Dec. 2003.

[74] H. K. Fauske, J. C. Leung, C. F. Askonas, T. . Fitzsimons, and Z. Wang, “Runaway Characterization and Vent Sizing based on DIERS Methodology,” in *Proceedings of the International Symposium on Runaway Reactions and Pressure Relief Deisgn*, pp. 186–199.

[75] K. Bell, S. D. Morris, and R. Oster, “Vent line void fractions and mass flow rates during top venting of high viscosity fluids,” *J. Loss Prev. Process Ind.*, vol. 6, no. 1, pp. 31–35, 1993.

[76] S. D. Morris, K. Bell, and R. Oster, “Top-venting of flashing high-viscosity fluids,” *Chemical Engineering and Processing: Process Intensification*, vol. 31, no. 5. pp. 297–305, 1992.

[77] S. Ordóñez, L. Bello, H. Sastre, R. Rosal, and F. V. Díez, “Kinetics of the deep oxidation of benzene, toluene, n-hexane and their binary mixtures over a platinum on γ-alumina catalyst,” *Appl. Catal. B Environ.*, vol. 38, pp. 139–149, 2002.

[78] G. Giacchetta, M. Leporini, B. Marchetti, and A. Terenzi, “Numerical study of choked two-phase fl ow of hydrocarbons fl uids through orifices,” *J. Loss Prev. Process Ind.*, vol. 27, 2014.

[79] J. E. Huff, “Pressure Relief System Flow: Results of the DIERS Phase II Projects,” in *Emergency Relief System Design Using DIERS Technology: The Design Institute for Emergency Relief Systems (DIERS) Project Manual*, .

[80] J. C. Leung, “A generalized correlation for one-component homogeneous equilibrium flashing choked flow,” *AIChE J.*, vol. 32, no. 10, pp. 1743–1746, Oct. 1986.

[81] J. C. Leung, “Two-phase flow discharge in nozzles and pipes — a unified approach,” *J. Loss Prev. Process Ind.*, vol. 3, no. 1, pp. 27–32, Jan. 1990.

[82] R. F. Tangren, C. H. Dodge, and H. S. Seifert, “Compressibility Effects in Two-Phase Flow,” *J. Appl. Phys.*, vol. 20, no. 7, p. 637, 1949.

[83] American Petroleum Institute, “Sizing, selection and installation of pressure relieving devices in refineries, part 1,” 2008.

[84] S. Richardson, S. Richardson, G. Saville, G. Saville, S. Fisher, S. Fisher, A. Meredith, A. Meredith, M. Dix, and M. Dix, “Experimental Determination of Two-Phase Flow Rates of Hydrocarbons Through Restrictions,” *Process Saf. Environ. Prot.*, vol. 84, no. 1, pp. 40–53, 2006.

[85] R. Britter, J. Weil, J. Leung, and S. Hanna, “Toxic industrial chemical (TIC) source emissions modeling for pressurized liquefied gases,” *Atmospheric Environment*, vol. 45, no. 1. pp. 1–25, 2011.

[86] R. Diener and J. Schmidt, “Sizing of throttling device for gas/liquid two-phase flow part 2: Control valves, orifices, and nozzles,” *Process Saf. Prog.*, vol. 24, no. 1, pp. 29–37, 2005.

[87] M. Sam Mannan, Ed., *Lees' Loss Prevention in the Process Industries.*, 4th ed. Oxford: Butterworth Heinemann, 2012.

[88] H. K. Fauske, M. A. Grolmes, and R. E. Henry, “Emergency Relief Systems - Sizing and Scale-Up,” *Plant/Operations Prog.*, vol. 2, no. 1, pp. 27–30, 1983.

[89] H. K. Fauske, “Flashing flows or: Some practical guidelines for emergency releases,” *Plant/Operations Prog.*, vol. 4, no. 3, pp. 132–134, 1985.

[90] H. L. Norris III, R. C. Puls, H. L. Norris, and R. C. Puls, “Single-phase or multiphase blowdown of vessels or pipelines,” in *68th Annual Technical Conference*, 1993, vol. Pi, pp. 519–528.

[91] H. L. Norris and R. C. Puls, “Hydrocarbon blowdown from vessels and pipelines,” in *69th Annual Technical Conference*, 1994, no. l, pp. 593–602.

[92] S. Selmer-Olsen, “Pressure Relief and Two-Phase Flow,” in *IChemE Symposium Series No. 130*, 1992.

[93] A. N. Skouloudis, “Benchmark exercises on the emergency venting of vessels,” *Journal of Loss Prevention in the Process Industries*, vol. 5, no. 2. pp. 89–103, 1992.

[94] D. V. Nichita, P. Khalid, and D. Broseta, “Calculation of isentropic compressibility and sound velocity in two-phase fluids,” *Fluid Phase Equilib.*, vol. 291, no. 1, pp. 95–102, 2010.

[95] M. Castier, “Thermodynamic speed of sound in multiphase systems,” *Fluid Phase Equilib.*, vol. 306, no. 2, pp. 204–211, Jul. 2011.

[96] H. Mahgerefteh, A. Oke, and O. Atti, “Modelling outflow following rupture in pipeline networks,” *Chem. Eng. Sci.*, vol. 61, no. 6, pp. 1811–1818, 2006.

[97] H. Mahgerefteh and S. M. . Wong, “A numerical blowdown simulation incorporating cubic equations of state,” *Comput. Chem. Eng.*, vol. 23, no. 9, pp. 1309–1317, 1999.

[98] H. Mahgerefteh, P. Saha, and I. G. Economou, “Modeling fluid phase transition effects on dynamic behavior of ESDV,” *AIChE J.*, vol. 46, no. 5, pp. 997–1006, 2000.

[99] H. Mahgerefteh, G. B. O. Falope, and A. O. Oke, “Modeling blowdown of cylindrical vessels under fire attack,” *AIChE J.*, vol. 48, no. 2, pp. 401–410, 2002.

[100] A. Oke, H. Mahgerefteh, I. Economou, and Y. Rykov, “A transient outflow model for pipeline puncture,” *Chem. Eng. Sci.*, vol. 58, no. 20, pp. 4591–4604, 2003.

[101] H. Mahgerefteh, P. Saha, and I. G. Economou, “Fast Numerical Simulation for Full Bore Rupture of Pressurized Pipelines,” *AIChE J.*, vol. 45, no. 6, pp. 1191–1201, 1999.

[102] M. F. Alfradique and M. Castier, “Modeling and simulation of reactive distillation columns using computer algebra,” *Comput. Chem. Eng.*, vol. 29, no. 9, pp. 1875–1884, Aug. 2005.

[103] M. L. Michelsen, “State function based flash specifications,” *Fluid Phase Equilib.*, vol. 158–160, pp. 617–626, Jun. 1999.

[104] W. H. Press, B. P. Flannery, S. A. Teukolsky, and W. T. Vetterling, *Numerical Recipes in Fortran 77: The Art of Scientific Computing*, 2nd ed. Cambridge University Press, 1992.

[105] C. N. Dorny, “Understanding dynamic systems approaches to modeling, analysis, and design.” Prentice Hall, Englewood Cliffs, N.J., 1993.

[106] M. Castier, “Automatic implementation of thermodynamic models using computer algebra,” *Comput. Chem. Eng.*, vol. 23, no. 9, pp. 1229–1245, Nov. 1999.

[107] M. L. Michelsen, “The isothermal flash problem. Part II. Phase-split calculation,” *Fluid Phase Equilib.*, vol. 9, no. 1, pp. 21–40, Dec. 1982.

[108] R. O. Espósito, M. Castier, and F. W. Tavares, "Calculations of thermodynamic equilibrium in systems subject to gravitational fields," *Chem. Eng. Sci.*, vol. 55, no. 17, pp. 3495–3504, Sep. 2000.

[109] M. L. Michelsen, "The isothermal flash problem. Part I. Stability," *Fluid Phase Equilib.*, vol. 9, no. 1, pp. 1–19, Dec. 1982.

[110] M. Castier, "Solution of the isochoric–isoenergetic flash problem by direct entropy maximization," *Fluid Phase Equilib.*, vol. 276, no. 1, pp. 7–17, Feb. 2009.

[111] A. Basha, "Rigorous Simulation of Accidental Leaks form High-Pressre Storage Vessels," Texas A&M University, 2014.

[112] T. Olewski, O. Basha, S. Waldram, S. Mannan, and L. Vechot, "Mitigation of LNG dispersion using two dimensional (2d) water curtains," in *IChemE Symposium Series No. 156*, 2011, no. 156, pp. 308–314.

[113] E. R. A. E. Lima, M. Castier, and E. C. B. Jr, "Differential-algebraic approach to dynamic simulations of flash drums with rigorous evaluation of physical properties," *Oil Gas Sci. …*, vol. 63, no. 5, pp. 677–686, 2008.

[114] H. L. Norris and H. L. Norris III, "Hydrocarbon blowdown from vessels and pipelines," in *Proceedings - SPE Annual Technical Conference and Exhibition*, 1994, vol. Pi, no. pt 1, pp. 593–602.

[115] L. Raimondi, "Rigorous Simulation of LPG Releases from Accidental Leaks," *Chem. Eng. Technol.*, vol. 26, pp. 63–68, 2012.

[116] M. Castier, "Dynamic simulation of fluids in vessels via entropy maximization," *J. Ind. Eng. Chem.*, vol. 16, no. 1, pp. 122–129, Jan. 2010.

[117] R. Kirk and D. Othmer, *Encyclopedia of Chemical Technology*, Fourth Ed. New York: Wiley, 1991.

[118] A. C. Hordijk and J. J. De Groot, "Experimental data on the thermal kinetics of organic peroxides," *Thermochimica Acta*, vol. 101. pp. 45–63, 1986.

[119] A. Aldeeb, "Systematic Approach For Chemical Reactivity Evaluation," Texas A&M University, 2003.

[120] M. Nandi, "The performance of di-tertiary-butyl peroxide as cetane improver in diesel fuels," *… -AMERICAN Chem. Soc. Div. FUEL …*, pp. 863–867, 1996.

[121] R. Blaine, “The search for kinetic reference materials for adiabatic and differential scanning calorimetry,” *J. Therm. Anal. Calorim.*, vol. 106, no. 1, pp. 25–31, Oct. 2010.

[122] HEL, “PHI-TEC Operating Manual Volume 3: Verification of Equipment Performance And Examples of Data,” vol. 3, no. September. pp. 1–15, 2004.

[123] Design Institute for Physical Properties, “Knovel Dippr Project 108.” AIChE, 2012.

[124] J. C. Oxley, J. L. Smith, E. Rogers, W. Ye, A. A. Aradi, and T. J. Henly, “Fuel combustion additives: A study of their thermal stabilities and decomposition pathways,” *Energy and Fuels*, vol. 14, no. 6, pp. 1252–1264, 2000.

[125] Y. Iizuka and M. Surianarayanan, “Comprehensive Kinetic Model for Adiabatic Decomposition of Di-tert-butyl Peroxide Using BatchCAD,” *Ind. Eng. Chem. Res.*, vol. 42, no. 13, pp. 2987–2995, 2003.

[126] A. Kimura and T. Otsuka, “Performance evaluation of differential accelerating rate calorimeter for the thermal runaway reaction of di-tert-butyl peroxide,” *J. Therm. Anal. Calorim.*, vol. 113, no. 3, pp. 1585–1591, Jul. 2013.

[127] L. Jiayu, C. Wanghua, C. Liping, T. Yingtao, and S. Xin, “Thermal Decomposition Analysis and Safety Study on Di-tert-butyl Peroxide,” *Procedia Eng.*, vol. 43, pp. 312–317, Jan. 2012.

[128] D. I. Townsend and J. C. Tou, “Thermal hazard evaluation by an accelerating rate calorimeter,” *Thermochim. Acta*, vol. 37, no. 1, pp. 1–30, Apr. 1980.

[129] Y. Duh, W. Wang, and C. Kao, “Novel validation on pressure as a determination of onset point for exothermic decomposition of DTBP,” *J. Therm. Anal. Calorim.*, 2014.

[130] Y. Y.-S. Duh, J.-M. J. Yo, W. W.-L. Lee, C. C.-S. Kao, and J.-M. Hsu, “Thermal Decompositions of Dialkyl Peroxides Studied by DSC,” *natasinfo.org*, no. 1, pp. 1–10, Jul. 2014.

[131] PerkinElmer, “Technical Specifications Thermal Analysis for the DSC 8000/8500 Differential Scanning Calorimeters.” 2010.

[132] Omega Engineering Inc., “Revised Thermocouple Reference Tables: K-type.” .

[133] C. Croarkin and P. Tobias, Eds., *NIST/SEMATECH e-Handbook of Statistical Methods*, Latest upd. 2003.

[134] A. Savitzky and M. J. E. Golay, “Smoothing and Differentiation of Data by Simplified Least Squares Procedures,” *Anal. Chem.*, vol. 36, no. 8, pp. 1627–1639, 1964.

[135] A. Savitzky, “A historic collaboration,” *Anal. Chem.*, vol. 61, no. 15, p. 921A–923A, 1989.

[136] B. E. Poling, J. M. Prausnitz, and J. P. O’Connell, *The Properties of Gases and Liquids*, 5th ed. New York: McGraw-Hill Professional, 2000.

[137] D.-Y. Peng and D. B. Robinson, “A New Two-Constant Equation of State,” *Ind. Eng. Chem. Fundam.*, vol. 15, no. 1, pp. 59–64, 1976.

[138] A. Firoozabadi and H. Pan, “Two-Phase Isentropic Compressibility and Two-Phase Sonic Velocity for Multicomponent-Hydrocarbon Mixtures,” *SPE Reserv. Eval. Eng*, vol. 3, pp. 335–341, 2000.

[139] A. A. Kossoy, J. Singh, and E. Y. Koludarova, “Mathematical methods for application of experimental adiabatic data – An update and extension,” *J. Loss Prev. Process Ind.*, vol. 33, no. 812, pp. 88–100, 2015.

[140] V. Casson Moreno, R. Kanes, J. Wilday, and L. Véchot, “Modeling of the venting of an untempered system under runaway conditions,” *J. Loss Prev. Process Ind.*, 2015.

[141] G. Wehmeier, F. Westphal, and A. Hoechst, “Pressure relief system design for vapour or two-phase flow?,” *Process Saf. Environ. …*, pp. 491–503, 1994.

[142] J. Etchells, T. Snee, and J. Wilday, “Relief System Design For Exothermic Runaway : The HSE Strategy,” in *IChemE SYMPOSIUM SERIES No. 147*, 2000, no. 147, pp. 1–13.

[143] HEL, “PHI-TEC Operating Manual Volume 1 Hardware Details,” Herts, 2007.

[144] Thermometrics, “Types of Thermocouples,” 2013. [Online]. Available: http://www.thermometricscorp.com/thermocouple.html.

[145] R. J. a. Kersten, M. N. Boers, M. M. Stork, and C. Visser, “Results of a Round-Robin with di-tertiary-butyl peroxide in Various Adiabatic Equipment for Assessment of Runaway Reaction Hazards,” *J. Loss Prev. Process Ind.*, vol. 18, no. 3, pp. 145–151, May 2005.

[146] J. L. Woodward, “An integrated model for discharge rate, pool spread, and dispersion from punctured process vessels,” *J. Loss Prev. Process Ind.*, vol. 3, no. 1, pp. 33–37, 1990.

[147] S. M. Richardson and G. Saville, “Blowdown of LPG pipelines,” *Process Saf. Environ. Prot.*, vol. 74, pp. 235–244, 1996.

[148] A. N. Skouloudis, K. Bell, and H. M. Kottowski, “Venting of vessels containing reacting fluids: a parametric study with SAFIRE and DEERS,” *J. Loss Prev. Process Ind.*, vol. 3, no. 1, pp. 13–16, 1990.

[149] K. H. Bendiksen, D. Maines, R. Moe, and S. Nuland, “The Dynamic Two-Fluid Model OLGA : Theory and Application,” *SPE Prod. Eng.*, no. May, pp. 171–180, 1991.

[150] D. W. Johnson and J. L. Woodward, *RELEASE: A Model with Data to Predict Aerosol Rainout in Accidental Releases*. New York: Center for Chemical Process Safety, AIChE, 1984.

[151] Det Norske Veritas Ltd, “Report 403: Flashing Liquid Jets and Two-Phase Dispersion,” 2002.

[152] H. Wiltox, “PVAP - Theory Document - Technical Reference.”

[153] H. Witlox, M. Harper, P. Bowen, and V. Cleary, “Flashing liquid jets and two-phase droplet dispersion. II. Comparison and validation of droplet size and rainout formulations,” *J. Hazard. Mater.*, vol. 142, no. 3, pp. 797–809, 2007.

APPENDIX A

PERKINELMER DSC 8500 HYPER-ENABLED DOUBLE-FURNACE DIFFERENTIAL SCANNING CALORIMETER

The PerkinElmer DSC 8500 Hyper-enabled Double-Furnace Differential Scanning Calorimeter is equipped with a 90% platinum alloy furnace that allows for superior thermal conductivity and fast furnace response. It can also operate with oxygen at temperatures greater than 873.15 K. It is also equipped with distributed platinum resistance temperature sensors, which are more accurate and linear for a wider temperature range. There are various cooling accessories, some of which are the chiller and LN2 cooler.

In terms of its calorimetric performance, it has a dynamic range of ±1300 mW, which allows applications with high-energy thermal transitions to be measured. The instrument's accuracy for heat flow measurements is <±0.2% while its precision is <±0.03%. Also, it can operate within a wide temperature range of 93.15 to 1023.15 K. Its accuracy with respect to temperature performance is <±0.05% while its precision is <±0.008%. Furthermore, the instrument has controlled heating and cooling rates of 0.01 to 1023.17 K/min, and an in-situ ballistic cooling to 2373.15 K/min and this enables experiments that simulate real-world processes. [131]

Its main operating governing principle of measurement is through power compensation. Here, the sample pan as well as the reference pan are placed in an identical set of furnaces/ovens. The temperature difference between the two is controlled through the power supply output to the sample furnace. In RC, there is an internal compensation heater that minimizes the temperature difference between the sample and the surroundings. The concept is the same in both cases, such that the power supplied to minimize the temperature difference is the measured variable. The difference between the power supplied and the baseline value when no reaction takes place is the quantity $\dot{Q}_s$ [17].

A.1 Apparatus description

The DSC consists of four major components: the main furnace for the sample and reference cells, the chiller, a crimping set and a computer control software. The main furnace, as shown in Figure 1, houses two small cells that can be made from various metallic compounds, as well the heater, and the thermocouples.

There are various cell types, or 'pans' to be more precise, than can be used, depending on the system and the pressure buildup. The Standard Sample Pans are available in aluminum, copper, or gold. Here, the sample is contained within a highly conductive capsule and distributed in a thin layer so that the internal resistance in the sample itself is very small. The operating temperature range vary with the material. For example, platinum and gold exhibit high thermal capabilities and thus can be used to 1000 K. The Stainless Steel Pans with O-ring are designed to suppress the vaporization of a solvent or a volatile reaction product, thus eliminating any effects of the heat of vaporization. These capsules can withstand an internal pressure of 40 atm, have a volume of 60 μL, and are to be operated between 233.15 K to 673 K. High pressure gold cells that can withstand up to 100 atm are also available.

Figure 1. DSC sample and reference cell furnace with vacuum wand.

Each pan needs to be crimped, so that it is sealed and the sample is protected from contamination. To do this a press kit is used. Each pan type has a special accessory to be used to crimp it or seal it shut. Care must be taken to avoid leaks and detect faulty pans.

The software used with the DSC is Pyris^{TM}. It allows for calibration of the baseline, heat flow and temperature sensors. It also has the ability to calculate conversion-time-temperature data along with the heat flow thermogram. Options such as onset calculation and peak area are also available.

A.2 Operating modes and procedures

In this research, Stainless Steel Pans with O-ring were used for both the sample and reference cells. First, a set of cells, one reference and one for the sample, were prepared by inserting the O-ring using a pair of fine tweezers around the inside the pan cover. The pan covers were then placed on top of the pan bottom and each is weighed separately using a microbalance. Then, the reference cell was crimped using the press kit and reweighed. The weight was recorded for each step. The pan cover was then removed from sample pan and using a micropipette; 10 μL were pipetted into the pan bottom. The cover was replaced and the weight of the sample pan with the contents was recorded. The difference in mass between the empty pan and pan with contents gives the mass of the sample/solution. The sample pan was also crimped and reweighed. This was to be able to denote any mass change or leaks during the experimental run.

Next, the furnace temperature was set to be 303.15 K using Pyris^{TM} and information about the weight sample and name of the run are inputted. The operation mode was set to temperature scanning. The program was constructed such that the instrument would hold for 1 minute at 303.15 K, then proceed with a heating rate of 5 K/min, until 573.15 K, where it will hold this temperature for another minute. After this the cooler will start taking the system back to preset initial temperature. The heating rate was changed frequently between run to 5 K/min, 10 K/min, 12.5 K/min and 15 K/min.

Finally, the sample and reference pans were loaded in the furnace in their allocated places using a vacuum wand. The run program was then set to start. The thermogram of heat flux with the progression of time and temperature was generated. The onset temperature and heat of reaction were determined using the Pyris^{TM} software. Conversion-time curves were generated as a function of the heat flux and calculated heat of reaction.

A.3 Data quality

To maintain high data quality, several tasks were carried out frequently. First, the equipment was placed on a stable non-vibrating table, with a clear area surrounding it. This reduced signal noise on the thermograms. Second, instrument calibration was performed every time there was drastic change in heating rate, or temperature range of study. The calibration standard used was Indium.

Also, frequent technician and servicing visits were scheduled to make sure the automated equipment mechanism, like door opening, was always working. Technicians also looked at several collected thermogram to check for quality of output signal. The furnace was cleaned after every run to avoid and vapors from remaining inside. Dust was also removed quite frequently.

APPENDIX B

ADIABATIC REACTION CALORIMETER PHI-TEC I&II

There are several characteristics of a suitable adiabatic calorimeter. The first of which is the calorimeter should indeed be adiabatic. This means that the sample is loaded into an internal vessel whose walls have good thermal insulation. Also, the software used should be able to regulate the heater to maintain the temperature of the surroundings equal to those the sample. Usually, the sample hold has volumes of 10 to 100 mL. The onset temperature detection for such calorimeters is usually when the self-heating rate is greater than 0.02 K/min. A wide temperature range (293.15 – 773.15 K), and pressure range (0 – 150 bar) can be used.

It is also recommended to work at conditions close to the industrial ones, so that scale-up is possible. The type of test cells should be indicative of the type of reactors used. Stirring should be simulated if industrial reactors use stirring. Not all conditions can reproduced at such a small scale, but as many as possible gives more accurate data for scale-up.

Furthermore, the thermal inertia, indicated by the phi-factor should be close to unity. Under adiabatic condition, heat released by the reaction goes only towards increasing the temperature of the sample. However, in a calorimeter, both the sample and vessel are under adiabatic mode, and thus some of the heat produced is used to heat up the vessel walls. In a laboratory scale, the thermal mass of the vessel is a much larger fraction of the total thermal mass.

It is recommended to use a phi-factor close to unity, or within a range of 1.05-1.1, since these generally better reflects industrial conditions. If the phi-factor rating of particular instrument is outside this range, the data obtained needs to be corrected before using it for vent sizing.

B.1 Apparatus description

PHI-TEC I (Figure 2–left) and PHI-TEC II (Figure 2–right) calorimeters are bench scale adiabatic calorimeters that allow safe investigations of runaway hazards. This part of the report describes both calorimeters and their operating conditions. Both the PHI-TEC I and II have the same basic design of an adiabatic calorimeter. The only difference between both of them is that PHI-TEC II is capable of using larger test cells (up to 120 ml) that have thinner cell walls (and hence lower ϕ) and it has an automatic pressure compensation system.

The common design features of PHI-TECs I and II will be described and then the differences between both calorimeters will be discussed in detail. Both PHI-TEC calorimeters can be broken down into the following main components: a containment vessel, heaters, test cells, instrumentation, electronics unit and a computer and interface cards.

The purpose of the containment pressure vessel is to house the test cell that itself contains the investigated reaction. The reason for having a pressure vessel is to provide a safe working environment for the personnel operating the calorimeter. The pressure vessel is designed to contain the cell and its components in case it blasts.

Figure 2. PHI-TEC I (Left) and PHI-TEC II (Right)

The pressure vessel is made of stainless-steel and rated at over 200 bars.[143] The pressure vessel is composed of the following parts: Main Unit, Top Plate, ‘O’ ring seal, and Top End Cap.[143] The Top Plate in PHI-TEC I serve as the Top End Cap. The main unit contains several ports for the connection of various instrumentation (pressure gauge, cables for the thermocouples, cables for the can heater…), feed line, and ball valve. The ‘O’ ring seal serves to ensure full isolation of the pressure vessel from the surrounding. The Top Plate contains three ports that are used for top guard heater power connections, thermocouples power connections, and connection to the agitation system. A schematic is shown in Figure 3.

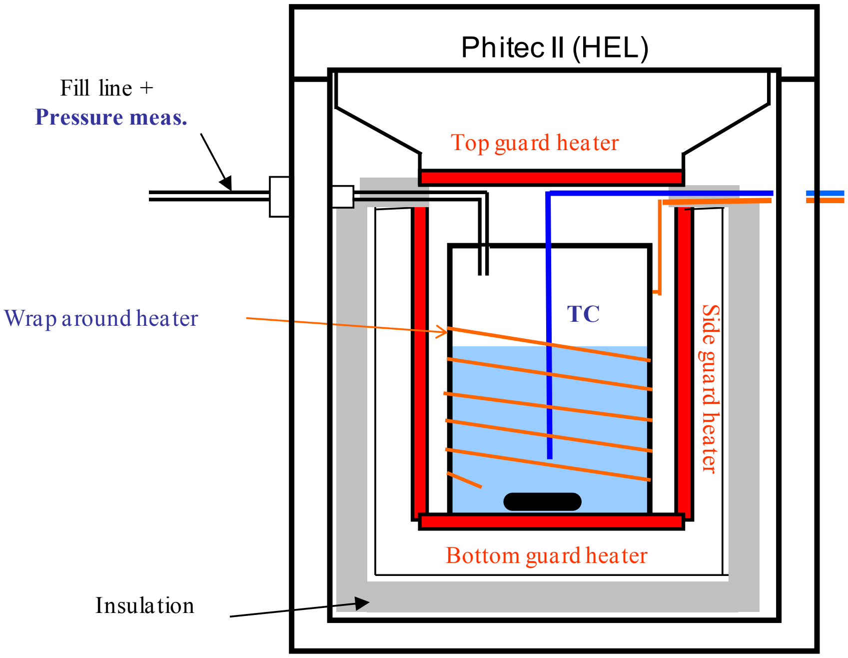

Figure 3. PHI-TEC II Pressure Vessel Assembly [143]

Both PHI-TEC calorimeters contain two types of heaters. The first one is the sample/can heater and the second one is the guard heaters. The sample heater in Figure 4 consists of a pre-coiled metallic wire that is designed to wrap around the test cell tightly. The sample heater is used in providing heat to the test cell (that contains the investigated mixture) until an exotherm is detected.

The purpose of the guard heater is to create an adiabatic environment for the reaction to take place. This mimics what happens in industry, whether in a large batch reactor or in a large vessel. The guard heater is divided into "Top heater assembly" and "Side/Bottom heater assembly". Each of the guard heaters is controlled independently using a "PID control algorithm".[143] The guard heaters maintain an adiabatic environment by adjusting their temperatures so that it is equal to the temperature inside the test cell. The test cell contains the investigated chemical/s and it is where the reaction takes place. Several test cells can be used of different material and sizes for PHI-TEC I and II.

PHI-TEC I test cells range from 8 ml to 11 ml. They are available in various materials. The test cells used for PHI-TEC I experiments were high pressure test cells that are 10 ml large – which is the most common test cell size. The test cells are made from stainless steel. These cells are relatively thicker than most common test cells that are used for PHI-TEC II. The thick test cell walls result in high ϕ factor. On the other hand, PHI-TEC II can use test cells that have thinner walls than the test cells used for PHI-TEC I. These cells are also made from stainless steel. The test cells used in PHI-TEC II were 110 ml large. The thin test cell walls result in a low ϕ factor that is almost 1 [143]. PHI-TEC II is also compatible with high-pressure test cells, however, these cells will have a high ϕ factor (usually between 1.5 and 2.0).

The main instruments that are used in PHI-TEC I and II are thermocouples and pressure sensors. Both calorimeters use thermocouples of type K. [143] These thermocouples can stand temperatures up to 1553.15 K [144]. The thermocouples read the temperatures inside the test cells and that of the various guard heaters. The readings are sent to a computer that serves as a data acquisition system by recording the data. The pressure sensors read the pressure inside the test cell and as the thermocouples; the readings are recorded and sent to the computer and recorded.

The difference between PHI-TEC II and PHI-TEC I is that the former one can use test cells with relatively thin walls (and thus with a lower ϕ factor). In order to avoid the test cells from crushing, PHI-TEC II uses an automatic pressure equalizer system. PHI-TEC II uses a differential pressure transducer to measure the pressure difference between the test cell and the pressure vessel. The pressure compensation system maintains a differential pressure less than 3 bar between the test cell and the pressure vessel. This is done by introducing nitrogen into the pressure vessel or by removing it to maintain the differential pressure less than 3 bar. The nitrogen is supplied from a standard lab nitrogen gas cylinder.

The differential pressure transducer is switched into an absolute pressure transducer when high-pressure test cells are used. In this case, the pressure transducer will measure the pressure inside the pressure vessel. In addition to that, the automatic pressure equalizer system is not activated when high-pressure test cells are used.

B.2 Operating modes and procedures

In this research, the adiabatic calorimeters were operated using the Heat Wait and Search (HWS) routine in order to be able to properly track the onset temperature of the sample. Heating steps of 1 K were used. This means that the instrument will heat the sample up by 1 degree from the set point temperature. Then, it will wait for the system to stabilize and reach this new temperature, upon which it will search to detect if there are any signs of a reaction exotherm. This is when the self-heating rate exceeds 0.02 ˚C/min. If no exotherm is detected, the instrument will heat the sample up by another degree, and so on, until an exotherm is detected. After this point, it will start tracking the rapid change in temperature and pressure buildup during a runaway. Figure 4 below depicts the steps of HWS routine, as well as the developed temperature and pressure profiles.

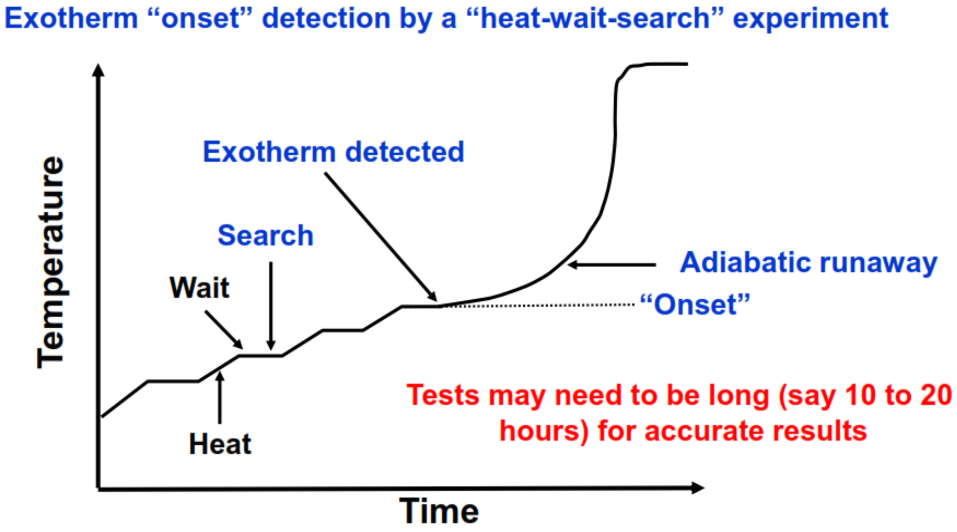

Figure 4. Heat Wait and Search routine

In the PHI-TEC II, the sample was loaded into the stainless steel cell using a glass syringe and a feeding pipe, and weighed. The cell was then attached to the reaction vessel by securing a Swagelok fitting, and then surrounding it with thermal insulation wool. After this, the pressure vessel was closed. Closed-cell HWS mode of study was then applied, with heating to temperatures about 15 K less than the expected onset temperature. The starting temperature and pressure were recorded. An initial waiting period of 40 minutes was set for temperature calibration. The waiting period between each HWS step was set to be 8 minutes. The maximum temperature to track for was 763.15 K and the maximum pressure to track for was 100 bars. Should the experiment exceed these values, shutdown procedures would be initiated.

At the end of the run, the sample was left to cool down and return to room temperature. The final temperature and pressure were recorded before the vessel was depressurized, and the cell was disconnected. The final weight of the sample was recorded, and the cell was then subsequently cleaned.

B.3 Data quality

To maintain high data quality, several tasks were carried out frequently. First, the instrument was cleaned after use with ethanol to make sure no residual vapors or drops interfere with the experiment. The thermal insulation wool used was also changed frequently, to avoid it contaminating newer runs. Second Swagelok fittings were replaced when the threads become worn and might leak.

Leak detection was first performed before loading the vessel, using Snoop® to determine whether there were any leaks in the line to the vessel. After the vessel was loaded, Snoop® was used to check the Swagelok fitting, and ensure the vessel itself was not leaking. Next, a pressure test was conducted by connecting a nitrogen line to the instrument and pressurizing the vessel to about 80 bars. This is to simulate the high pressures that can be developed by the sample. The software was used to run an isothermal test at room temperature and track pressure change. Calibration of thermocouples was also performed, whenever new ones were installed. This prevents any positive or negative deviations that may affect the adiabatic conditions of the system.

B.4 Correcting for the phi-factor

When using adiabatic data, it is assumed that the temperature rise is proportional to the conversion at the each point, and the rate constant follows the Arrhenius law with respect to temperature dependency. In order to replicate large scale conditions, wherein the heat capacity of the vessel walls is negligible compared the heat capacity of the fluid it contains, the walls of a given cell used in calorimeter have to be ideally non-extremely thin. This results in a cell that has small fraction of the total thermal mass, as is the case of large-scale operation. However, this is not feasible on a small laboratory scale, where the cell mass fraction is large compared to the total thermal mass. This is characterized by the thermal inertia, quantified using the phi-factor, ϕ, where subscript s denotes the sample, and subscript c denotes the cell,

$$\phi = \frac{\left(mC_p\right)_s + \left(mC_p\right)_c}{\left(mC_p\right)_c} \tag{1}$$

It must be noted that these values are all static; dynamic phi-factor values are difficult to measure both in an experimental and large scale. Usually, phi-factor values vary between 1 and 1.05 in industrial plants, indicating that the heat produced by the reaction is used solely to heat up the reaction temperature. Any heat losses from the experimental sample into either the environment or the vessel wells, reduces the sample temperature. This leads to incorrect predictions of onset temperature in cases of runaway. For experimental data with high phi-factors, the data is to be corrected to a phi-factor equal to unity before their use to predict runaway parameters and for vent sizing [17]. The effect of the phi factor on experimental data, such as the temperature profile and its derivative can be seen in Figure 5.

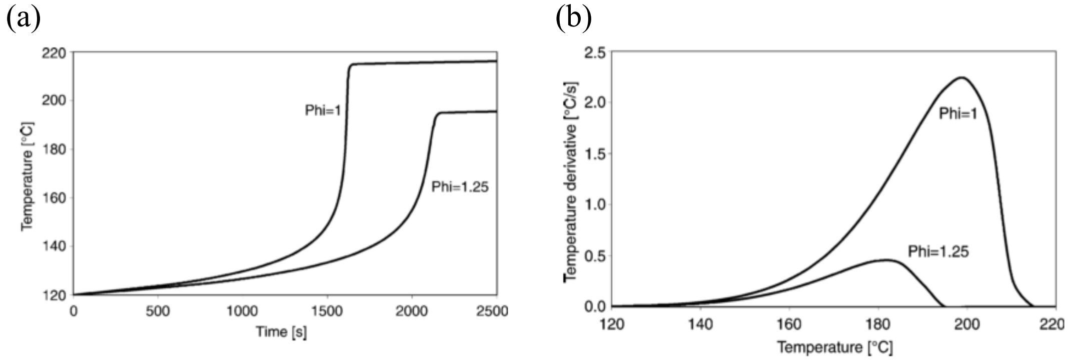

Figure 5. Influence of phi-factor on (a) temperature profile (b) self-heating rate profile. Adapted from R.J.A. Kersten et al. [145]

For an accurate kinetic and thermodynamic description of the system, the adiabatic temperature increase can be found directly from experimental data

$$\Delta T_{ad} = \left(T_{end} - T_{onset}\right) \tag{2}$$

This can then be corrected for using the phi-factor using

$$\Delta T_{ad,\mathrm{corr}} = \phi \Delta T_{ad} \tag{3}$$

Next, the onset temperature, T_o, obtained from experimental data, can be corrected as proposed by Fisher [19]

$$\frac{1}{T_{o,corr}} = \frac{1}{T_o} + \frac{R}{E_a} \ln \phi \tag{4}$$

For equipment with a phi-factor higher than 1, the onset detection is lower than ideal conditions, and thus it over-estimates the onset point. The corrected value, $T_{o,corr}$, is expected to be lower than the experimental value.

The remaining experimental temperatures, T, after the onset are then also corrected

$$T_{corr} = T_{0,corr} + \phi \cdot \left(T - T_{0,corr}\right) \tag{5}$$

The heating rate from the adiabatic energy balance is given by Eq. (6) and (7). For the same degree of conversion, at different temperatures T_1 and T_2, the equivalent heating rates are

$$\left(\frac{dT}{dt}\right)_{T=T_1} = \frac{\Delta H_r}{C_p} \exp\left(\frac{-E_a}{RT_1}\right) f\left(X\right) \tag{6}$$

$$\left(\frac{dT}{dt}\right)_{T=T_2} = \frac{\Delta H_r}{C_p} \exp\left(\frac{-E_a}{RT_2}\right) f\left(X\right) \tag{7}$$

This is similar to having different phi-factors for the same degree of conversion. For a phi-factor of 1, the temperature is going to be higher than for a phi-factor greater than one, thus

$$\left(\frac{dT}{dt}\right)_{\phi=1} = \frac{\Delta H_r}{C_p}\exp\left(\frac{-E_a}{RT_{\phi=1}}\right)f\left(X\right) \tag{8}$$

$$\left(\frac{dT}{dt}\right)_{\phi>1} = \phi\frac{\Delta H_r}{C_p}\exp\left(\frac{-E_a}{RT_{\phi>1}}\right)f\left(X\right) \tag{9}$$

APPENDIX C

COMPUTER PROGRAMS

C.1 LEKCON

In 1990, Woodward et al. [146] developed LEAKR, a computer program for the Environment of Canada, which calculates single or two phase discharge rates based on Fauske's equilibrium rate model for sonic releases. This work was later extended to form LEAKER, using technology from DIERS and DIPPR (Design Institute of Physical Properties Research) to calculate discharge rates from vessels. In 1989, LEAKER and a series of other similar programs were integrated to form LEKCON, a single tool capable of predicting the effects of an accidental release from a process vessel [146]. The program accounts for various geometries (horizontal, vertical and spherical cylinders), vessel elevation, insulation, liquid level and puncture height.

C.2 BLOWDOWN

The depressurization of major process vessels may occur through blowdown to the flare system onsite. A hazard associated with sudden depressurization is the fall in temperature of the vapor/gas phase. This causes the vessel walls to drop in temperature, and leads to condensation of the vapor, creating liquid droplets which may enter the flare header [87]. BLOWDOWN was developed by Richardson, Saville, and co-workers, at

Imperial College London, to predict vessel wall temperature in order to prevent brittle failures of the vessel and estimate the resulting flow to the flare. Its application was mostly for the offshore oil platforms, and was later extended to include pipelines [147].

The program uses an equation of state based on the extended corresponding states principle to estimate thermodynamic properties such as the pressure, temperature, density. Also, it is able to deal with three phases, and assumes thermodynamic non-equilibrium. The flow is assumed to be quasi-steady irrespective of the number of phases, however, if it is two-phase, then it has to be homogeneous.

BLOWDOWN divides the vessel into three zones: a top zone of gaseous hydrocarbons; a middle zone of liquid hydrocarbons, and a bottom zone of free water. Finally, depressurization is broken down over increments of pressure instead of time, as it is more pertinent, and in order to be able to appropriately follow vessel behavior during the rapid process [147].

C.3 SAFIRE

SAFIRE is a vessel depressurization program developed by Fauske & Associates for DIERS, to model the multi-phase hydro-dynamics for pressure vessels, equipped with an ERS [148]. It is mostly used for batch processing chemicals where runaway reactions may occur. It is capable of dealing with various vessel flow regimes by using the drift-flux model, and thermodynamic equilibrium is assumed. The basic concept of the drift-flux model is that it considers that mixture was a whole rather than consisting of two phases. It should be noted that with this simplifying formulation, some characteristics of two-phase flow might be lost. However, since the vessel is modelled as a single control volume, the range of its applicability is limited [148]. Skouloudis, in his bench mark study of computer programs related to emergency relief venting [93], suggests there is a need to analyze the venting processes by using 1-D modelling for the vessel and the vent line. Also, numerical robustness was found to be a problem [72].

C.4 OLGA

OLGA is a dynamic two-fluid program developed by Bendelksen et al. [149] for simulation of two-phase oil and gas flows in pipelines. The program had the ability to accurately predict the pressure drop, liquid hold-up and flow-regime transitions. OLGA was tested against experimental data from SINTEF two-phase flow laboratory and from literature, and its predictions were in good agreement with both [149].

C.5 RELEASE

In order to simulation continuous steady state flow of a liquid discharge from an orifice, RELEASE was developed in 1999. It was assumed that the chemical system was non-reactive, and the discharge resulted in jet spreading. RELEASE can predict the vessel depressurization, and the rate of the fluid discharge. It can also handle flashing and formation of liquid drops, entrainment of drops into vapor cloud, jet spreading and rate of liquid rainout to a pool on the ground [150].

C.6 PHAST

PHAST is a consequence modeling software developed by DNV that includes models for atmospheric release of vessel discharges. For pressurized releases from vessels/pipes, PHAST uses a ‘flash model’ to calculate depressurization phenomena such as external expansion and flashing, from the exit pressure to the ambient pressure [151]–[153].